ATRX Mediated Restriction of Herpes Simplex Virus 1

ATRX Mediated Restriction of Herpes Simplex Virus 1

A dissertation presented

by

Joseph Michael Cabral

to

The Division of Medical Sciences

in partial fulfillment of the requirements

for the degree of

Doctor of Philosophy

in the subject of

Virology

Harvard University

Cambridge, Massachusetts

May 2019

Dissertation Advisor: Dr. David Knipe Joseph Michael Cabral

ATRX Mediated Restriction of Herpes Simplex Virus 1

Abstract

A key regulator of gene expression and chromosome stability during development, replication, and genome maintenance, ATRX also restricts invading DNA viruses. We undertook a series of experiments to investigate the mechanisms by which ATRX affects viral gene regulation, formation of viral heterochromatin, and restriction of DNA virus replication using herpes simplex virus (HSV).

We used herpes simplex virus to investigate the role of ATRX in gene silencing and *de novo* heterochromatin formation on repeat rich, nucleosome-free DNA *in vivo*. Viruses with bioorthogonally labeled genomes were used to detect colocalization of HSV DNA with PML, IFI16, ATRX at PML-nuclear bodies within minutes of infection. ATRX depletion by siRNA and CRISPR-Cas9 mediated knockout resulted in elevated mRNA accumulation, early viral DNA synthesis, and unexpectedly revealed that ATRX was not required for initial histone deposition or modification to HSV DNA. Rather, ATRX was required for heterochromatin maintenance on input viral DNA during times of chromatin stress.

We next investigated the roles other H3 chaperones play in restriction of HSV. Using siRNAs to systematically deplete human fibroblasts of nuclear H3 chaperones, we found that the ATRX/DAXX complex is unique among nuclear H3

chaperones in its capacity to restrict HSV infection and that H3 deposition to HSV DNA occurs in a highly redundant manner. ChIP-seq for total H3 showed that the entire HSV genome was loaded with high levels of H3, but HSV in ATRX-KO cells exhibited reduced H3 accumulation. Furthermore, ATAC-seq analysis revealed that HSV DNA was not largely organized into full nucleosomes during lytic infection, and ATRX-KO globally increases viral DNA accessibility and a delayed progression of infection. Together, these findings support a model in which the unique restrictive activity of ATRX is mediated through enhanced chromatin stability, reduced viral gene accessibility, and delayed viral kinetics during lytic HSV infection.

Table of Contents

Chapter One: Introduction

1.1 Herpesvirus Classification

1.1.1 The Family *Herpesviridae*

Herpesvirales is a large order of enveloped double-stranded DNA (dsDNA) viruses that share common morphological features. The linear dsDNA genomes of these viruses range in size from 125-290 kilo base pairs (kbp) and are contained within an icosahedral capsid embedded in an amorphous proteinaceous matrix, known as the tegument (Davison et al., 2009). The capsid and tegument are surrounded by a lipid bilayer envelope decorated with viral glycoproteins. Members of *Herpesvirales* utilize a wide range of animals as host species, including reptiles, fish, bivalves, birds, and mammals. Of particular interest are members of family *Herpesviridae*, often referred to simply as herpesviruses, that infect rodents, sea turtles, chickens, monkeys, and, importantly, humans.

Mammalian herpesviruses are divided into three subfamilies (*Alphaherpesvirinae, Betaherpesvirinae, and Gammaherpesvirinae)* that share 43 core genes facilitating essential functions such as DNA replication, packaging of viral DNA into capsids, capsid structure and formation (Davison et al., 2009; Pellett and Roizman, 2013). Herpes viruses also share the capacity to establish both lytic and latent infection of host cells. While both modes of infection occur in the host cell nucleus, lytic infection is typically highly productive and results in the death of the host cell. In contrast, latent infection is characterized by the establishment of a

life-long quiescent infection that displays little to no viral replication except upon rare stress-induced episodes of reactivation.

1.1.2 *Herpesviridae* Subfamilies

Viruses of the *Alphaherpesvirinae* subfamily can infect a wide range of host organisms and cell types, but they typically undergo efficient productive infection in epithelial cells, resulting in the rapid accumulation of progeny virions and host cell death. These pathogens can also establish a life-long latent infection in the sensory ganglia of host organisms in which little viral gene expression or DNA replication can be detected. Notable members of this subfamily include well known human pathogens herpes simplex virus 1 and 2 (HSV-1 and HSV-2), which typically cause oral and genital lesions, respectively, and varicella zoster virus (VZV) which is the etiological agent of chicken pox and shingles.

Lytic infections of epithelial cells by viruses of *Betaherpesvirinae*, typified by human cytomegalovirus (HCMV), produce progeny virions more slowly than alpha-herpesviruses. These viruses tend to establish latency in lymphocytes rather than sensory ganglia. While most beta-herpesvirus infections go unnoticed by the host organism, HCMV can lead to severe disease in immunocompromised individuals, and vertical transmission of HCMV from-mother-to-child can results in congenital abnormalities.

Unlike alpha-herpesviruses and beta-herpesviruses, members of *Gammaherpesvirinae* are restricted to replication in lymphoid cells or monocytic

cells. Epstein-Barr virus (EBV) is the etiological agent responsible for mononucleosis and is associated with the development of Burkitt's lymphoma. Infection by another gamma-herpesvirus, Kaposi's sarcoma-associated herpesvirus (KSHV), can result in Kaposi's sarcoma in immunocompromised individuals, particularly those with human immune deficiency virus (HIV) derived acquired immunodeficiency syndrome (AIDS).

1.2 Herpes Simplex Viruses

1.2.1 HSV Epidemiology

Herpes simplex virus (HSV) is one of the most ubiquitous human pathogens. Underlying the success of HSV is its ability to establish a lifelong latent infection in sensory ganglia following primary infection of epithelial cells at mucosal surfaces. The establishment of latency followed by periodic reactivation affords HSV a decades-long vehicle through which to disseminate to naïve hosts. In the United States, the seroprevalence of HSV-1 and HSV-2 are 48.1% and 12.1%, respectively. By age 49, 59.7% of Americans are HSV-1 positive (McQuillan et al., 2018). The global prevalence of HSV-1 and HSV-2 in 2012 was reported to be 67% and 11.3% of the total world population, respectively (Looker et al., 2019a; Looker et al., 2019b). While the prevalence of HSV-2 spikes in sexually active age groups (>20 years of age), most individuals become seropositive for HSV-1

between 5-9 years of age. By age 49, 79% of the global population tests seropositive for HSV-1 (Looker et al., 2019a). But the global burden of HSV is asymmetrically distributed with the highest rates of HSV found in Africa where the prevalence of HIV is extremely high. This overlap is a public health concern as HIV rates of acquisition are three times higher in HSV seropositive individuals (Freeman et al., 2006; Looker et al., 2017).

Humans are the sole natural host for HSV, and transmission occurs during close personal contact between a naïve individual and an individual who is shedding virus. HSV-1 has traditionally been associated with oral lesions, commonly referred to as fever blisters or cold sores. However, an increasing number of genital herpes cases are directly attributable to infection by HSV-1 (Roizman et al., 2013). In rare cases, HSV infection can lead to severe and even life-threatening disease states. Despite a seroprevalence of 20-30% in pregnant women, infection of the neonate occurs in only 1 in 3200 births (Pinninti and Kimberlin, 2013). Although rare, neonatal HSV infection can result in encephalitis, respiratory failure, seizures, and is accompanied by a high mortality rate. Neonatal HSV infection of the central nervous system (CNS) is often followed by subsequent developmental deficiencies.

1.2.2 Organization of the HSV Genome

Despite diverging nearly 8 million years ago, HSV-1 and HSV-2 have an overall identity of 83% (Dolan et al., 1998; Kosakovsky Pond et al., 2014). The HSV

genome largely exists as a linear, nucleosome-free dsDNA strand while inside the viral capsid. The HSV-1 genome is approximately 152 kbp with a high G+C content of 68% while the HSV-2 genome is approximately 154 kbp with 70% G+C content (Roizman et al., 2013). The HSV genome is organized into two major domains, Long (L) and Short (S). Each of these domains consists of a region of unique sequence, the unique long (U_L) and unique short (U_S) regions, which are bracketed by inverted repeat regions repeat long (R_L) and repeat short (R_S), respectively (Wadsworth et al., 1975). The L and S regions are covalently joined at the junction of the internal R_L and R_S features. Most HSV genes exist as single copy genes. However, several genes, such as infected cell protein 0 (ICP0), infected cell protein 4 (ICP4), and latency associated transcript (LAT) are encoded in repeat regions, thus genomes maintain two copies of these genes. Upon release from the capsid into the nucleus, the terminal R_L and R_S regions of the HSV genome are joined to form a circular DNA template for transcription and replication (Garber et al., 1993; Jongeneel and Bachenheimer, 1981; Strang and Stow, 2005).

1.2.3 Viral Entry

Entry of HSV into cells occurs through a fusion of the viral envelope with the host cell plasma membrane or through an endocytosis mechanism. This process is mediated by viral glycoproteins that decorate the envelope of the virion and may occur through two distinct pathways. Heparan sulfate, found on the surface of the

human host cell, acts as an attachment factor for the HSV virion through an interaction with viral glycoproteins gB and/or gC. Once attached, another viral glycoprotein, gD, can interact with one of the three known HSV receptors: Nectin-1, the herpesvirus entry mediator (HVEM), or 3-O-sulfated heparan sulfate (Roizman et al., 2013). These interactions are thought to cause changes in gH and gL that leads to the activation of gB which then triggers fusion of the viral envelope with the plasma membrane. HSV can then enter by either direct membrane fusion or through an endocytosis or phagocytosis-like pathway [reviewed in (Roizman et al., 2013)].

When the viral envelope fuses with the host cell membrane or a vesicular membrane, the contents of the virion are released into the interior of the cell. Proteins that make up the proteinaceous tegument layer surrounding the capsid are released into the cytoplasm after de-envelopment; although, some remain with the capsid. Some tegument proteins, such as virion protein 16 (VP16), re-localize to the nucleus to aid in viral gene expression. Others remain in the cytoplasm to affect other functions, such as the virion host shutoff protein (VHS) which degrades host messenger RNA (mRNA) (Roizman et al., 2013). The HSV capsid is trafficked from the site of de-envelopment to the nuclear pore via retrograde transport along microtubules as mediated by interaction with dynein motor proteins (Dohner et al., 2002). Once the capsid reaches a nuclear pore, it releases its viral dsDNA payload into the nucleus.

1.2.4 Lytic Infection

Upon entry and circularization, the HSV-1 genome is rapidly chromatinized by host-cell machinery (Cliffe and Knipe, 2008; Lee et al., 2016; Oh and Fraser, 2008), and begins a well-regulated cascade of viral gene expression (Honess and Roizman, 1974) of more than 80 viral gene products. The immediate-early (IE) genes are the first to be expressed. The products of these genes drive the expression of early (E) genes of which many are involved in driving the process of viral DNA replication. Late (L) gene expression follows viral DNA replication and results in gene products required for the assembly of progeny virions.

To facilitate viral gene transcription and DNA replication, the virus commandeers cellular macromolecular synthesis machinery while concurrently shutting down host cell gene expression. The HSV tegument protein VP16 localizes to the nucleus upon release from the virion. Once in the nucleus, VP16 enhances the expression of IE genes through the formation of an activator complex with host cell factors Oct1 (POU2F1) and HCF-1 (Stern et al., 1989; Wilson et al., 1993). The Oct1 component of the VP16-Oct1-HCF-1 complex then binds to an IE gene promoter response element, TAATGAGAT, to recruit additional host factors that enhance the transcription of IE genes (Ace et al., 1989). Two of the six IE genes, *ICP4* and *ICP27*, are essential for viral gene expression and replication. ICP4 acts as a required regulator of viral gene expression through interaction with TFIIB and either the TATA-binding protein (TBP) or TFIID (Smith et al., 1993). ICP27 is a multifunctional regulatory protein. In conjunction with VHS, ICP27 aids in

coordinating host cell shut off through inhibition of pre-mRNA splicing (Hardwicke and Sandri-Goldin, 1994; Phelan et al., 1993) and export of spliced transcripts (Sandri-Goldin, 1998). ICP27 also the binds to the C-terminal domain of RNA polymerase II (POLII) (Zhou and Knipe, 2002), recruits it to the viral genome (Dai-Ju et al., 2006) and stimulates the expression of viral genes. The remaining four IE gene products, ICP0, ICP22, ICP47, and $U_S1.5$, are not strictly required, but enhance the efficiency of E gene expression and the viral infection [reviewed in (Roizman et al., 2013)].

Viral E gene expression is driven by the products of IE genes. Proteins encoded by E genes, such as the single-stranded DNA binding protein (ICP8), subunits of the primase-helicase complex, and the viral DNA polymerase, are required for successful HSV genome synthesis by rolling circle replication (Jongeneel and Bachenheimer, 1981; Skaliter et al., 1996; Strang and Stow, 2005). HSV L genes are efficiently transcribed after the onset of viral DNA synthesis and encode for proteins essential for viral genome packaging, virion assembly, and egress. The rolling circle replication of HSV yields concatemerized genomes that are later cleaved during the process of virion assembly and are subsequently packaged into pre-formed capsids.

There are multiple models by which virion egress might occur. A prominent model suggests that the virion is enveloped as it buds into the peri-nuclear space through the inner nuclear membrane and subsequently de-enveloped as it buds from the outer nuclear membrane into the cytoplasm. The model then describes a process by which the virion re-acquires an envelope by passage through the Golgi apparatus before its subsequent release from the plasma membrane [reviewed in (Roizman et al., 2013)].

1.2.5 Latent Infection

Following primary lytic infection, HSV can spread into sensory neurons at axonal termini. Upon entry, the nucleocapsid is trafficked from the site of entry along microtubules in the axon via retrograde transport to the nucleus located in the cell body (Bearer et al., 2000). In the nuclei of infected neurons, HSV DNA persists in a quiescent episomal state with no detectable viral replication. Several factors are thought to contribute to the establishment to neuron specific latency. One factor may be the inefficient transport of VP16 from the site of entry to the nucleus of the neuron (Roizman et al., 2013). A neuron-specific host miRNA, miR-138, was recently reported to restrict expression of ICP0 and promote latency (Pan et al., 2014). Additionally, the viral long non-coding RNA, LAT, promotes the repression of IE gene expression (Wang et al., 2005).

Viral lytic gene expression is repressed during latency; however, LAT is expressed at high levels from a neuron-specific promoter (Zwaagstra et al., 1990). During the establishment of latency, expression of LAT promotes the accumulation of repressive heterochromatin on the HSV genome (Cliffe et al., 2009; Wang et al., 2005). Numerous viral microRNAs are also expressed during latency and are thought to contribute to viral gene repression but may also regulate host cell factors. Latent virus can be reactivated upon stimulation of the host cell by external stress such as injury, exposure to UV radiation, and even emotional stress. During reactivation, a wave of lytic gene expression is followed by productive reactivation and the production of infectious virus (Cliffe et al., 2015).

The nascent virions then travel via anterograde transport down the axon to the site of original infection where the virus may cause a recurring infection and result in shedding of infectious virus.

1.3 Cellular Innate and Intrinsic Resistance to DNA Virus Infection

1.3.1 Innate Immune Sensors of DNA Virus Infection

The sensing of pathogen-associated molecular patterns (PAMPs) by cellular pattern recognition receptors (PRRs) is a critical cellular function that enables detection of invading pathogens. By detecting PAMPs, cells can trigger signaling pathways that result in the transcription and production of antimicrobial factors such as type I interferons (IFNα and IFNβ) that can be secreted from the infected cell to alert nearby cells to the presence of pathogen and trigger an anti-viral state [reviewed in (Thompson et al., 2011)]. HSV may be detected by numerous PRRs that recognize different cognate ligands such as DNA, RNA, or protein. Toll-like receptors (TLRs) are a family of membrane-spanning PRR proteins that are involved in detecting a variety of PAMPs at different cellular locations and ports of cellular entry. TLR2 is found on the outer plasma membrane of cells and has been shown to recognize viral glycoproteins upon attachment to the cell surface and activate innate immune signaling (Leoni et al., 2012).

HSV DNA has several features that are recognized by host-cell DNA sensors. TLR3 and TLR9 are localized to endosomal compartments and recognize the dsDNA and unmethylated CpG features of HSV genomes, respectively (Lund et al., 2003; Zhang et al., 2007). Interferon γ-inducible protein 16 (IFI16) is a nuclear DNA sensor that has been shown to induce activation of interferon regulatory factor 3 (IRF3) and drive the production of IFNβ during HSV infection (Orzalli et al., 2012). Cytosolic DNA sensor cGMP-AMP synthase (cGAS) and IFI16 were both shown to be required for *IFNβ* induction in human foreskin fibroblasts (HFFs) with cGAS contributing to IFI16 stabilization (Orzalli et al., 2015). Not all cells express the same PRRs, thus viral DNA sensing and the subsequent innate immune response may function in a cell type-dependent manner and contribute to the restrictive or permissive nature different cells exhibit to HSV infection.

1.3.2 Cellular Intrinsic Resistance to HSV Infection

The innate responses to viral infection induce *de novo* production of effector molecules, a process that takes time and, at least in part, is designed to limit the spread of a pathogen to neighboring cells. However, cells also constitutively express proteins that can act directly to restrict invading pathogens should infection occur. This intrinsic antiviral resistance is the front-line defense against invading viruses (Bieniasz, 2004). Intrinsic effector proteins may be different for each virus depending on factors such as genetic material (DNA versus RNA) and location of viral replication (cytoplasm versus nucleus).

DNA damage response proteins play a complicated role in the HSV lifecycle and can act to both inhibit and enhance viral replication (Lilley et al., 2005; Lilley et al., 2011; Taylor and Knipe, 2004; Wilkinson and Weller, 2006). Cellular ubiquitin ligases RNF8 and RNF168 were shown to affect the localization of DNA damage response proteins to sites adjacent to HSV DNA and promyelocytic leukemia nuclear bodies (PML-NBs). Loss of either of these proteins resulted in resulted in elevated levels of IE gene mRNA (Lilley et al., 2011) suggesting that the re-localization of DNA damage proteins in response to viral infection acts to restrict efficient viral gene expression.

PML-NBs have been implicated in a range of cellular activities such as DNA-damage response, DNA repair, transcriptional regulation, telomere homeostasis, p53-associated apoptosis, and intrinsic resistance to DNA virus infection [reviewed in (Chang et al., 2018)]. Promyelocytic leukemia protein (PML) protein acts as a scaffold for the formation of the nuclear bodies. PML-NBs can vary in size and composition which may be context specific. PML-NB assembly is a dynamic process that is, in part, governed by PML isoform composition and SUMOylation state (Brand et al., 2010; Weidtkamp-Peters et al., 2008). Individual components of PML-NBs, such as PML, SP100, α-thalassemia X-linked intellectual disability (ATRX), and death domain associated protein (DAXX), have been shown to localize at PML-NBs associated with sites of HSV DNA and contribute to intrinsic antiviral immunity against HSV infection (Alandijany et al., 2018; Everett et al., 2008; Everett et al., 2006; Jurak et al., 2012; Lukashchuk and

Everett, 2010). The mechanisms of each of these proteins are still under investigation, but recent studies, including the work presented here, suggest restriction may be mediated through epigenetic regulation of viral DNA (Albright and Kalejta, 2016; Merkl et al., 2018; Saffert and Kalejta, 2006; Shalginskikh et al., 2013).

1.3.3 HSV-1 Infected Cell Protein 0: Viral Countermeasure

RNF8, RNF168 and the PML-NB proteins act as intrinsic anti-viral defenses against invading HSV. But they also have something else in common: their degradation is promoted by the HSV-1 E3 ubiquitin ligase, ICP0. ICP0 is an immediate early gene product expressed from two gene copies, one located in each of the R_L features of the HSV genome L segment. The protein exhibits E3 ubiquitin ligase activity from its C_3HC_4 really interesting new gene (RING) finger domain (Boutell et al., 2002). ICP0 uses this activity to dismantle host intrinsic and innate immune machinery by promoting the proteasome-dependent degradation of host cell restriction factors.

ICP0 uses its E3 ubiquitin ligase activity to drive a rapid proteasome-dependent degradation of PML during HSV-1 infection. ICP0 has two mechanisms for degrading PML isoforms – one SUMO-dependent and one SUMO-independent (for PML.I) (Boutell et al., 2011; Cuchet-Lourenço et al., 2012). ICP0 recruits cellular E2 ubiquitin conjugation enzymes UbcH5a and UbcH6 to facilitate the degradation of PML and SP100 during the early stages of lytic infection (Boutell et

al., 2002; Gu and Roizman, 2003). Loss of these proteins can be observed as early as 2 to 3 hours post infection (hpi) (Chelbi-Alix and de The, 1999). Likewise, degradation of RNF8 and RNF168 occurs between 2 and 4 hpi (Lilley et al., 2010). ICP0-promoted degradation of IFI16 is proteasome dependent and can be observed by 4 hpi (Orzalli et al., 2012), but the short 2 hour half-life of IFI16 makes it difficult to determine if the loss of protein is a direct or indirect effect of ICP0 (Orzalli et al., 2015). In contrast, ATRX degradation during HSV infection is ICP0 and proteasome dependent, but loss of ATRX is not observed until somewhere between 4-8 hpi (Jurak et al., 2012). While it cannot be ruled out that degradation of ATRX is the result of direct ICP0 targeting, the relatively late loss of ATRX suggests that its degradation may be an indirect effect, possibly a consequence of PML-NB destabilization and displacement of ATRX from PML-NBs. Additionally, both HSV-1 and HSV-2 encode microRNAs (miRNAs) that target ATRX and can decrease endogenous levels of the protein (Jurak et al., 2012). From these examples, it is clear HSV has evolved ICP0 and other countermeasures to effectively disable host cell intrinsic and innate resistance.

1.4 Epigenetic Regulation of HSV Gene Expression

1.4.1 Viral Chromatin During Lytic Infection

The double-stranded DNA genome of HSV is not associated with nucleosomes in the viral particle (Oh and Fraser, 2008; Pignatti and Cassai, 1980). Rather, the HSV virion contains spermine and spermidine which are thought to neutralize up

to 40% of the negative charge in the DNA to enable DNA compaction and packaging (Gibson and Roizman, 1971). Because viral dsDNA is naked as it enters the nucleus, it acts as a potent substrate for nucleosome or nucleosome-like structure formation (Cereghini and Yaniv, 1984). Upon entry into the nucleus, the HSV genome is rapidly associated with histone H3 and silencing histone modifications, histone 3 lysine 9 trimethylation (H3K9me3) and histone 3 lysine 27 trimethylation (H3K27me3), in as little as 1-2 hpi (Cliffe and Knipe, 2008; Lee et al., 2016; Oh and Fraser, 2008). The rapid formation of restrictive heterochromatin likely reflects a cellular defense mechanism that leverages existing host cell infrastructure and epigenetic factors to silence foreign DNA that penetrates the nucleus (Lilley et al., 2011).

Despite the rapid association of chromatin with viral DNA, studies investigating nucleosome occupancy and DNA protection from nuclease digestion suggest that nucleosomes do not occupy viral genome with the same ordered regularity observed on cellular chromatin. Early nuclease digestion assays of HSV DNA during lytic infection found that only a small fraction of viral DNA yielded fragment sizes consistent with nucleosome occupation (Leinbach and Summers, 1980; Muggeridge and Fraser, 1986). Another study suggested that while nucleosome-like structures associate with viral DNA, they do not do so in a regular repeating structure (Kent et al., 2004). A more recent study suggested that nucleosome-like structures associate only loosely with HSV genomes and observed that the susceptibility of viral DNA to nuclease digestion changed during

the course of infection (Lacasse and Schang, 2010). It is important to note, however, that none of the nuclease digestion studies were performed in normal human cell lines. The same is true for studies that identified histone H3-variant H3.3 chaperones HIRA (Placek et al., 2009) and ASF1A (Oh et al., 2012) as factors that both promote H3 occupation on viral DNA and promote viral growth. Both studies were conducted in HeLa cells. Aberrant cellular growth, ploidy, gene copy number, and number of translocations observed in transformed cell lines are likely the result of underlying changes in the activity of chromatin remodelers involved in replication, gene regulation, and chromatin stability. While this does not invalidate the observations made during these studies, the above factors should be considered when interpreting the resulting data.

In the presence of ICP0, viral chromatin is short lived. ICP0 promotes the stepwise removal of the newly deposited heterochromatin from viral promoters (Cliffe and Knipe, 2008; Lee et al., 2016). Levels of H3 and histone modifications H3K9me3 and H3K27me3 were similar between ICP0^{+} and ICP0^{-} for the first two hours of infection. ICP0^{+} viruses then promoted the removal of H3 from viral DNA followed by removal of H3K9me3 and H3K27me3. In contrast, ICP0^{-} viruses were unable to remove viral heterochromatin which persisted for up to 12 hpi (Lee et al., 2016). Similarly, viral transcription activator ICP4 was shown to be required for increased histone dynamics during lytic infection, a process the authors suggest is through the disruption of nucleosome stability (Gibeault et al., 2016). The rapid loading of chromatin on viral DNA and the dynamic changes to viral chromatin

during lytic infection likely represent the push and pull between the efforts of the cells to epigenetically silence the invading pathogen and the viral countermeasures that seek to reverse restriction.

1.4.2 Viral Chromatin During Latent Infection

Latent HSV infection is typified by low levels of HSV lytic transcripts. Unlike lytic infection, nuclease digestion of latent HSV genomes reveals that they are arranged in regular arrays with banding patterns typical of nucleosomal cellular chromatin (Deshmane and Fraser, 1989). In the absence of robust gene expression, viral lytic gene promoters are enriched for H3K9me3 and H3K27me3 modified H3 (Cliffe et al., 2009; Wang et al., 2005). The particular abundance of the facultative heterochromatin modification, H3K27me3, has been suggested to contribute to a state of poised latency which aids reactivation of HSV transcription (Cliffe et al., 2009; Lee et al., 2018b). Poised latency allows the virus to evade cellular immune detection while remaining ready to reactivate given the proper stimulus.

1.5 ATRX Mediated Restriction of Viral Infection

1.5.1 Histone H3 Chaperones and DNA Viruses

The kinetics and composition of viral chromatin have been well-studied in both lytic and latent HSV infections. However, studies describing the mechanisms by which viral heterochromatin forms and which chromatin factors are involved have been less definitive. As described above, a study investigating the role of HIRA in the formation of HSV-associated chromatin expressed tagged H3.3 or H3.1 in HeLa cells and performed chromatin immunoprecipitation experiments (ChIP). Tagged H3.3 was observed to be the dominant form of H3 associated with the coding region of several HSV genes, and HIRA was found to contribute to H3.3 deposition before the onset of replication (Placek et al., 2009). After replication, tagged H3.1 became the dominant H3 form associated with the viral genes. Counterintuitively, it was also observed that depletion of HIRA negatively affected viral gene expression and DNA replication, suggesting that HIRA acts in a manner that promoted viral growth. Likewise, ASF1A was shown to promote H3 incorporation on the viral genome and both ASF1A and ASF1B were shown to support viral growth (Oh et al., 2012; Peng et al., 2010). As discussed above, it is important to note that these studies were conducted in HeLa and African green monkey cells and not in normal human cells. It also interesting to note that HIRA was detected at HSV replication forks in MRC5 (diploid human fetal lung fibroblasts) cells (Dembowski et al., 2017), but ASF1A and ASF1B were not

detected at viral replication forks, with input, nor with nascent viral DNA in MRC5 cells during targeted mass spectrometry studies (Dembowski and DeLuca, 2018; Dembowski et al., 2017). These studies also identified components of the transcription-coupled FACT H3 chaperone complex as interacting with input viral genomes from 2 hpi. But as with HIRA and ASF1A/B, the FACT complex has been suggested to facilitate HSV gene expression rather than restrict it (Fox et al., 2017).

Another H3 chaperone, DEK, was detected as interacting with input HSV DNA from 2 hpi, with viral replication forks, and with nascently replicated HSV DNA (Dembowski and DeLuca, 2018; Dembowski et al., 2017). DEK has been reported to interact with DAXX (Hollenbach et al., 2002) and influence the trafficking of H3.3 between HIRA, DAXX, ATRX, and PML-NBs (Ivanauskiene et al., 2014). The effects of DEK on viral chromatin and gene expression are not currently known. ATRX and DAXX form a H3.3-specific chaperone complex that has been implicated in numerous chromatin remodeling activities discussed in greater detail below. Importantly, ATRX and DAXX are constitutive components of PML-NBs and have been shown to restrict a diverse range of DNA viruses and promote H3 occupation on HCMV and EBV genomes at late times post-infection (Albright and Kalejta, 2016; Lukashchuk and Everett, 2010; Tsai et al., 2014). A recent study has suggested HIRA and ATRX/DAXX may perform redundant roles in promoting histone occupation on quiescent HSV genomes (Cohen et al., 2018).

Interestingly, the ATRX/DAXX complex has been the only H3 chaperone complex that has been shown consistently to restrict DNA virus infection.

1.5.2 Role of ATRX in Heterochromatin Maintenance

The SWI/SNF chromatin remodeler α-thalassemia X-linked intellectual disability (ATRX) has recently gained attention as a crucial epigenetic regulator of eukaryotic gene expression and steward of silenced heterochromatin. ATRX is highly conserved and shares an ancestral core with both fish and plants (Park et al., 2004). *ATRX* is a large gene with 38 exons spanning 281 kbp of the X chromosome. The ATRX protein has two major isoforms: a full length ~280-kD protein and a ~180-kD truncated protein (Garrick et al., 2004). The ATRX protein has several protein-protein interaction domains and two functional domains. The N-terminal ADD domain displays homology to DNMT3 family of DNA methytransferases, and it is comprised of a zinc finger domain, a plant homeodomain (PHD), and an alpha-helical region. The C-terminal domain contains a SNF2 ATPase/helicase domain (Bérubé, 2011). Mutations of the *ATRX* gene in coding regions for either the ADD domain or the ATPase/helicase domain can result in a serious developmental disorder, α-thalassemia X-linked intellectual disability (ATR-X) syndrome (Berube et al., 2000; Gibbons et al., 2003). Mutations in the functional domains of ATRX have also been observed in 15 human cancer types (Koschmann et al., 2016), including gliomas in which 31% of pediatric glioma samples were reported to harbor *ATRX* mutations (Schwartzentruber et al.,

2012). Therefore, deciphering the many functions of ATRX in epigenetic regulation of chromatin and its implications in human disease is of great importance.

ATRX and DAXX form an H3.3-specific chaperone complex that promotes H3.3 deposition into repeat-rich regions of heterochromatin (Drane et al., 2010; Goldberg et al., 2010; Lewis et al., 2010). This complex has been identified as crucial for H3.3 incorporation at pericentromeric repeats and telomeres (Drane et al., 2010; Lovejoy et al., 2012; McDowell et al., 1999). Accordingly, loss of ATRX leads to reduced H3.3 levels at pericentric heterochromatin and telomeres, telomere instability, and contributes to activation of the alternative lengthening of telomeres (ALT) pathway (Lewis et al., 2010; Lovejoy et al., 2012). More recently, ATRX has been implicated in promoting H3.3 and repressive H3K9me3 modification mediated silencing of endogenous retroviruses, imprinted alleles, and hypomethylated tandem repeat sequences during development (Elsasser et al., 2015; He et al., 2015; Voon et al., 2015). While ATRX and DAXX have been shown to have nucleosome deposition and remodeling activity *in vitro (Drane et al., 2010; Lewis et al., 2010), in vivo* studies have largely investigated the effects of ATRX or DAXX depletion at elements where chromatin may have previously been established. Reported observations of reduced H3.3 or H3K9me3 could also conceivably be attributed to defective chromatin maintenance rather than *de novo* chromatin formation.

ATRX is known to promote heterochromatin independently from its H3.3 chaperone activity. Interestingly, ATRX itself is a histone tail reader and can

interact directly with histone modification H3K9me3 through its ADD domain and promote heterochromatin spreading (Iwase et al., 2011). Using a H3.3-binding deficient DAXX mutant, histone chaperone activity was shown to be dispensable for ATRX-mediated H3K9me3 modifications to histones at a retrotransposon reporter element (Sadic et al., 2015). This activity was attributed to the interaction of ATRX with a histone methyltransferase (HMT) complex comprised of SETDB1 and KAP1. Adding to the complexities of the relationship between ATRX and heterochromatin, a series of recent studies have implicated several long non-coding RNAs in the regulation of ATRX activity, including targeting the polycomb repressive complex 2 (PRC2) to the X chromosome through interaction with the XIST RNA (Chu et al., 2017; Lee et al., 2018a; Sarma et al., 2014).

1.5.3 Role of ATRX in the DNA Damage Response

ATRX has recently been shown to play critical roles in homologous recombination through interaction with PCNA and RFC1 to facilitate H3.3 loading during DNA repair synthesis (Juhász et al., 2018) and in repairing stalled replication forks in heterochromatin through interaction with the MRN complex (Clynes et al., 2014; Huh et al., 2016; Leung et al., 2013). ATRX has also been reported to inhibit alternative lengthening of telomeres (ALT) through sequestration and inhibition of MRE11 (Clynes et al., 2015). PCNA and MRE11, were reported to occupy HSV replication forks (Dembowski et al., 2017) and localize with input viral genomes by 3hpi (Dembowski and DeLuca, 2018). Additionally, ATRX has been demonstrated

to be important for maintaining genome stability as illustrated by the copy loss of ribosomal DNA (rDNA) in ATRX-knockout murine embryonic stem cells (Udugama et al., 2018).

1.5.4 Restriction of DNA Virus Infections by ATRX/DAXX

The ATRX/DAXX complex has been reported to restrict a diverse range of DNA viruses. While ATRX/DAXX restriction of herpesviruses is perhaps the best studied, many questions remain regarding the mechanisms by which this restriction occurs. Because ATRX/DAXX complex acts as a H3.3 chaperone complex, it is perhaps not surprising that the complex has been shown to promote H3.3 incorporation on HCMV, adenovirus (AdV), and EBV genomes at 18, 24, and 72 hpi, respectively (Albright and Kalejta, 2016; Schreiner et al., 2013; Tsai et al., 2014). However, the role ATRX plays in *de novo* viral chromatin formation upon viral nuclear entry is currently unknown.

Both ATRX and DAXX have been shown to restrict HSV-1 IE gene expression and viral growth (Lukashchuk and Everett, 2010). This study also revealed that deletion of the ATRX-interaction domain of DAXX ablated restriction of HSV-1 infection revealing that DAXX requires the activity of ATRX to restrict HSV-1. The ICP0 degradation of PML disperses the components of PML-NBs including DAXX and ATRX (Everett, 2000; Jurak et al., 2012). Additionally, HSV-1 encodes a microRNA, miR-H1, that has been shown to repress expression of ATRX and may play a role in reactivation from latency (Jurak et al., 2012). Indeed,

the ATRX/DAXX complex has been detected at latent viral genomes in neurons of mice (Catez et al., 2012) and has been suggested to play a role in histone occupation on quiescent HSV genome (Cohen et al., 2018). However, the mechanisms of ATRX-mediated restriction of HSV are not well understood.

Because the ATRX/DAXX complex restricts DNA virus gene expression, many DNA viruses have evolved varied mechanisms to specifically target and manipulate the ATRX/DAXX complex. Much of what is known about the restrictive properties of ATRX and DAXX have been revealed through studies of their interactions with viral proteins that target them. The EBV protein BNRF1 has been shown to bind to DAXX and separate it from the ATRX/DAXX complex (Tsai et al., 2011). Depletion of DAXX or ATRX resulted in reactivation of EBV in lymphoblastoid cells. BNRF1 has also been shown to increase H3.3 mobilization and turnover during FRAP experiments through its interaction with DAXX (Tsai et al., 2014). HCMV tegument protein pp71 has been reported to degrade DAXX and displace ATRX from PML-NBs (Saffert and Kalejta, 2006). Trichostatin A (TSA), alleviated IE gene restriction when DAXX degradation was blocked with a proteasome inhibitor, suggesting that DAXX may restrict HCMV infection through recruitment of an HDAC (Saffert and Kalejta, 2006).

In contrast to its intrinsic immune functions, there is evidence that DAXX may also have functions that benefit some viral infections. Depletion of DAXX in U2OS cells was reported to down-regulate HPV early gene expression and genome replication (Kivipõld et al., 2015). DAXX was previously shown to interact

with ICP27 and possibly ICP4 and ICP8 in the form of a complex (Tang et al., 2003). A recent study verified the interaction between DAXX and ICP27 and reported that the ICP27-DAXX interaction repressed NF-κB activity through altering DAXX SUMOylation (Kim et al., 2017), a function of DAXX that has been previously reported (Park et al., 2007). Further supporting these findings, dengue virus (DENV) capsid protein (DENV C) was reported to disrupt the interaction between DAXX and NF-κB resulting in NF-κB activation of *CD137* transcription and CD137 mediated apoptosis (Netsawang et al., 2014). Unlike DAXX, the activity of ATRX has thus far been shown only to result in restriction of viral infection. This may explain why some DNA viruses have evolved mechanisms to disrupt the ATRX/DAXX complex or target ATRX directly rather than DAXX.

Chapter Two: ATRX Promotes Maintenance of Herpes Simplex Virus Heterochromatin During Chromatin Stress

A version of this chapter has been published:

Cabral, J. M., Oh, H. S. & Knipe, D. M. (2018)

eLife 7, e40228, doi:10.7554/eLife.40228

Abstract

The mechanisms by which mammalian cells recognize and epigenetically restrict viral DNA are not well defined. We used herpes simplex virus with bioorthogonally labeled genomes to detect host factors recruited to viral DNA shortly after its nuclear entry and found that the cellular IFI16, PML, and ATRX proteins colocalized with viral DNA by 15 min post infection. HSV-1 infection of ATRX^{-} depleted fibroblasts resulted in elevated viral mRNA and accelerated viral DNA accumulation. Despite the early association of ATRX with vDNA, we found that initial viral heterochromatin formation is ATRX-independent. However, viral heterochromatin stability required ATRX from 4-8 h post infection. Inhibition of transcription blocked viral chromatin loss in ATRX-knockout cells; thus, ATRX is uniquely required for heterochromatin maintenance during chromatin stress. These results argue that the initial formation and the subsequent maintenance of viral heterochromatin are separable mechanisms, a concept that likely extrapolates to host cell chromatin and viral latency.

Introduction

Recognition and restriction of foreign DNA is ubiquitous to all cells. It is imperative that cells prevent foreign DNA from expressing its genes or integrating into the cellular genome lest foreign gene products disrupt normal cellular function. Bacteria possess restriction endonucleases and CRISPR-Cas9 mechanisms to recognize and cleave foreign DNA (Barrangou et al., 2007; Tock and Dryden, 2005). Eukaryotic cells, however, recognize foreign DNA and redirect existing chromatin machinery to epigenetically silence the DNA by modifying it with repressive heterochromatin. Epigenetic modification of chromatin, such as DNA methylation and covalent modification of histone tails, is critical for regulating gene expression to ensure proper cellular function and expression of regulated genes at only the appropriate times (Kanherkar et al., 2014). Likewise, epigenetic modifications also allow for the effective silencing of foreign DNA that is often associated with invading pathogens, for example DNA viruses. DNA virus genomes are recognized by nuclear DNA sensors, such as interferon-inducible protein 16 (IFI16), and are subject to epigenetic regulation by host cell factors during both lytic and latent infection (Knipe, 2015; Knipe et al.; Orzalli and Knipe, 2014). Nuclear unintegrated retroviral DNAs are also associated with nucleosomes and silencing histone modifications (Wang et al., 2016). Indeed, retroviral genomes are epigenetically silenced even after integration into the host genome (Yao et al., 2004).

Both boon and bane for DNA viruses, viral chromatin enables DNA viruses to establish and maintain persistent latent infections in which the virus is poised for reactivation, but it also impedes productive viral transcription and replication during lytic infection (Knipe et al., 2013). Viruses must overcome host-cell silencing mechanisms for reactivation from latency or for lytic infections to proceed. The double-stranded DNA genome of herpes simplex virus (HSV) is not associated with histones within the virion (Pignatti and Cassai, 1980). However, during lytic infection, nucleosomes are rapidly assembled on the viral DNA upon its entry to nuclei of epithelial or fibroblast cells (Cliffe and Knipe, 2008; Lee et al., 2016; Oh and Fraser, 2008). Newly formed viral chromatin is immediately associated with silencing histone tail modifications, specifically H3 lysine 9 trimethylation (H3K9me3) and histone H3 lysine 27 trimethylation (H3K27me3), that peak in density within 1-2 h post infection (hpi) (Lee et al., 2016). The resulting viral heterochromatin acts as an epigenetic barrier to viral gene expression and replication. Consequently, viral gene expression occurs in the regulated cascade of immediate-early (IE), early (E), and late (L) viral gene products that drive viral transcription, viral DNA synthesis, and virion assembly, respectively (Knipe and Cliffe, 2008). HSV proteins VP16 and ICP0, a viral E3 ubiquitin ligase, promote viral gene expression, and removal of viral heterochromatin (Cliffe and Knipe, 2008; Herrera and Triezenberg, 2004; Lee et al., 2016). However, the cellular machinery that drives formation of viral heterochromatin and epigenetic silencing

of viral gene expression during the early stages of DNA virus infections are still not well described.

The SWI/SNF chromatin remodeler protein, α-thalassemia X-linked intellectual disability (ATRX), has recently gained attention as a crucial epigenetic regulator of eukaryotic gene expression and steward of silenced heterochromatin. ATRX is also known to play a role in restriction of DNA viruses (Lukashchuk and Everett, 2010). ATRX and death domain-associated protein (DAXX) together form a histone chaperone complex specific for the non-canonical histone variant 3.3 (H3.3) (Drane et al., 2010; Lewis et al., 2010). This complex is critical for maintaining repressive heterochromatin at many repeat-rich regions, including telomeres (Lovejoy et al., 2012), pericentric repeats (19), and endogenous retroviruses (Elsasser et al., 2015), and mutations in the ATRX gene are linked to a developmental disorder and several cancer types (18). ATRX and DAXX are also two of the core components of promyelocytic leukemia protein (PML) nuclear bodies (PML-NBs), nuclear punctate structures that have been implicated in a range of cellular activities including the DNA-damage response, transcriptional regulation, and restriction of viral infection (Chang et al., 2018). In this context, ATRX and DAXX have been shown to restrict gene expression from DNA viruses and integrated retrovirus DNA (Lukashchuk and Everett, 2010; Schreiner et al., 2013; Shalginskikh et al., 2013; Tsai et al.; Woodhall et al., 2006). The ATRX/DAXX complex also appears to be important for maintaining DNA virus

latency as depletion of either ATRX or DAXX was reported to induce EBV reactivation from latently infected cells (Tsai et al., 2011).

In response, DNA viruses have evolved numerous strategies for alleviating the effects of host restriction factors and epigenetic silencing. The Epstein-Barr virus (EBV) BNFR1 protein interacts with DAXX to displace ATRX from the complex, effectively reprogramming DAXX and resulting in the activation of early gene transcription (Tsai et al., 2014; Tsai et al., 2011), while degradation of DAXX is promoted by pp71 and E1B-55K during human cytomegalovirus (HCMV), and adenovirus (AdV) infections, respectively (Saffert and Kalejta, 2006; Schreiner et al., 2013). During HSV infection, proteasome-dependent degradation of PML, ATRX, and IFI16 is promoted by ICP0 (Boutell et al., 2003; Chelbi-Alix and de The, 1999; Gu and Roizman, 2009; Jurak et al., 2012; Orzalli et al., 2012). Though ATRX and DAXX have proven to be important host restriction factors, the mechanism of their antiviral activity is less clear.

While ATRX and DAXX have been shown to possess nucleosome deposition and remodeling activity *in vitro* (Drane et al., 2010; Lewis et al., 2010), *in cellulo* studies have largely investigated the effects of ATRX or DAXX depletion at integrated reporter elements or viral genomes during late stage infection, after chromatin had already formed. For instance, DAXX has been reported to promote H3.3 incorporation on HCMV, AdV, and EBV genomes at 18, 24, and 72 hpi, respectively (Albright and Kalejta, 2016; Schreiner et al., 2013; Tsai et al., 2014). While the histone chaperones HIRA and ASF1A have been implicated in the initial

loading of histones onto HSV DNA during the first few hours of infection, these reports also demonstrated that HIRA and ASF1A actually promote productive viral infection (Oh et al., 2012; Placek et al., 2009). Thus, the mechanisms underpinning *de novo* formation of restrictive heterochromatin on viral DNA remain unclear. Lytic HSV infection provides a temporal reference point that can be used to determine the sequential order of events and dissect the function of cellular chromatin remodelers with greater resolution. Therefore, we used HSV to investigate *de novo* viral heterochromatin formation and maintenance in the presence or absence of chromatin remodeler and host restriction factor ATRX.

Here we report on the mechanisms of viral gene restriction mediated by ATRX during the first 8 h of infection. We used HSV with bioorthogonally-tagged genomes to quantitatively track viral entry and host restriction factor recruitment as a function of time. Along with nuclear DNA sensor IFI16, we detected ATRX and PML recruitment to viral DNA by 15 min post infection (mpi), almost immediately upon nuclear entry. Although ATRX restricted the expression of viral mRNA, ATRX had no effect on the initial formation of viral heterochromatin assembly at 2 and 4 hpi. However, ATRX was required for the maintenance of viral heterochromatin between 4-8 hpi during challenges to chromatin stability. Our findings argue for a biphasic model of epigenetic regulation in which *de novo* assembly of heterochromatin on viral genomes is ATRX-independent but that ATRX is required for viral heterochromatin stability during chromatin stress, such as replication and transcription.

Results

HSV genomes colocalize with host restriction factors IFI16, ATRX, and PML upon entry into the nucleus.

To investigate early interactions of HSV genomes with host proteins that could potentially initiate chromatinization of viral DNA, we generated nucleoside analog-labeled HSV-1 preparations that could be used for the detection of input viral DNA in infected cells. First, we prepared labeled HSV (HSV-EdC) stocks by infecting confluent human foreskin fibroblasts (HFF) with HSV-1 in the presence of the nucleoside analog 5-ethynyl-2′-deoxycytidine (EdC, 0.5 μM). HSV-EdC DNA could be detected by fluorescence microscopy after a copper-catalyzed bioorthogonal cycloaddition (click chemistry) of biotin to EdC incorporated into viral DNA followed by incubation with a streptavidin-fluorophore probe (Figure 2.1A; Supplemental Figure 2.1B). HSV-EdC genomes were detected as punctate nuclear foci that colocalized with the HSV immediate-early protein ICP4, considered a marker for viral DNA, at 2 h post infection (hpi) (Supplemental Figure 2.2A). We also observed that HSV-EdC viral DNA (vDNA) colocalized with early replication compartments, as defined by immunofluorescence (IF) staining for the viral early protein ICP8 at 4 hpi (Supplemental Figure 2.2B). As recently reported (Sekine et al., 2017), HSV-EdC genomes that colocalized with ICP8 underwent a morphological decompaction that could be prevented by treatment with viral DNA synthesis inhibitor phosphonoacetic acid (PAA, 400 μg/ml) (Supplemental Figure 2.2B). HSV-EdC demonstrated only a slight decrease in ICP8 protein levels at

4hpi but no differences in either ICP4 or ICP8 levels by 8hpi (Supplemental Figure 2.2C). Intracellular HSV-EdC foci were prevented by treatment with heparin (50 μg/mL), which blocks viral attachment and entry to cells (Bender et al., 2005) (Supplemental Figure 2.2D). Labeling of host cell chromatin during infection with EdC-labeled viral preparations was not observed. In total, these results validated the use of EdC labeling of HSV to detect input HSV DNA and showed that the course of infection with HSV-EdC virus was normal.

To determine the kinetics of restrictive host protein recruitment to input viral DNA, we quantitatively mapped the spatiotemporal kinetics of incoming HSV-EdC genome colocalization with host restriction factors IFI16, PML, and ATRX (Figure 2.1A,C-E; Supplemental Figure 2.3A-B). To measure colocalization of viral DNA and restriction factor foci in host cell nuclei, we first defined nuclear fluorescent foci using a software bot (Cicconet et al., 2017) and then used additional customized features of the software to define foci as colocalizing when the centers were within a distance threshold of 5 pixels, ~350nm (see Materials and Methods for detailed description of software). Using this method, we observed click chemistry labeled viral genomes in the nuclei of HFFs as early as 15 mpi (Figure 2.1B). The percentage of infected cells increased steadily over the first 30 min of infection. HSV genomes were stably maintained at 2-3 per infected nucleus from 50 mpi (Supplemental Figure 2.3C). ATRX colocalization with HSV DNA peaked between 40-100 mpi (Figure 2.1E), with 80% of viral DNA colocalizing with ATRX.

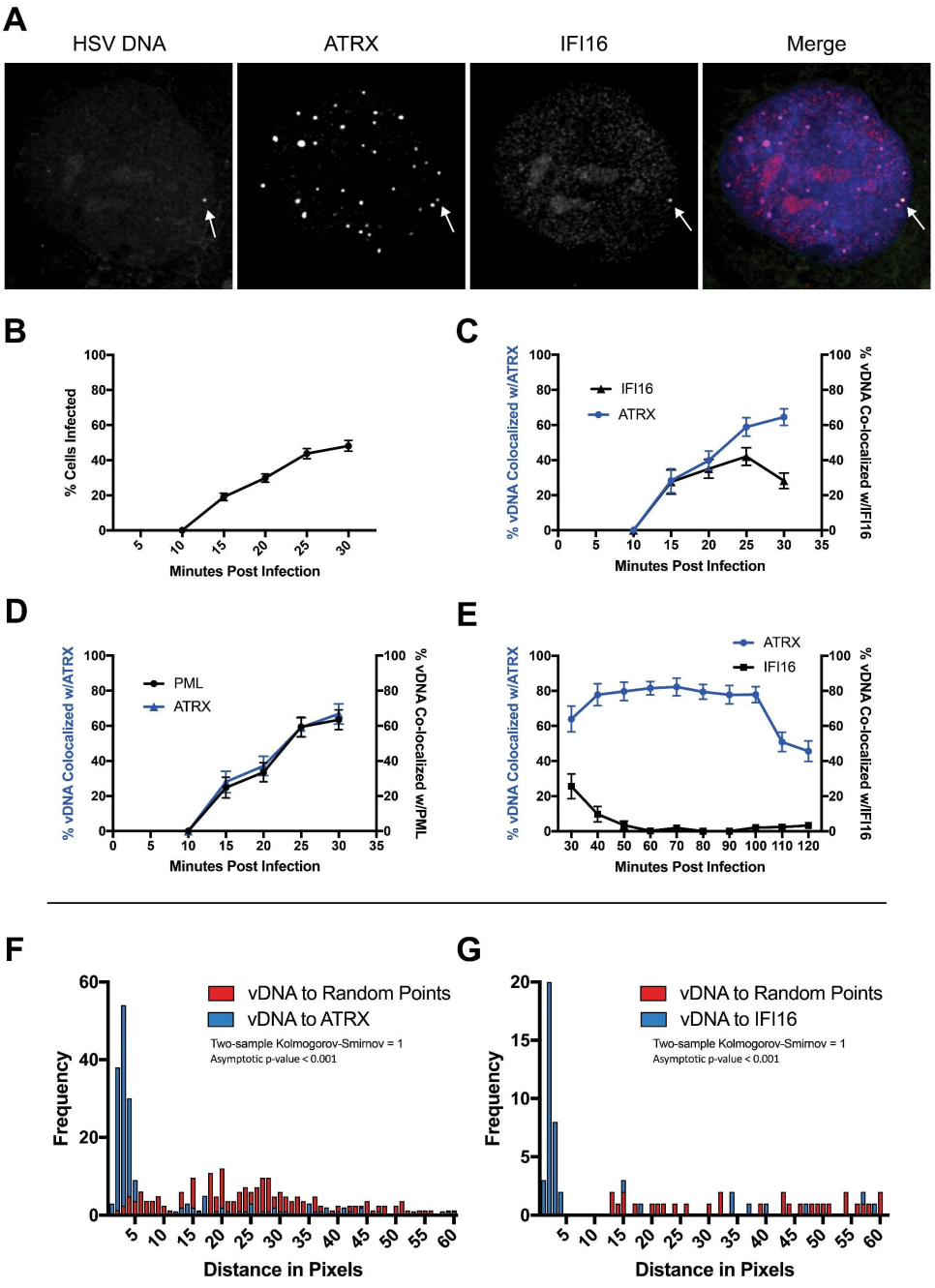

Figure 2.1: HSV genomes colocalize with host restriction factors upon nuclear entry.

HFFs were infected with HSV-EdC at an MOI of 5 and fixed at times post infection as indicated. Host proteins were detected by immunocytochemistry, and HSV genomes were detected with

Figure 2.1 (Continued) click chemistry and a streptavidin-fluorophore probe. (A) Representative confocal image showing colocalization of ATRX and IFI16 with vDNA as indicated by the white arrows. (B) Percentage of cells with at least 1 HSV-EdC focus within the nucleus as determined by foci detection software. $n \geq 270$ total cell population per time point from 15-30 mpi derived from 3 independent experiments. Percentage of vDNA foci colocalized with (C) ATRX (blue) or IFI16 (black) and (D) ATRX (blue) or PML (black) from 15-30 mpi in 5 min intervals as determined by foci detection and colocalization software (see Materials and Methods). $n \geq 150$ total cell population per time point from 15-30 mpi derived from 3 independent experiments. (E) Percentage of vDNA foci colocalized with ATRX (blue) or IFI16 (black) from 30-120 mpi in 10 min intervals as determined by foci detection and colocalization software. $n \geq 65$ total cell population per time point from 30-120 mpi derived from 3 independent experiments. (F) Frequency distribution of distances from the center of a vDNA focus to the center of the nearest neighbor ATRX focus within a 60 pixel radius of the vDNA focus (blue) vs a distribution of distances from vDNA to randomly generated points within the nucleus equal to the number of ATRX foci (see Figure 1 – figure supplement 1A). Distance values were binned in increments of 1 pixel with the center of the first bin set to 0.5 pixels. Kolmogorov-Smirnov test was used to compare distributions and generate a p value. 0 = same underlying distribution, 1 = d distributions are significantly different (see Materials and Methods). n = 183 vDNA foci. (G) Frequency distribution of distances (as in F) from the center of a vDNA focus to the center of an IFI16 focus vs vDNA to random points. n = 51 vDNA foci. All data are reported $\pm$ standard error of the mean.

We observed IFI16 and ATRX colocalizing with viral DNA at similar frequencies by 15 mpi (Figure 2.1C). IFI16 has been shown to form transient foci at the nuclear periphery in response to HSV infection (Diner et al., 2016; Everett, 2016). The kinetics of IFI16 colocalization with viral DNA supported this hypothesis as our observations revealed an early peak of IFI16-vDNA colocalization (20-30 mpi) that rapidly decreased after 30 mpi (Figure 2.1C,E). Little to no IFI16-vDNA colocalization was observed from 60 mpi (Figure 2.1E). These results indicated that, under our conditions, IFI16 and ATRX localize with HSV genomes almost immediately upon nuclear entry, and while the majority of IFI16 colocalization with input viral DNA occurs between 15 and 30 mpi, ATRX colocalization is stable between 15 and 100 mpi.

PML and ATRX colocalization with viral DNA occurred with nearly identical kinetics (Figure 2.1D). We attempted to analyze the kinetics of DAXX colocalization with HSV DNA. However, several antibodies, while providing a signal for immunoblotting, gave little or no signal in IF experiments. ATRX colocalization with viral DNA began to wane by 100 mpi (Figure 2.1E). The HSV E3 ubiquitin ligase, ICP0, has been shown to promote degradation of both PML and ATRX (Chelbi-Alix and de The, 1999; Jurak et al., 2012). Indeed, we observed that the presence of ATRX foci in infected nuclei generally diminished as the presence of ICP0 increased across the infected population (Supplemental Figure 2.3D). By 90 minutes post infection, ICP0 was observed to localize to ATRX foci that also colocalized with HSV genomes (Supplemental Figure 2.3E). Though the

percentage of infected cells positive for ICP0 did not change between 90 and 120 minutes, the percentage of infected cells positive for ATRX foci decreased by more than half (Supplemental Figure 2.3D). This may reflect a period of time in which ICP0 drives the dissolution of PML-NBs; however, the ICP0 antibody exhibited a high background signal that rendered it difficult to perform precise colocalization studies that would be needed to further define the spatiotemporal relationship between ICP0 and ATRX.

To test whether the colocalization of vDNA with ATRX or IFI16 was due to random events, we compared the distances of vDNA to restriction factors with the distances of random intranuclear points to vDNA. Frequency distribution analysis of pixel distances from HSV-EdC genomes to nearest-neighbor (nn) ATRX foci revealed a non-parametric distribution of distances that had a median distance of 2.83 pixels (~200nm), within the optical resolution of the system (Figure 2.1F). Similarly, vDNA-to-nnIFI16 foci had a mean median distance of 2.24 pixels (~150nm) (Figure 2.1G). We used a custom software script to generate foci at randomly positioned x,y coordinates in numbers equal to the ATRX (or IFI16) foci that fell within a given nucleus (see Materials and Methods for detailed description of software). We then compared the frequency distribution of vDNA-to-nnATRX foci (or vDNA-to-nnIFI16 foci) distances with the distribution of distances of vDNA to randomly generated x,y coordinates (Supplemental Figure 2.1A). The frequency distributions of distances from vDNA-to-nnATRX foci and vDNA-to-nnIFI16 foci versus the distribution of distances from vDNA-to-nnRandom points at

30 mpi were highly significant ($p<0.001$) (Figure 2.1F,G). These results argued that IFI16 and PML-NB proteins localize to viral DNA very early and are candidates for the DNA sensors that initially respond to nuclear entry of viral genomes.

ATRX colocalization with HSV genomes is independent of IFI16 but dependent on the histone chaperone DAXX.

We next investigated if IFI16 affects ATRX colocalization with HSV-EdC genomes or vice versa. We reported that IFI16 and PML recruitment to viral genome complexes are independent (Orzalli et al., 2013), while another study observed only a 10% reduction in cells showing PML recruitment to genome complexes when IFI16 was depleted (Cuchet-Lourenco et al., 2013). We depleted HFFs of IFI16 using small interfering RNAs (siRNAs) against IFI16 (siIFI16) (Figure 2.2A,C). Cells treated with siIFI16 and infected at a multiplicity of infection (MOI) of 5 with HSV-EdC showed no significant reduction in ATRX colocalization with viral genomes at 30mpi (Figure 2.2A,D). Likewise, depletion of ATRX via siRNA (siATRX) did not change the colocalization frequency of IFI16 with labeled HSV genomes (Figure 2.2B,E). Interestingly, treatment with siRNAs reduced the frequency of IFI16 foci formation in both siNon-Targeting (siNT) and siATRX treated HFFs (Figure 2.2E), perhaps due to an innate immune response to transfected siRNA (Whitehead et al., 2011). While ATRX recruitment to viral DNA appears to be independent of IFI16, it has been reported that mutation or

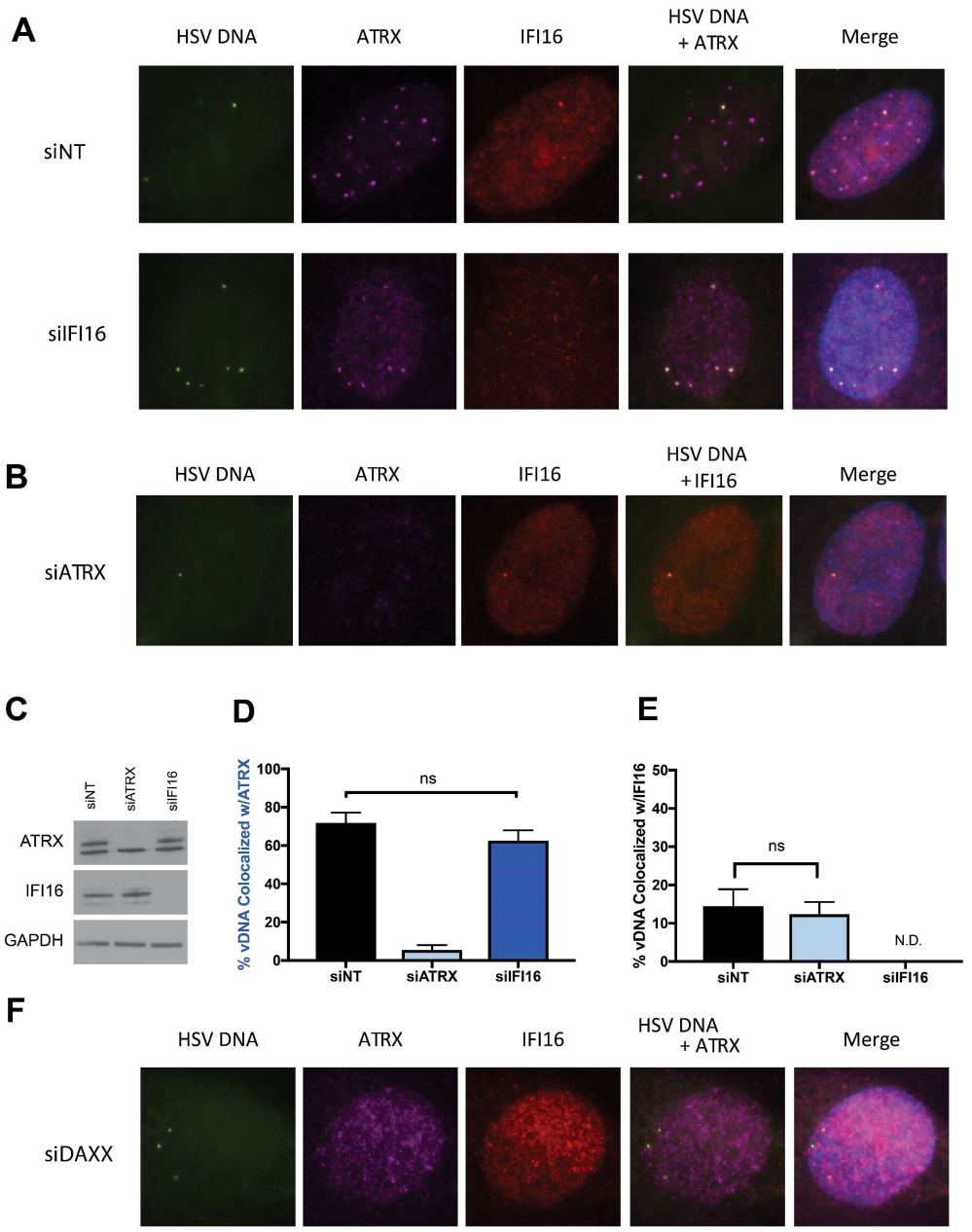

Figure 2.2: ATRX and IFI16 independently localize to viral DNA.

HFFs were treated with siRNAs targeting ATRX (siATRX), IFI16 (siIFI16), DAXX (siDAXX), or non-targeting (siNT). 72 h post siRNA treatment, cells were infected with HSV-EdC at an MOI of 5. (A) Colocalization of ATRX (magenta) and IFI16 (red) with vDNA (green) in HSV-EdC infected HFFs treated with either siNT or siIFI16 at 1 hpi. (B) Colocalization of ATRX and IFI16 with vDNA in

Figure 2.2 (Continued) HSV-EdC infected HFFs treated with siATRX at 30 mpi. (C) Immunoblot detection of ATRX and IFI16 in lysates from HFFs treated with siRNA against either ATRX or IFI16 72 h post treatment. GAPDH was used as a loading control. Percentage of vDNA that colocalizes with (D) ATRX or (E) IFI16 in cells treated with siNT, siATRX, or siIFI16 30 mpi as determined by foci detection and colocalization software. $n \geq 120$ total cell population derived from 2 independent experiments, one-way ANOVA. All data are reported $\pm$ standard error of the mean. (F) Colocalization of ATRX and IFI16 with vDNA in HSV-EdC infected HFFs treated with siDAXX at 30 mpi.

alteration of the ATRX interaction domain of DAXX abolished ATRX localization to PML-NBs and early replication compartments (Lukashchuk and Everett, 2010). Indeed, ATRX colocalization with vDNA and PML-NBs was lost in HFFs depleted for DAXX, resulting in diffuse nuclear ATRX staining (Figure 2.2F, Supplemental Figure 2.4A). These results demonstrated IFI16 is not required for ATRX colocalization to viral DNA, as recently reported for PML and IFI16 (Alandijany et al., 2018), and argued that ATRX and IFI16 are in distinct DNA sensing pathways that simultaneously detect input viral DNA as it enters the nucleus.

ATRX and DAXX act together to restrict HSV gene expression via an IFI16-independent pathway.

We next investigated the functional effects of ATRX on epigenetic silencing of viral DNA. Depletion of ATRX from HepaRG cells was reported to increase viral plaque formation and slightly increase viral early protein UL42 as detected by immunoblotting (Lukashchuk and Everett, 2010). Because ICP0 promotes the dissolution of PML-NBs and the proteasome-mediated degradation of ATRX, we performed the following studies using the HSV-1 7134 virus that is ICP0-null. ATRX colocalized with input viral DNA from 15-100 mpi; therefore, we investigated if ATRX was associating with the viral DNA. We performed chromatin immunoprecipitation followed by quantitative polymerase chain reaction (ChIP-qPCR) on chromatin from HFF cells infected with HSV 7134 virus. We found that ATRX could be detected at viral gene promoters for both *ICP27* and *ICP8* at levels

higher than GAPDH by 1 hpi, and to significantly higher levels by 4 hpi (Figure 2.3A). Detection of ATRX at viral gene promoters suggested that ATRX may play a role in epigenetically regulating viral gene expression by associating with viral DNA.

We next measured viral gene expression in siATRX-treated HFFs infected with HSV 7134. We harvested infected cells at 2-hour intervals from 2-8 hpi and measured viral transcripts by reverse transcription (RT) -qPCR (Figure 2.3B-D). ATRX-depleted HFFs showed significant increases in transcripts from genes of all kinetic classes, with the most significant effects on expression occurring from IE (*ICP27*) and L genes (*gB*) at 6 and 8 hpi (Figure 2.3B,D), while E gene *ICP8* expression was significantly elevated at 8hpi (Figure 2.3C). In parallel with the above experiment, we tested the impact of viral DNA replication on ICP0-null HSV gene expression in HFFs depleted of ATRX. To accomplish this, we treated cells with a viral DNA polymerase inhibitor, PAA (400 μg/ml), from 1 h prior to infection and maintained PAA throughout the experiment. While overall viral gene expression was reduced in the presence of PAA, depletion of ATRX still resulted in significant increases in ICP0-null gene expression from each gene of the three kinetic classes (Figure 2.3B-D). The increased accumulation of viral mRNA upon ATRX depletion argued that ATRX plays a role in preventing transcription from viral genes, and the increase in viral gene expression with and without PAA demonstrated that ATRX restricts gene expression from both input and progeny viral DNA.

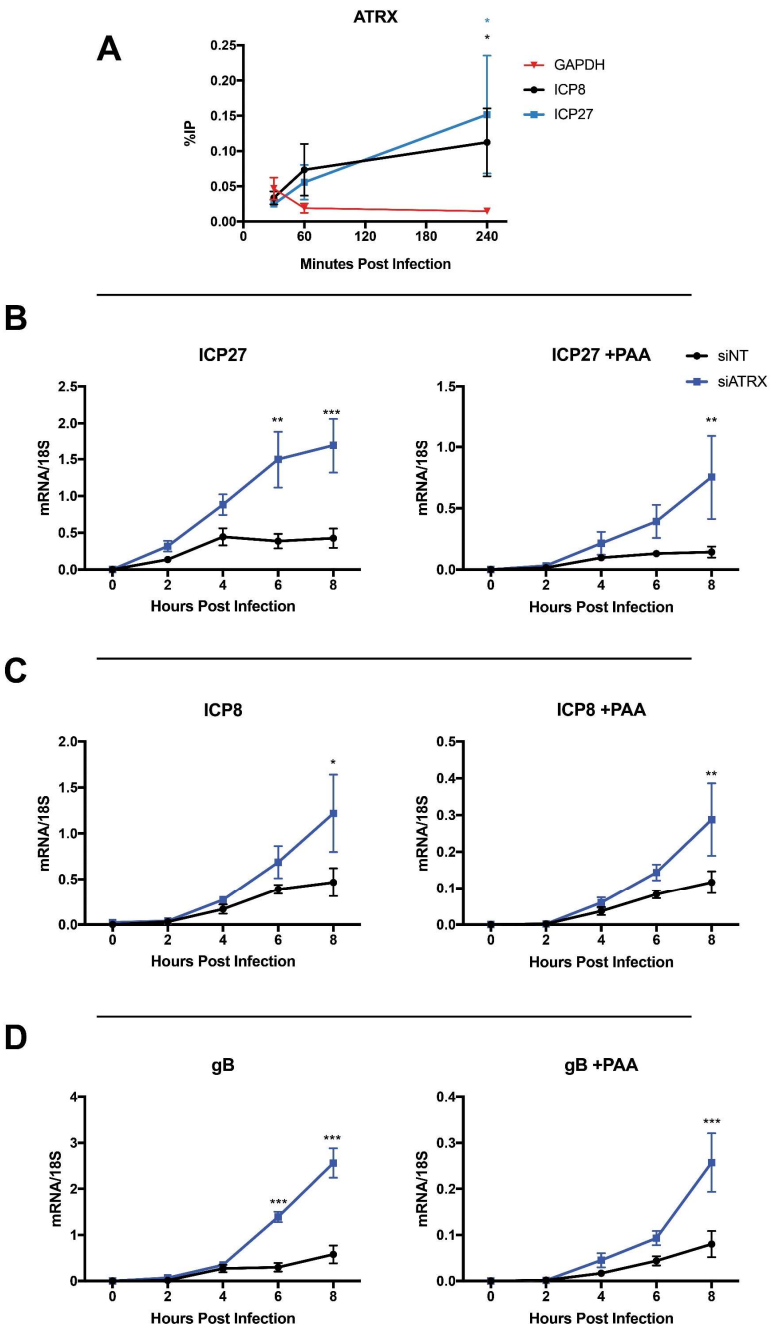

Figure 2.3: ATRX restricts HSV gene expression from input and progeny viral DNA.

(A) HFFs were infected with HSV 7134 at an MOI of 3, and infected cells were fixed and harvested 30, 60, and 240 minutes post infection. ChIP-qCPR and HSV specific primers were used to detect

Figure 2.3 (Continued) chromatin enrichment of ATRX at ICP27 (blue) and ICP8 (black) gene promoters. Two-tailed t-tests were used to compare ATRX enrichment at viral gene promoters compared to GAPDH. (B) HFFs were treated with siNT or siATRX and infected with HSV 7134 at an MOI of 5 in the absence (left panels) or presence (right panels) of PAA. Relative viral transcripts for (B) *ICP27*, (C) *ICP8*, or (D) *gB* were quantified by qPCR at 0, 2, 4, 6, and 8 hpi. Viral mRNA levels were normalized to cellular 18S transcripts. Results were analyzed by two-way ANOVA. All data for Figure 2.3 are reported as the average of 3 independent experiments ± standard error of the mean; $p < 0.05$ (*), $p < 0.01$ (**), $p < 0.001$ (***).

To facilitate our functional studies of ATRX and DAXX, we used CRISPR-Cas9 mediated gene editing to establish an ATRX-knockout cell line (ATRX-KO) derived from hTERT immortalized human fibroblasts (Albright and Kalejta, 2016; Bresnahan et al., 2000). We also established a control cell line (Control) in parallel that expresses Cas9 but no guide RNA, resulting in passage-matched ATRX-KO and Control cell lines (Supplemental Figure 2.5A). The immortalized fibroblasts were not permissive for single cell cloning; therefore, we used a population of ATRX-KO cells maintained under puromycin selection. ATRX-KO cells yielded significantly higher viral titers of ICP0-null virus than Control cells (MOI 3) (Supplemental Figure 2.5B). Similar to our observations in siRNA treated cells, *ICP27* gene expression from ICP0-null HSV was significantly greater in ATRX-KO cells than Control cells by 4 hpi, with both *ICP8* and *gB* exhibiting significantly elevated expression levels by 6 hpi (Supplemental Figure 2.5C).

DAXX has also been shown to reduce HSV U_L42 protein levels during ICP0-null HSV infection (Lukashchuk and Everett, 2010); however, the effects of double depletion of ATRX and DAXX on viral mRNA levels have yet to be investigated. We treated ATRX-KO and Control cells with siRNAs against DAXX, ATRX, or a non-targeting control (Supplemental Figure 2.5D). Control cells treated with siDAXX exhibited elevated expression of *ICP27* transcripts and a slight increase in *ICP8* transcript levels by 8 hpi (Figure 2.4A). In contrast, siDAXX-treated ATRX-KO cells did not exhibit elevated expression of either *ICP27*

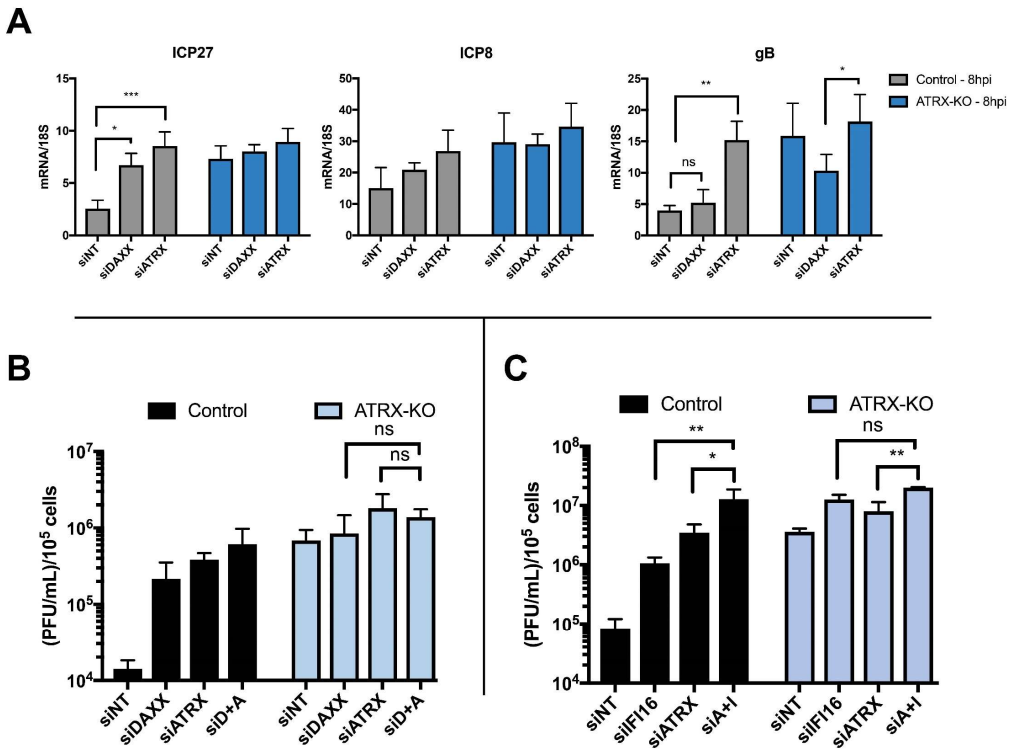

Figure 2.4: ATRX and DAXX cooperatively restrict HSV gene expression via an IFI16-independent pathway.

(A) Relative viral transcripts for *ICP27*, *ICP8*, and *gB* detected by qPCR in whole cell lysates collected from ATRX-KO or Control cells treated with siNT, siDAXX, or siATRX for 72 h then infected with HSV 7134 at an MOI of 5. Lysates were collected at 4 and 8 hpi. Results were analyzed by two-way ANOVA. (B) Viral yields from ATRX-KO and Control cells treated with siRNAs against non-targeting, ATRX, DAXX, or ATRX + DAXX (siD+A) and infected with HSV 7134 at an MOI of 0.1. Viral lysates were collected at 48 hpi and titrated on U2OS cells. Yields were normalized to (PFU/mL)/1x10^5 cells. Results were analyzed by two-way ANOVA. (C) Viral yields from ATRX-KO and Control cells treated with siRNAs against non-targeting, ATRX, IFI16, or ATRX + IFI16 (siA+I) and infected with HSV 7134 at an MOI of 0.1. Viral lysates were collected at 48 hpi and titrated on U2OS cells. Yields were normalized to (PFU/mL)/1x10^5 cells. Results were analyzed by two-way ANOVA. All data for Figure 2.4 are reported as the average of 3 independent experiments ± standard error of the mean; $p < 0.05$ (*), $p < 0.01$ (**), $p < 0.001$ (***).

or *ICP8* in comparison to siNT and siATRX treated ATRX-KO at 8 hpi (Figure 2.4A). Slightly elevated viral gene expression from ATRX-KO cells treated with siATRX is likely due to increased depletion efficiency in the heterogeneous ATRX-KO population. These results argued that DAXX works in conjunction with ATRX to restrict viral gene expression. Interestingly, siDAXX treated ATRX-KO cells exhibited a significant decrease in *gB* transcripts at 8 hpi when compared to siATRX treated ATRX-KO cells (Figure 2.4A). Similarly, Control cells treated with siDAXX did not exhibit an increase in *gB* expression at 8 hpi. These results indicated that DAXX restricts viral gene expression while in complex with ATRX, but after ATRX is degraded by the activity of ICP0 (Jurak et al., 2012), it may have a separate role in promoting *gB* and potentially other viral late gene expression or replication.

We next investigated the effects of DAXX depletion in ATRX-KO cells on viral yield. ATRX-KO cells treated with siDAXX and infected with ICP0-null HSV at either MOI 0.1 or 3 exhibited no increase in viral yield in comparison to cells treated with siATRX and siATRX + siDAXX (Figure 2.4B, Supplemental Figure 2.5E). Treatment with siNT decreased viral yield in both ATRX-KO and Control cells compared to untreated samples, possibly due to the cellular response to siRNA transfection as discussed above (Supplemental Figure 2.5E). Unlike siDAXX treatment in ATRX-KO cells, siIFI16 and siATRX treatment resulted in a significant increase in viral yield over siATRX treatment alone in ATRX-KO cells

(Figure 2.4C). We recently reported similar additive effects on ICP0-null HSV yield in cells depleted for both DAXX and IFI16 (Merkl et al., 2018). These results supported a model in which ATRX restricts HSV gene expression in coordination with DAXX, and this pathway is distinct from IFI16 sensing and restriction of viral DNA.

ATRX depletion increases ICP0-null HSV DNA replication and removal of heterochromatin.

ATRX and DAXX have been reported to promote H3.3 deposition on viral DNA promoters of AdV and HCMV (Albright and Kalejta, 2016; Newhart et al., 2013; Schreiner et al., 2013); however, the role(s) that ATRX and DAXX play in chromatin deposition on HSV DNA remain unknown. To investigate if ATRX plays a role in the initial chromatin deposition on input viral DNA, we performed ChIP-qPCR. ATRX-KO and Control cells were infected with ICP0-null 7134 virus at an MOI of 3, and cell lysates were harvested at 2, 4, and 8 hpi. Chromatin was immunoprecipitated with antibodies specific for total H3, H3.3, H3K9me3, and H3K27me3. We then quantified the recovered chromatin via qPCR. Surprisingly, we detected little to no difference in chromatin occupation at either the *ICP27* or *ICP8* gene promoter at 2 and 4 hpi for each of the chromatin markers tested in ATRX-KO and Control cells (Figure 2.5A-D; Supplemental Figure 2.6A-D). However, by 8 hpi, we observed lower levels of viral chromatin in ATRX-KO cells, with H3, H3.3, H3K9me3, and H3K27me3 all exhibiting significantly decreased

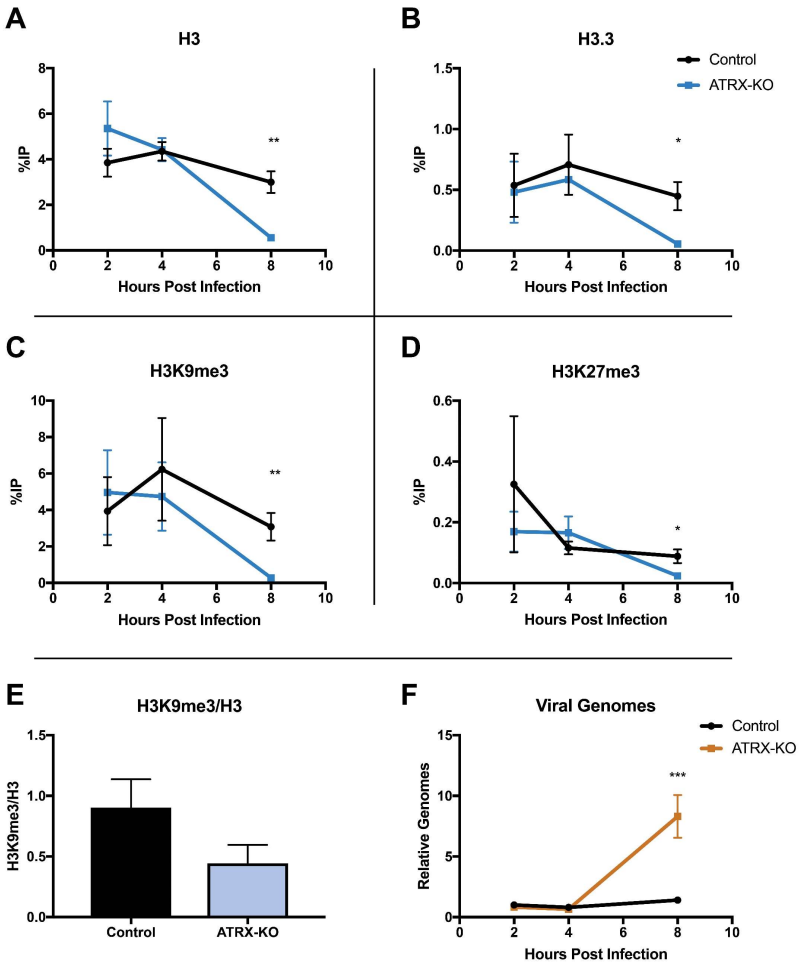

Figure 2.5: ATRX depletion enhances ICP0-null HSV DNA Replication and removal of heterochromatin.

ATRX-KO or Control cells were infected with HSV 7134 at an MOI of 3. Infected cells were fixed and harvested 2, 4, and 8 hpi. ChIP-qCPR and HSV specific primers were used to detect chromatin enrichment of (A) H3, (B) H3.3, (C) H3K9me3, and (D) H3K27me3 at the viral gene promoter for *ICP27*. Results are reported as the percent of input immunoprecipitated by each antibody. Two-tailed t-tests were used to compare results from ATRX-KO versus Control cells for each antibody and each time point. (E) H3K9me3 enrichment per H3 for the *ICP27* promoter. (F) Chromatin input for *ICP8* relative to input *GAPDH* to determine relative viral genome copy numbers. All data for Figure 2.5 are reported as the average of 4 independent experiments ± standard error of the mean; $p < 0.05$ (*), $p < 0.01$ (**).

levels compared to Control cells at both *ICP27* and *ICP8* gene promoters (Figure 2.5A-D; Supplemental Figure 2.6A-D). The overall density of H3K9me3 modifications per H3 at 8 hpi in ATRX-KO cells was less than half of those in Control cells (Figure 2.5E). This argued that loss of H3K9me3 occurred at a greater rate than the removal of H3. Indeed, H3K9me3 levels were reduced by greater than 10-fold at the *ICP27* promoter in ATRX-KO cells compared to Control. DNA replication was also enhanced in ATRX-KO cells, indicating an earlier onset of viral DNA synthesis (Figure 2.5F). These findings were supported by the observation that when infected with an ICP0-positive virus, 7134R, there was no significant difference in viral gene expression between ATRX-KO and Control cells (Supplemental Figure 2.6F). This argued that the unique restrictive effects exerted by ATRX on ICP0-null HSV gene expression occurred later than 2 hpi, when ICP0 disrupted PML-NBs (Supplemental Figure 2.3D), possibly in response to chromatin stability challenges, such as replication and transcription. From these results we concluded that ATRX promotes maintenance of stable viral heterochromatin during infection and delays the onset of viral DNA replication but is not uniquely required for the *de novo* formation of chromatin on input viral genomes.

ATRX promotes accumulation of heterochromatin on input viral genomes. To determine if the changes in heterochromatin composition on ICP0-null HSV genomes were dependent on viral DNA synthesis, we performed ChIP-qPCR in

ATRX-KO and Control cells with or without viral DNA synthesis inhibitor. ATRX-KO and Control cells were pretreated with PAA for 1 h prior to infection and maintained for the duration of the experiment. We infected cells with HSV 7134, harvested at 4 and 8 hpi, and performed ChIP-qPCR as described above. Consistent with our previous results, untreated ATRX-KO cells exhibited reduced H3, H3.3. H3K9me3, and H3K27me3 at both the *ICP27* and *ICP8* promoters compared to their Control cell counterparts (Supplemental Figures 2.7A-D and 2.8A-D). However, when viral DNA synthesis was inhibited with PAA (Figure 2.6E), viral chromatin density was similar in all conditions at 4 hpi (Figure 2.6A-D). Viral heterochromatin continued to accumulate from 4-8 hpi in PAA-treated Control cells while it remained near 4-hour levels in PAA treated ATRX-KO cells; however, removal of heterochromatin was largely blocked by PAA treatment (Figure 2.6A-D). Interestingly, H3.3 increased in occupancy at the *ICP8* promoter from 4-8 hpi in ATRX-KO cells treated with PAA suggesting that H3.3 deposition may be differentially regulated at the *ICP8* promoter (Supplemental Figure 2.8C). Overall, these results argued that ATRX maintained virus genome-associated heterochromatin on input HSV DNA, promoted increased viral heterochromatin stability and density from 4-8 hpi, and that removal of heterochromatin was enhanced by viral DNA replication.

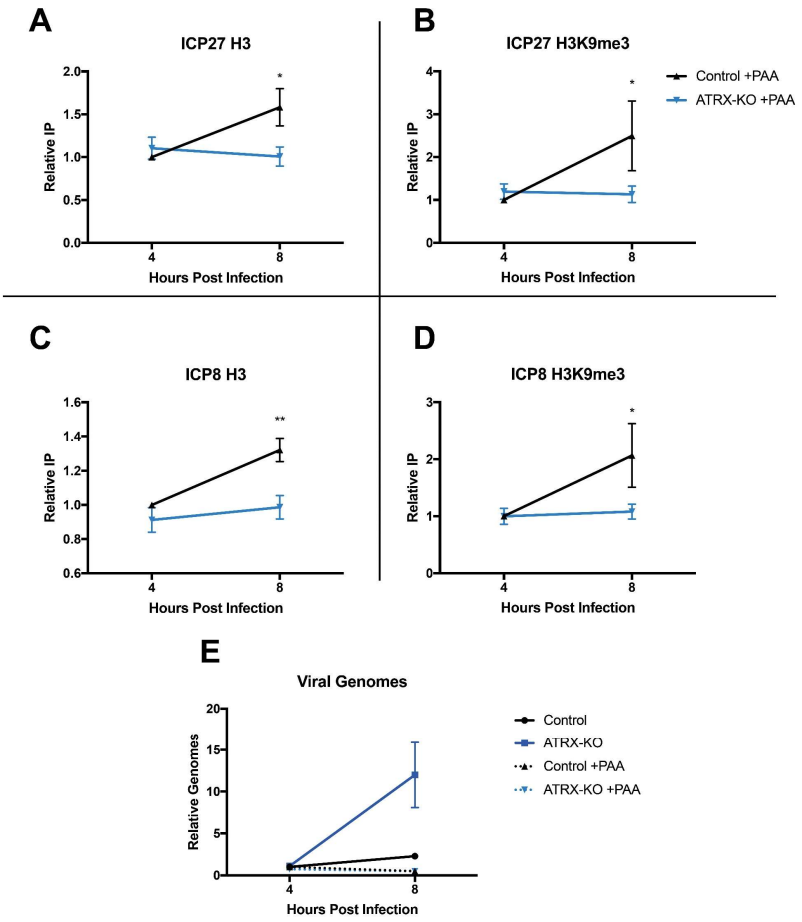

Figure 2.6: ATRX promotes maintenance of heterochromatin on input viral genomes.

ATRX-KO or Control cells were infected with HSV 7134 at an MOI of 3. Infected cells were fixed and harvested 8 hpi. ChIP-qCPR and HSV specific primers were used to detect chromatin enrichment of at the viral gene promoters in the absence (Figure 6 – figure supplement1A-D) or presence of PAA. Enrichment of (A) H3 and (B) H3K9me3 at the *ICP27* gene promoter. Enrichment of (C) H3 and (D) H3K9me3 at the *ICP8* gene promoter. Results reported as Relative IP (the percent of input immunoprecipitated by each antibody normalized to the 4 hour control sample - set to 1.0 for each replicate). (E) Chromatin input for *ICP8* relative to input *GAPDH* to determine relative viral genome copy numbers in the absence or presence of PAA. All data for Figure 2.6 are reported as the average of 4 independent experiments ± standard error of the mean; two-tailed t-test, $p < 0.05$ (*), $p < 0.01$ (**).

Transcription contributes to HSV heterochromatin instability in the absence of ATRX.

Chromatin structure is dynamic by nature and requires active maintenance in response to stability challenges including replication and transcription (Nair et al., 2017; Schwabish and Struhl, 2004). To assess the effects of transcription on viral chromatin composition, we infected Control and ATRX-KO cells with transcriptionally silent HSV *d*109 virus. ATRX-KO cells showed no difference in either H3 or H3K9me3 levels at the *ICP8* gene promoter at both 4 and 8 hpi (Figure 2.7A). To further investigate the effects of ATRX on chromatin during transcription, we inhibited transcription with the CDK9 inhibitor flavopiridol. Cells were treated with flavopiridol (1 μM, 1 h pretreatment) (Supplemental Figure 2.10E) and infected with HSV. As previously observed in untreated cells, H3 and H3K9me3 levels on HSV DNA were similar at 4 hpi in ATRX-KO and Control cells but lower by 8 hpi in ATRX-KO fibroblasts (Supplemental Figure 2.9A,B). However, treatment with flavopiridol blocked heterochromatin loss and resulted in H3 and H3K9me3 accumulation from 4-8 hpi in ATRX-KO cells (Figure 2.7B, Supplemental Figure 2.10A). Likewise, treatment with polymerase inhibitor α-amanitin (2 μg/ml, 16 h pretreatment) (Supplemental Figure 2.10F) blocked removal of H3 and H3K9me3 in ATRX-KO cells and resulted in heterochromatin accumulation from 4-8 hpi (Figure 2.7C, Supplemental Figures 2.9C,D and 2.10B). We also infected Control and ATRX-KO cells with HSV 7134 and added the

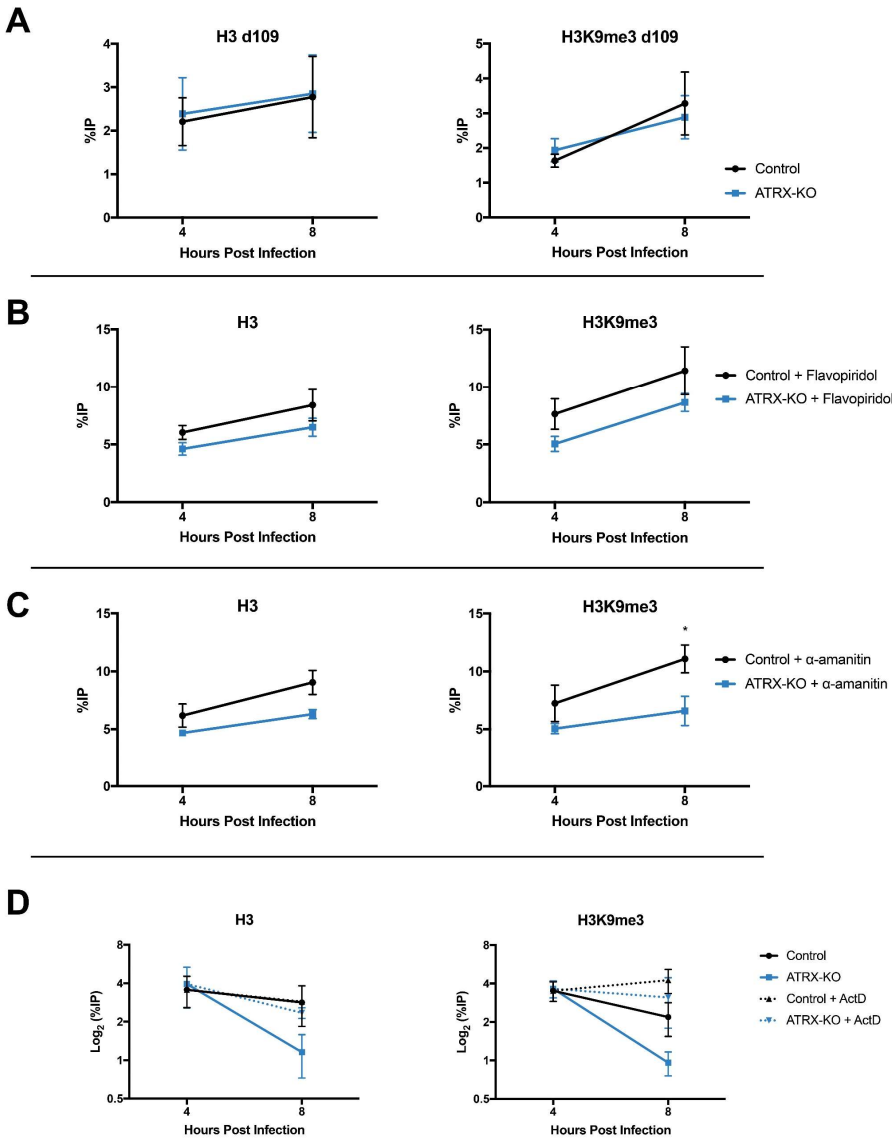

Figure 2.7: ATRX promotes heterochromatin maintenance during challenges to chromatin stability.

(A) ATRX-KO and Control cells were infected with HSV *d*109 at an MOI of 3 and fixed and harvested at 4 and 8 hpi. ChIP-qPCR was used to detect H3 and H3K9me3 enrichment at the *ICP8* promoter. (B) ATRX-KO and Control cells were treated with flavopiridol (flavopiridol; 1 μM) from 1 h prior to infection until time of harvest. Treated and untreated (Figure 7 – figure supplement 1A-B) cells were infected with HSV 7134 at MOI 3 and fixed at 4 and 8 hpi. ChIP-qPCR was used to detect H3 and H3K9me3 enrichment at the *ICP8* promoter. (C) ATRX-KO and

Figure 2.7 (Continued) Control cells were treated with α-amanitin (2 µg/mL) from 16 h prior to infection until time of harvest. Treated and untreated (Figure 7 – figure supplement 1C-D) cells were infected with HSV 7134 at MOI 3 and fixed at 4 and 8 hpi. ChIP-qPCR was used to detect H3 and H3K9me3 enrichment at the *ICP8* promoter. (D) ATRX-KO and Control cells were infected with HSV 7134 at a MOI of 3 and treated with ActD (5 µg/mL) at 4 hpi. Samples were fixed and collected a 4 and 8 hpi. Chromatin enrichment is reported as percent input immunoprecipitated by antibodies specific for H3 and H3K9me3 as detected by qPCR using specific primers for the promoter of *ICP8*. All data for Figure 2.7 are reported as the percent of input immunoprecipitated by each antibody and are the average of 3 independent experiments $\pm$ standard error of the mean; two-tailed t-test, $p < 0.05$ (*).

transcriptional inhibitor actinomycin-D (actD, 5 μg/ml) at 4 hpi. Addition of actD prior to infection blocked chromatin loading to HSV DNA (not shown), so we added actD at 4 hpi to arrest transcription once viral chromatin had been established. Treatment with actD at 4 hpi stabilized chromatin resulting in no loss of H3 or H3K9me3 in ATRX-KO and Control cells between 4 and 8 hpi (Figure 2.7D; Supplemental Figure 2.10C). Taking these results together, we concluded that ATRX plays a role in a process that protects against chromatin destabilization during transcription.

PML promotes maintenance of viral chromatin during infection.

Because PML has recently been implicated in influencing ATRX/DAXX activity (Delbarre et al., 2017), we next investigated if PML affects viral chromatin maintenance. We infected HFFs stably expressing a short hairpin against PML (shPML) (Wagenknecht et al., 2015) with HSV 7134, and we observed that at 4 hpi, PML-depleted cells (Figure 2.8A) showed no significant differences from shControl cells for H3 but a slight decrease in H3K9me3 at the *ICP27* and *ICP8* viral gene promoters (Figure 2.8B-D). However, by 8 hpi, we observed a significant reduction of chromatin in shPML cells that was similar to what was observed in ATRX-KO fibroblasts (Figure 2.8B-D). Though PML may play a minor role in promoting early H3K9me3 density at viral gene promoters, these results indicated that PML, like ATRX, is not uniquely required for the formation of viral

heterochromatin. However, ATRX and PML are both required for the maintenance of viral heterochromatin stability.

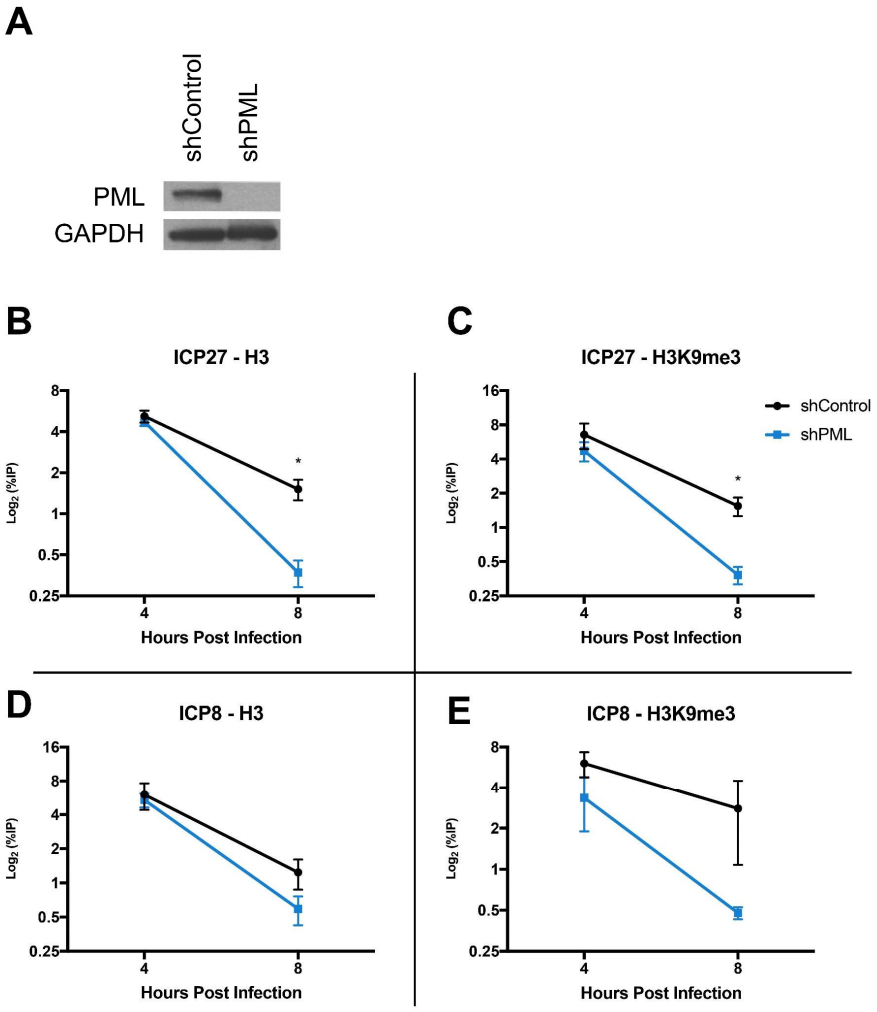

Figure 2.8: PML promotes maintenance of viral chromatin.

(A) Immunoblot for PML in shControl and shPML cells. shPML and shControl cells were infected with HSV 7134 at an MOI of 3. Samples were fixed and harvested at 4 and 8 hpi. ChIP-qPCR for (B) H3 and (C) H3K9me3 at the *ICP27* viral gene promoter. ChIP-qPCR for (D) H3 and (E) H3K9me3 at the *ICP8* viral gene promoter. Figure 2.8 B-E are reported as the percent of input immunoprecipitated by each antibody and are the average of 3 independent experiments ± standard error of the mean; two-tailed T test, $p < 0.05$ (*).

Discussion

The results presented here argue that viral DNAs are concurrently detected by multiple DNA sensing and restriction pathways and that the initial deposition of chromatin on the HSV genome and the maintenance of viral chromatin are mediated by separate mechanisms. ATRX and IFI16 are both recruited to incoming viral DNA, but they do so independently and then restrict viral infection through independent pathways. Although ATRX has been reported to be important for H3.3 occupation on both cellular and viral genomes, direct examination of the role ATRX plays in *de novo* heterochromatin formation *in vivo* has yet to be described. Despite possessing H3.3-specific chaperone activity when in complex with DAXX, here we report that ATRX is dispensable for the initial deposition of histones and repressive histone modifications on naked viral DNA. But ATRX is required to maintain the stability of viral heterochromatin in the face of chromatin stress. This observation reveals new insights into the specificity of histone chaperone activity and may prove to be important in understanding the complex roles ATRX plays in regulating gene expression, heterochromatin maintenance and telomere homeostasis on host cell chromatin.

Multiple restriction pathways detect incoming viral DNA.

Our results revealed that incoming viral DNA is detected and epigenetically silenced by multiple host-cell restriction pathways. We detected IFI16, PML, and

ATRX colocalizing with viral DNA by 15 mpi, the earliest time point at which we were able to detect viral DNA in the nuclei of HFFs. This observation argued that these host restriction factors detect HSV almost immediately upon nuclear entry. IFI16 has been observed to form transient foci at the nuclear periphery during early HSV infection (Diner et al., 2016; Everett, 2016), but there was no definite way to connect the IFI16 foci to incoming viral DNA without labeling of the viral DNA as presented here. IFI16 colocalization with viral DNA was temporally limited, suggesting an initial detection of viral DNA followed by a displacement by additional factors or modifications, perhaps by nucleosomes which are known to impede IFI16 oligomerization (Stratmann et al., 2015). In contrast, we observed ATRX stably colocalizing with viral genomes until PML-NBs were disbursed by ICP0 around 2 hpi. We previously showed that depletion of IFI16 does not affect recruitment of PML to ICP4, a marker for viral DNA (Orzalli et al., 2013). Furthermore, during the preparation of this manuscript, it was reported that IFI16 does not influence PML recruitment to labeled HSV DNA (Alandijany et al., 2018). The latter report supports our own observations that ATRX and IFI16 are independently recruited to incoming viral DNA. Providing additional support for this argument, we showed the restrictive effects of ATRX and IFI16 on ICP0-null HSV replication are additive. These results echo our recent findings regarding the additive restrictive effects of DAXX and IFI16 (Merkl et al., 2018). Together, these results argue that IFI16 and PML-NB components represent distinct nuclear DNA

sensing pathways that act in parallel to detect and restrict invading viral DNA almost immediately upon nuclear entry.

Formation of viral chromatin does not require the ATRX/DAXX complex. Our results revealed that ATRX is not required for H3/H3.3 deposition on viral DNA for the first 4 hpi; however, we cannot rule out the possibility that other histone chaperones or assembly complexes may compensate for the loss of ATRX/DAXX histone chaperone activity, as HIRA does for depletion of CAF-1 (Ray-Gallet et al., 2011). In fact, CAF-1 has been reported to compensate for loss of Daxx in murine cells (Drane et al., 2010), and NAP1 can assemble H3.3-containing nucleosomes *in vitro* (Lewis et al., 2010). However, it is important to note that ATRX and DAXX have roles in promoting heterochromatin that do not require histone chaperone activity (Sadic et al., 2015). Because ATRX can also act as a H3K9me3 reader (Eustermann et al., 2011; Iwase et al., 2011), restrictive effects of ATRX and DAXX on HSV infection may not require the H3.3 chaperone activity of the ATRX/DAXX complex during lytic infection. Individual and combinatorial depletion of other histone loaders and nucleosome formation complexes will be required to identify the cellular factors needed for the initial loading of heterochromatin on the HSV genome.

We also cannot rule out the possibility that the observed effects are due to an indirect effect as a consequence of depleting ATRX. Depleting cells of a histone chaperone will likely result in changes to cellular chromatin and altered

gene expression. However, changes in viral chromatin density in ATRX-KO cells are not observable until after 4 hours post infection, so we do not believe the observed to be effects to be the consequence of enhanced global histone mobility. Additionally, we observed the association of ATRX with viral gene promoters by 4 hours post infection. This finding is consistent with a direct role for ATRX in viral chromatin regulation. Furthermore, as both siRNA and CRISPR depletions of ATRX have very similar effects on viral yield and viral gene expression, it seems unlikely that this is due to off-target effects.

Our results suggest that DAXX may have ATRX-independent functions during viral infection. Here we report that siRNA depletion of DAXX in ATRX-KO cells significantly decreased the expression of *gB* transcripts during productive ICP0-null HSV infection. Similar dual anti-viral and pro-viral effects have recently been reported for PML (Newhart et al., 2013; Xu et al., 2016), and the H3.3-specific chaperone, HIRA, has been shown to both enhance and restrict viral infection depending on context (Placek et al., 2009; Rai et al., 2017). It is possible that DAXX is restrictive while in complex with ATRX but at a later stage of infection, after dispersion of PML-NBs and degradation of ATRX, DAXX may promote HSV gene expression or replication. Our results contribute to a growing body of literature that is revealing ATRX-independent functions of DAXX that may have important implications for viral restriction, cancer biology, and epigenetics (He et al., 2015; Hoelper et al., 2017).

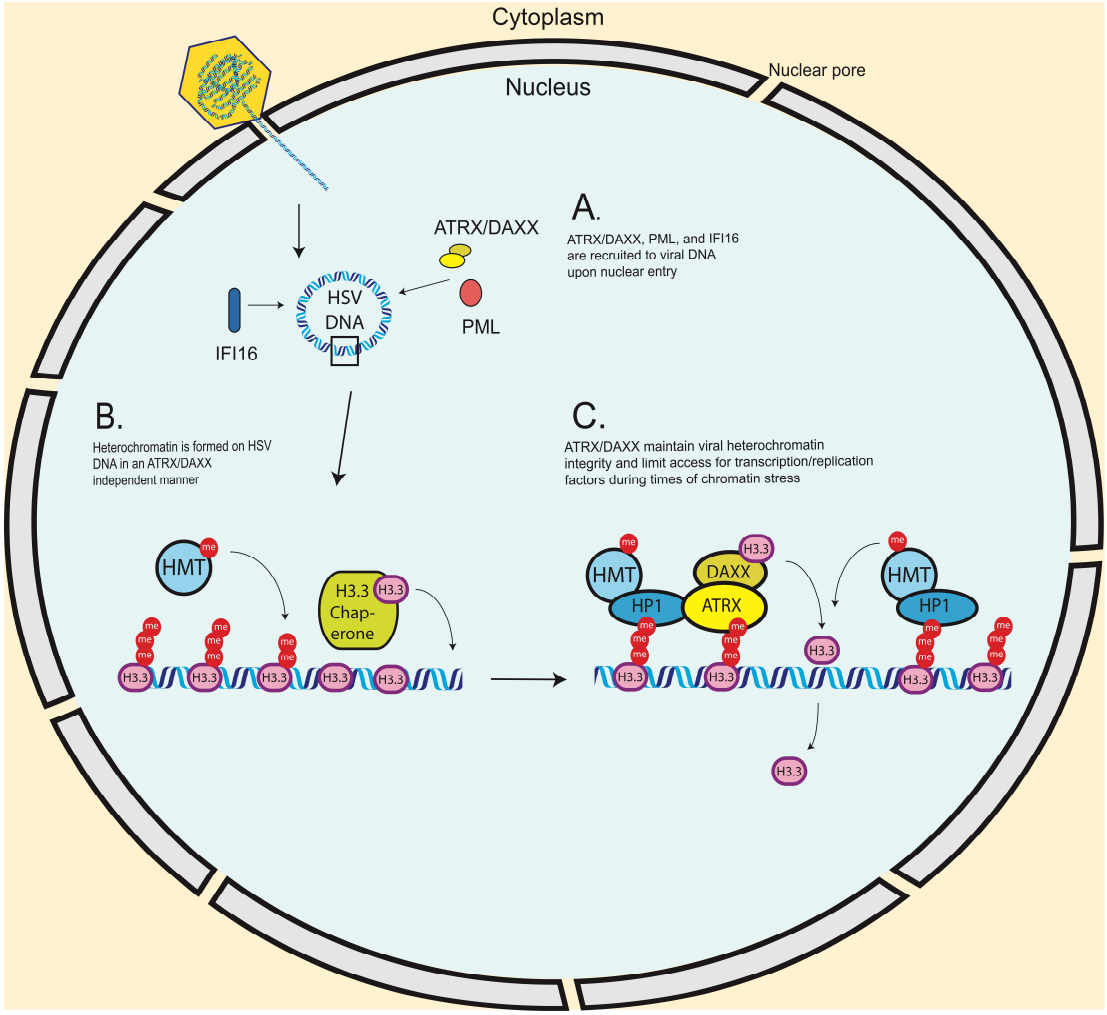

Figure 2.9: Model – ATRX promotes heterochromatin maintenance during challenges to chromatin stability.

(A) Incoming HSV genomes are rapidly sensed by IFI16, PML, and ATRX upon nuclear entry. (B) The *de novo* formation of heterochromatin on input viral genomes occurs in an ATRX-independent manner, possibly through a HIRA/ASF1A mediated pathway in conjunction with histone methyltransferases (HMTs). However, our results indicate that ATRX is required to maintain viral heterochromatin stability during destabilizing events such as transcription or replication. (C) We hypothesize that ATRX maintains viral heterochromatin integrity resulting in reduced chromatin dynamics, stabilized heterochromatin, and reduced access for transcription factors, viral replication factors, and polymerases.

ATRX mediates HSV heterochromatin stability during chromatin stress.

We hypothesize that ATRX restricts viral infection by maintaining viral heterochromatin stability, resulting in DNA that is less accessible to transcription and viral replication factors (Figure 2.9). Though *de novo* formation of HSV-associated heterochromatin was unaffected by the absence of ATRX (Figure 2.9B), decreased histone retention or histone reloading in the absence of ATRX/DAXX could conceivably explain the observed loss of H3 and H3K9me3 on HSV genomes, elevated levels of viral transcription, and the enhanced accumulation of nascent viral DNA that we observed by 8 hpi in ATRX-KO cells. Decreased histone retention may lead to increased histone dynamics, reduced nucleosome density, and transiently expose transcription factor binding sites, resulting in elevated transcription (Huang and Zhu, 2014) and increased accessibility for viral replication factors. Similarly, if nucleosomes are lost from viral DNA during transcription or DNA synthesis, new nucleosomes will need to be rapidly formed and modified with repressive histone tail modifications to maintain epigenetic silencing. These ideas are consistent with our findings that ATRX promotes the maintenance and continued accumulation of viral heterochromatin, both histones and histone modifications, during times associated with viral transcription and DNA synthesis. When viral DNA synthesis was blocked with PAA, HSV DNA in Control cells continued to accumulate H3 and H3K9me3 from 4-8 hpi. In contrast, HSV DNA-associated H3 and H3K9me3 did not accumulate significantly in ATRX-KO cells from 4-8hpi, suggesting that in the absence of

ATRX, histone exchange rates had reached an equilibrium by 4 hpi. While there may be more than one way to explain these observations, we think the model that best fits these observations is one in which ATRX promotes heterochromatin accumulation by mediating modified histone retention.

ATRX is known to be recruited to heterochromatin through the interaction of its ADD domain with the H3K9me3 histone tail modification (Iwase et al., 2011), and is known to be required for both H3.3 and H3K9me3 maintenance on regions of cellular DNA (17, 53, 58). It can also be recruited by direct interaction with heterochromatin protein 1 (HP1) (Berube et al., 2000; Eustermann et al., 2011), a chromatin remodeling factor which has been reported to localize to HSV gene promoters during infection (Ferenczy and DeLuca, 2009). ATRX may act to recruit DAXX to viral DNA through its interaction with H3K9me3 or HP1 and promote rapid replacement of histones that dissociate from viral DNA (Figure 2.9C). These histones could then be rapidly modified with H3K9me3 by histone lysine methyltransferases SUV39H1 or SETDB1 that are known to be recruited by HP1, thus maintaining heterochromatin composition and density on the HSV DNA. Our model is also likely relevant to the maintenance of DNA virus latency. The EBV protein BNRF1 has been shown to bind to DAXX and separate it from the ATRX/DAXX complex (Tsai et al., 2011). That study also showed that depletion of DAXX or ATRX led to EBV reactivation in lymphoblastoid cells. Through its interaction with DAXX, BNRF1 was shown to promote increased mobilization and turnover of H3.3 during FRAP experiments (Tsai et al., 2014). The observed

increase in H3.3 turnover has been proposed to facilitate expression of viral latent genes and the establishment of latent EBV infection. ATRX and DAXX have also been detected localizing to viral genomes in neurons of mice latently infected with HSV-1 (Catez et al., 2012). These reports are consistent with our model that ATRX/DAXX promotes heterochromatin integrity to enhance epigenetic silencing of viral genes and proposes that this mechanism may be important for both lytic and latent DNA virus infections. Further studies are needed to define how ATRX reduces the loss of chromatin during times of increased viral transcription and replication.

This model may also be relevant to cellular heterochromatic loci that are maintained by ATRX. Transcription by RNA Pol II evicts histones which are then quickly replaced (Schwabish and Struhl, 2004) by the FACT complex, which has been implicated in both the disassembly and reassembly of histone components during transcription (Belotserkovskaya et al., 2003; Mason and Struhl, 2003; Xin et al., 2009). The result is a dynamic equilibrium of nucleosome formation, retention, and eviction. Based on our observations of viral chromatin and viral gene expression in the absence of ATRX, we expect that as the level of transcription increases in the absence of ATRX, the equilibrium between eviction and deposition could shift in favor of eviction and result in an apparent reduction in H3.3 and H3K9me3. Supporting this idea, ATRX has been shown to be required to silence transcription of an eGFP-retrotransposon reporter in response to continuous dox-induced transcription (Sadic et al., 2015). In that study, ATRX

depletion had minor effects on the initial establishment of H3K9me3 at the reporter element, but it was required for the efficient re-establishment of H3K9me3 after transcriptional challenge was ended. Similarly, ATRX protected against expression of minor satellite sequences in mouse embryonic stem cell derived neurons upon neuronal stimulation (Noh et al., 2015b).

Like ATRX, PML was not strictly required for the initial deposition of histone H3 or H3K9me3 on viral DNA but required for maintenance of heterochromatin from 4-8 hpi. PML was recently reported to influence ATRX/DAXX complex activity and loss of PML may increase H3.3 turnover at PML-associated domains (PADS) (Delbarre et al., 2017). Because ATRX is required for heterochromatin maintenance at both pericentric heterochromatin and telomeres (Goldberg et al., 2010; Lewis et al., 2010; McDowell et al., 1999), it is not surprising that pericentric heterochromatin and telomeres have both been shown to exhibit high levels of chromatin stability with very low histone turnover (Kraushaar et al., 2013). Consequently, we suggest that a major function of ATRX in heterochromatin maintenance is in stabilizing chromatin density and promoting histone retention. However, increased histone retention is not the only possible mechanism of action. ATRX could also be promoting the re-establishment of heterochromatin in the wake of RNA Pol II mediated transcription, perhaps in a fashion similar to the FACT-complex. Likewise, ATRX could be stabilizing chromatin by inhibiting transcription or replication through a DNA damage pathway. Further mechanistic

studies will be required to define the precise mechanism through which ATRX exerts its influence on viral chromatin.

Epigenetic regulation of viral DNA occurs in two stages.

Our finding that ATRX restricts HSV gene expression by promoting the maintenance of viral heterochromatin raises the idea that there are at least two stages of epigenetic regulation involved in restriction of viral gene expression: 1. Initial loading of heterochromatin; 2. Maintenance of heterochromatin during chromatin stress, such as transcription and replication. Although viral chromatin structure is known to be dynamic (Gibeault et al., 2016), before this report, the formation of viral chromatin and the maintenance of viral chromatin were not understood to be separate mechanisms. Importantly, DNA viruses have evolved specific mechanisms for dismantling or disabling the ATRX/DAXX pathway rather than blocking the initial formation of heterochromatin. This argues that there may be some role for the early formation of chromatin in the viral life cycle. This is supported by reports that HIRA and ASF1A promote histone occupation on HSV DNA during the first few hours of infection but do not appear to be restrictive during this same period of time (Oh et al., 2012; Placek et al., 2009). Conversely, the heterochromatin maintenance mechanism mediated by ATRX appears to act as a critical restrictive hurdle to productive infection.

The multiple stages of epigenetic restriction of viral genomes uncovered here involve cellular chromatin factors. Therefore, their roles in epigenetically

silencing viral DNA may reflect their functions in cellular chromatin assembly and maintenance. Cellular chromatin structure must be maintained during transcription, DNA synthesis, and mitosis. Thus, it is likely that multiple mechanisms exist to deal with each of these chromatin stressors. The stages of viral epigenetic regulation by the host cell as defined here will serve to identify host epigenetic factors that may function in similar host cell pathways, and this knowledge could provide insights critical to the development of epigenetic therapies for both viral and host diseases.

Materials and Methods

Cell culture, viruses, and infections

HFF, U2OS, and HEK293T cells were obtained from the American Type Culture Collection (Manassas, VA). hTERT immortalized fibroblasts were a kind gift from Robert Kalejta and originally described in Bresnahan et al. HFFs expressing a short hairpin against PML (shPML) were a kind gift from Thomas Stamminger (Wagenknecht et al., 2015). All cells are regularly tested for the presence of mycoplasma contamination. Cells used in this study were mycoplasma free.

All fibroblast cells and HEK293T cells were maintained in Dulbecco's Modified Eagle's medium (DMEM; Corning, Corning NY) supplemented with 10% (v/v) fetal bovine serum (FBS) in humidified 5% CO_2 incubators at 37ºC. Cells were serially passaged by trypsin-EDTA (0.05%; Corning) treatment and transfer to fresh media. shPML fibroblasts were maintained under 5 µg/ml puromycin.

HSV-1 KOS was used as the wild type virus in this study. HSV-1 KOS 7134 (Cai and Schaffer, 1992) was used for experiments requiring an ICP0-null HSV. HSV-1 7134R is an ICP0$^+$ virus. HSV-1 *d*109 does not express HSV immediate-early genes (Samaniego et al., 1998). Cells were infected with viruses at the indicated MOI in PBS containing 1% (w/v) glucose and 1% (v/v) bovine calf serum (BCS). Infections were carried out at 37ºC with constant agitation with 1 h adsorption time unless otherwise indicated. After 1 h, the inoculum was removed and replaced with DMEM supplemented with 1% BCS (DMEV) and then incubated at 37ºC until times indicated. ICP0-null viral yields were determined by infecting U2OS cells with serial dilutions of viral lysates collected at indicated times. For experiments testing the effects of viral DNA synthesis, PAA (Sigma-Aldrich; St. Louis, MO) was added to the media (400 µg/ml) with 10mM HEPES at the time of infection and maintained until time of harvest. Actinomycin-D (5 µg/ml; Sigma) and flavopiridol (1 µM; Selleck Chemicals, Houston, TX) were added to cells 4 hpi and 1 h prior to infection, respectively, and maintained until time of harvest. Cells were pre-treated with α-amanitin (2 µg/ml; Sigma) for 16 h prior to infection and maintained until time of harvest. To block viral attachment and entry to cells, heparin was added to the viral inoculum (50 µg/ml), and heparin was maintained for the duration of the infection.

CRISPR/Cas9-mediated knockout of ATRX

DNA oligos coding encoding sgRNAs specific for ATRX were designed using the Optimized CRISPR Design tool (http://crispr.mit.edu/; Zhang Lab, MIT) and cloned into the lentiCRISPR v2 vector (Busskamp et al., 2014). HEK293T cells were grown to 70% confluency in 6-well plates and either lentiCRISPR v2 expressing Cas9 or co-expressing an sgRNA targeting ATRX were co-transfected with the psPAX2 and pVSV-G packaging plasmids using Effectene Transfection Reagent per manufacturer's instructions (Qiagen). hTERT immortalized fibroblasts seeded in a 6-well plate were transduced with supernatant (1:1) harvested from HEK293T cells 48 h post transfection that had been filtered through a 0.45 μm sterile syringe filter (MilliporeSigma; Burlington, MA). Transduced cells were maintained for two days then placed under puromycin selection (5 μg/ml) and expanded for two weeks.

Oligo sequences for anti-ATRX sgRNA expression:

sgATRX 1 F TCTACGCAACCTTGGTCGAA

sgATRX 1 R TTCGACCAAGGTTGCGTAGA

sgATRX 2 F CGAAACTAACAGCTGAACCC

sgATRX 2 R GGGTTCAGCTGTTAGTTTCG

Preparation of EdC-labeled HSV-1 stocks

HFFs were grown to confluency in T-150 flasks, and then left at confluency for 2-3 days. The confluent HFFs were infected with HSV-1 HSV at a MOI of 10 and

incubated at 34ºC. At 4 hpi, the medium was replaced with fresh medium containing 0.5 μM of the nucleoside analog, EdC. At 34 hpi, the HSV-infected HFFs were washed twice with 5 mL DMEV per wash, and 20 mL of fresh EdC-free media was added to the cells. The infected HFFs were incubated for an additional 2 h at 34ºC. At 36 hpi, cells were harvested by scraping the flasks in 2.5 mL DMEV and 2.5mL sterile skim milk. The viral lysate was then sonicated using a Misonix S-4000 probe sonicator on setting 30 for 3 cycles: 30 seconds on, 30 seconds off. The HSV-EdC lysate was aliquoted and stored at -80ºC. Infection of Vero cells with serially diluted virus was used to determine viral titer via plaque assay.

Protein Depletions

To deplete cells of endogenous proteins, siRNAs were transfected into $1x10^5$ cells plated in a 12-well dish using Lipofectamine RNAiMAX Reagent (Invitrogen). At 48 h post transfection, cells were re-seeded into assay-appropriate dishes and infected 24 h later.

siRNAs used in this study:

siNT: Dharmacon ON-TARGETplus Non-targeting pool D-001810-10

siATRX: Dharmacon ON-TARGETplus ATRX pool D-006524-00

siIFI16: Dharmacon ON-TARGETplus IFI16 pool D-20004-00

siDAXX: Dharmacon ON-TARGETplus DAXX pool D-004420-10

Antibodies

The following antibodies were used in this study:

IFI16 Abcam ab50004

PML Bethyl A301-167A (immunoblot only)

PML Abcam ab96051 (immunofluorescence only)

DAXX Sigma D7810 (immunoblot only)

GAPDH Abcam ab8245 (immunoblot only)

ICP8 (Knipe et al., 1987)

ICP4 (Showalter et al., 1981)

ICP0 East Coast Bio H1A207

ATRX Abcam 97508

H3 Abcam ab1791 (ChIP)

H3K9me3 Abcam ab8898 (ChIP)

H3K27me3 Active Motif 39156 (ChIP)

H3.3 Millipore 09-838 (ChIP)

Negative control rabbit IgG Millipore NG1893918 (ChIP)

Immunoblots

Cells were harvested at times indicated in lithium dodecyl sulfate (LDS) sample buffer and incubated at 95ºC for 10 min. Protein samples were run on NuPAGE 4-12% bis-Tris gels (Invitrogen). Proteins were transferred from the gel to

nitrocellulose or PVDF membranes for imaging via LI-COR Odyssey imager (Lincoln, NE) or film, respectively. Membranes were blocked in either LI-COR blocking solution or 5% powdered milk-PBS containing 0.1% Tween 20 (PBST) for 1 h. After blocking, membranes were incubated with primary antibody overnight at 4ºC. Membranes were washed 3 times with PBST, incubated in secondary antibody for 1 h at room temperature (IRDye 800CW Goat anti-Mouse IgG and IRDye 800CW Goat anti-Rabbit IgG for LI-COR; α-mouse IgG^{+}HRP and α-Rabbit IgG^{+}HRP, Cell Signaling 7076s and 7074s, respectively for film). Membranes were washed 3 times in PBST. Nitrocellulose membranes were imaged with a LI-COR Odyssey imager. PVDF membranes were incubated with SuperSignal West Pico chemiluminescent substrate (Thermo Scientific) and exposed to film.

Immunofluorescence and detection of EdC-labeled HSV-1 genomes

Transfected or infected cells were fixed with 2% methanol-free formaldehyde (ThermoFisher), permeabilized with 0.1% Triton-X 100. Permeabilized cells were incubated with primary antibodies for 30 min at 37ºC and washed twice with 0.1% PBST for 5 min each, followed by one wash with PBS. Alexa Fluor 594- and 647-conjugated secondary antibodies (Invitrogen; A11032 and a21246, respectively) and DAPI were incubated with cells for 30 min at 37ºC. All antibodies were used at 1:500. The coverslips were washed as described above and either mounted on slides with ProLong Gold antifade reagent (Invitrogen) or incubated with click chemistry reagents as follows. After incubation with secondary antibodies,

coverslips were incubated with 10 μM biotin-picolyl azide (Click Chemistry Tools, Scottsdale, AZ), 10 mM sodium ascorbate (Sigma-Aldritch A4034), and 2 mM $CuSO_4$ (Fisher) for 2 h in the dark. Coverslips were washed twice with 0.1% PBST and once with PBS. Coverslips were then incubated with Alexa Fluor 488-conjugated streptavidin (1:1000; Invitrogen S32354) for 30 min in the dark. Coverslips were washed twice in PBS and mounted as described above. Images were acquired using NIS-Elements AR imaging software (Nikon) controlling a Nikon Ti-E inverted microscope system using a Plan Apo 100x/1.45 objective with a Zila sCMOS camera (Andor) and SPECTRA X light engine (Lumencor) or a Nikon Ti-E inverted spinning disk confocal system using laser lines 488, 514, 561 and 640 and a Plan Apo 100x/1.45 objective. Image J (FIJI) was used to minimally adjust contrast and generate 3D projections of exported images.

Quantitative Image Analysis

The Image and Data Analysis Core (IDAC) at Harvard Medical School developed a custom MATLAB-based software for nuclear foci and co-localization detection in microscopy images based upon their previously described nuclear foci detection software (Cicconet et al., 2017). In brief, unaltered images were analyzed by the software to detect signal intensity over a set threshold to define foci above background. The software then uses DAPI staining to generate a mask that defines nuclear areas in the image. Only foci above the fluorescence threshold and within the nuclear masks were scored. The software determines

colocalization based on the distance between the centers of nuclear foci in a reference channel (vDNA) to foci in other channels of the image. The centers of compared foci must be ≤ 5 pixels (~350 nm at approximately 70 nm per pixel) in distance to be considered colocalized (user definable). An additional MATLAB script uses nuclear masks and foci center x,y coordinate data from each channel to determine distances of nearest neighbor foci in a second channel from foci in the reference channel and generate distance frequency data (78). The script then generated the same number of random x,y points within the nuclear mask as were detected in the second channel. The distances from the centers of reference channel foci to nearest neighbor random points was then calculated and reported to within a user defined radius (60-pixel radius for data in this paper) of each reference focus. The resulting frequency distributions of reference-to-test channel distances and reference-to-random points were compared by the non-parametric Kolmogorov-Smirnov test. If the test rejects the null hypothesis at 5% significance, the test returns a value of 1, and 0 if the null hypothesis is not rejected. The test also returns an asymptotic p-value and a list of distances in pixel values which can then be plotted and further analyzed using GraphPad Prism (as it was here) or other data analysis packages. Foci detection and colocalization software and nearest neighbor analysis script are available for use: doi:10.5061/dryad.95fs76f; https://datadryad.org/review?doi=doi:10.5061/dryad.95fs76f

RT-qPCR quantification of viral transcripts

Total RNA was isolated using the Qiagen RNeasy kit per manufacturer's instructions. Resulting RNA was quantified, treated with DNAse (DNAfree Kit, Ambion), and reverse transcribed (High Capacity cDNA RT Kit, Applied Biosystems) to produce cDNA. Quantitative PCR was performed using Fast SYBR Green reagents (ThermoFisher) on a StepOnePlus from Applied Biosystems (ThermoFisher). Oligos for qPCR reactions are as follows:

ICP27 (mRNA) for GCATCCTTCGTGTTTGTCATT

ICP27 (mRNA) rev GCATCTTCTCTCCGACCCCG

ICP8 (mRNA) for GTCGTTACCGAGGGCTTCAA

ICP8 (mRNA) rev GTTACCTTGTCCGAGCCTCC

gB (mRNA) for TGTGTACATGTCCCCGTTTTACG

gB (mRNA) rev GCGTAGAAGCCGTCAACCT

18S (mRNA) for GCCGCTAGAGGTGAAATTCTTG

18S (mRNA) rev CTTTCGCTCTGGTCCGTCTT

Chromatin Immunoprecipitation

ChIP experiments were carried out as previously described in detail (Lee et al., 2016) with minor changes. Briefly, infected cell monolayers were fixed in 1% formaldehyde (Sigma-Aldrich) at 37ºC for 15 min. Fixation was quenched with

glycine at a final concentration of 125 mM for 3 min. Cells were washed 3 times in ice cold PBS supplemented with 1 mM phenylmethanesulfonylfluoride (PMSF), collected in PBS + PMSF, and pelleted at 2000 rpm for 5 min at 4ºC. Cell pellets were re-suspended in 1 mL lysis buffer (1% SDS, 10 mM EDTA, 50 mM Tris, pH 8.1), transferred to 15 mL polystyrene tubes and sonicated at 4ºC in a Diagenode Biorupter on high setting for 9 cycles of 5 min each (30 sec ON, 30 sec OFF). An aliquot of recovered chromatin was used for each IP reaction in 1 ml IP dilution buffer (150 mM NaCl, 10 mM Na_2HPO_4, 2 mM EDTA, 1.1% Triton, 0.1% SDS). An aliquot of a no antibody IP reaction was retained as 10% input sample. IPs were performed with 2.5 µg (6.0 µg for ATRX ab) of ChIP grade antibody (see Antibodies) per reaction and incubated overnight at 4ºC. 20 µl of MagnaChIP protein A magnetic beads (Millipore) were added for 2.5-3 hrs at 4ºC with rotation, washed 3 times with a cold low-salt buffer (150 mM NaCl, 20 mM Tris·HCl, pH 8.1, 2 mM EDTA, 1% Triton X-100, and 0.1% SDS, 1 mM PMSF) and 3 times with cold LiCl wash buffer (50 mM HEPES pH 7.5, 250 mM lithium chloride, 1 mM EDTA, 1% NP-40, 0.7% sodium deoxycholate, 1 mM PMSF), and washed once with cold Tris-EDTA buffer (10 mM Tris-HCl, pH 8, 1 mM EDTA). DNA-protein complexes were eluted in 100 µl of elution buffer (1% SDS, 0.1 M $NaHCO_3$) at 65ºC for 20 min. Protein-DNA crosslinks were reversed by adding NaCl (0.2 M final concentration) and incubating at 95ºC for 30 min followed by 1 h RNase A (Ambion) treatment at 37ºC and Proteinase K treatment (Roche) at 45ºC for 2 h.

DNA was purified using a QIAquick PCR purification kit (Qiagen) end eluted twice with 50 µl buffer EB for a final volume of 100 µl.

Quantitative-PCR was performed to quantify DNA using Fast SYBR Green reagents (ThermoFisher) on a StepOnePlus from Applied Biosystems (ThermoFisher). Oligos for qPCR reactions are as follows:

ICP27 Promoter (genomic)

FWD ACCCAGCCAGCGTATCCACC

REV ACACCATAAGTACGTGGC

ICP8 promoter (genomic)

FWD GAGACCGGGGTTGGGGAATGAATC

REV CCCCGGGGGTTGTCTGTGAAGG

GAPDH promoter (genomic)

FWD CAGGCGCCCAATACGACCAAAATC

REV TTCGACAGTCAGTCAGCCGCATCTTCTT

Author contributions:

J.M.C designed and executed research, analyzed data, and wrote the manuscript with the guidance and supervision of D.M.K. Significant assistance with developing methodologies associated with EdC-labeled virus and CRISPR-Cas9 knockout cell lines was provided by H.S.O.

Chapter Three: ATRX limits the accessibility of histone H3-occupied HSV genomes during lytic infection

Abstract

Histones are rapidly loaded on the HSV genome upon entry into the nucleus of human fibroblasts, but the effects of histone loading on viral replication have not been defined. To further investigate the roles that ATRX and other H3 chaperones play in restriction of HSV, we infected human fibroblasts that were systematically depleted of nuclear H3 chaperones. We found that the ATRX/DAXX complex is unique among nuclear H3 chaperones in its capacity to restrict ICP0-null HSV infection. No individual nuclear H3 chaperone was required for *de novo* deposition of H3 to input viral genomes, suggesting that H3 deposition occurs via redundant mechanisms. ChIP-seq for total H3 showed that HSV DNA is loaded with high levels of histones across the entire viral genome during infection. ATAC-seq analysis revealed that HSV DNA is accessible across the entire genome. However, HSV accessibility was enhanced in ATRX-KO cells, arguing that ATRX mediates viral DNA accessibility. Together, these findings support a model in which ATRX restricts viral infection by promoting chromatin stability through H3 retention and globally reduced accessibility of viral DNA during lytic HSV infection.

Introduction

Epigenetic regulation is fundamental to the control of appropriate basal cellular gene expression and changes in expression in response to replication, stress, and invading pathogens. Eukaryotic DNA is wrapped around nucleosomes which allow for higher orders of compaction and the formation of larger chromatin domains [reviewed in (Dixon et al., 2016)]. Nucleosomes are comprised of an octamer that contains 2 copies each of four core histone proteins, H2A, H2B, H3, and H4, around which can wrap a 147 base pair (bp) segment of DNA [reviewed in (Cutter and Hayes, 2015)]. DNA-wrapped nucleosomes can assemble into a 10nm fiber and form higher order structures that enhance DNA compaction (Maeshima et al., 2014) and form regions of active or inactive gene expression. Post-translational modifications (PTMs), such as methylation, can be added to the tails of core histone proteins that comprise nucleosomes to further define regions of active and inactive gene expression (Cutter and Hayes, 2015).

As a DNA virus, herpes simplex virus (HSV) is subject to epigenetic regulation by host cell machinery. The double-stranded DNA (dsDNA) genome of HSV is not associated with histones in the virion (Oh and Fraser, 2008; Pignatti and Cassai, 1980). However, several studies have shown that HSV genomes are rapidly loaded with histone H3 which is subsequently modified with repressive histone modifications such as histone H3 lysine 9 trimethylation (H3K9me3) and histone H3 lysine 27 trimethylation (H3K27me3) (Cabral et al., 2018; Cliffe and

Knipe, 2008; Kent et al., 2004; Lee et al., 2016; Oh and Fraser, 2008). The components of the cellular chromatin machinery that are responsible for loading histones onto viral DNA upon nuclear entry and whether the virus-associated histones are organized into proper nucleosomes are questions that remain to be answered.

Eukaryotic cells encode an array of histone chaperone proteins and complexes that are have roles in loading histones onto DNA. Histone chaperones preferentially affect specific histone deposition pathways. This is partially governed by their affinities for particular histone variants that are expressed at different points of the cell cycle or are associated with specific activities, such as the role that phosphorylated histone H2AX plays in DNA damage signaling . Histone H3 variants H3.1 and H3.2, for example, are only expressed during S phase while H3.3 is expressed throughout the cell cycle (Tagami et al., 2004). Histone variant/chaperone specificities can therefore influence deposition activity. The chromatin assembly factor-1 (CAF-1) complex preferentially loads canonical H3.1/3.2 onto DNA to replicating DNA (Tagami et al., 2004). Conversely, the α-thalassemia X-linked intellectual disability (ATRX) and death domain-associated (DAXX) proteins form a complex that preferentially promotes H3.3 occupation at telomeres and pericentric repeats in a replication-independent process while the HIRA and ATRX/DAXX complexes preferentially load H3.3 in a replication independent manner (Benson et al., 2006; Lewis et al., 2010). HIRA has a more generalized role in H3.3 loading, including histone loading at actively transcribed

genes and a gap-filling chromatin maintenance function that can compensate for CAF-1 loss during replication (Ray-Gallet et al., 2011; Tagami et al., 2004).

Conflicting reports have precluded consensus on the roles that H3 chaperones play in viral chromatin formation and restriction.(Cabral et al., 2018; Huh et al., 2016; Juhasz et al., 2018; Lukashchuk and Everett, 2010; McFarlane et al., 2019; Rai et al., 2017). HIRA and an upstream H3 chaperone, ASF1A, have been implicated in H3.3-biased occupation of histones on HSV DNA during lytic infection of HeLa cells . Unexpectedly, these reports also suggested that HIRA and ASF1A promote viral gene expression and replication. Conflicting with these observations, it was recently reported that during HSV infection, HIRA localizes to promyelocytic leukemia nuclear bodies (PML-NBs) after interferon stimulation and promotes the expression of interferon-stimulated genes . ATRX and DAXX have been well documented to inhibit numerous DNA viruses. The proteins have been shown to promote H3.3 occupation on the human cytomegalovirus (HCMV) (Albright and Kalejta, 2016), Epstein-Bar virus (EBV) (Tsai et al., 2014), and adenovirus (AdV) (Schreiner et al., 2013) genomes at late times post infection. However, we recently showed that histone deposition on HSV DNA did not strictly require ATRX but that ATRX stabilized HSV chromatin during lytic infection and inhibited viral gene expression [Chapter 2; (Cabral et al., 2018)]. Highlighting the importance of this pathway in DNA virus restriction, HSV, HCMV, EBV, AdV, and Kaposi's Sarcoma Associated Herpesvirus (KSHV) all encode proteins that disrupt

or degrade the ATRX/DAXX complex (Full et al., 2014; Jurak et al., 2012; Saffert and Kalejta, 2006; Schreiner et al., 2013; Tsai et al., 2011).

To gain a clear understanding of the mechanism and machinery that govern chromatin formation during early lytic HSV infection, we investigated which H3 chaperones are responsible for *de novo* deposition of H3 to the HSV genome and what restrictive potential they might have during lytic infection. Using a series of combinatorial depletions of nuclear H3 chaperones, we found that only the ATRX/DAXX complex could significantly restrict replication of an ICP0-null virus. When transcription was inhibited globally, we found that only a combinatorial depletion of ATRX/HIRA/ASF1A resulted in a significant decrease in total H3 deposition by 4 hours post infection, suggesting a highly redundant mechanism for chromatinizing naked DNA. Although not strictly required for *de novo* H3 deposition, ATRX was important for H3 retention on the viral genome, and ATAC-seq analysis revealed ATRX to be important for limiting HSV DNA accessibility before viral genome replication. The presence of ATRX also slowed the accumulation of open chromatin that was triggered by a virus-induced stress response. The results presented here argue for a model in which *de novo* H3 deposition happens in a redundant manner but requires ATRX for efficient retention of H3 during infection. Our results also argue that ATRX restricts viral DNA accessibility, possibly through enhanced H3 retention, and effectively delays progression of the viral lifecycle.

Results

The ATRX/DAXX complex is uniquely restrictive of HSV.

HSV encodes an E3 ubiquitin ligase, ICP0, that disrupts the restrictive effects of the ATRX/DAXX complex (Lukashchuk and Everett, 2010). It was reported previously that ICP0 promotes the proteasome-dependent degradation of ATRX during lytic HSV infection (Jurak et al., 2012). In agreement, we observed that the loss of ATRX requires ICP0, and loss of ATRX can be detected by 6-8 hpi (Supplemental Figure 3.1A). Using an EdC-labeled wild-type HSV (KOS-EdC) [Chapter 2; (Cabral et al., 2018)] we were able to verify that in the presence of ICP0, PML-NBs are disrupted and that PML staining is decreased by 2-3 hpi (Supplemental Figure 3.1B). Unlike PML, ATRX staining was not abolished; rather, it became diffuse throughout the nucleus of the infected cell. By four hours post-infection, just under 20% of infected cells displayed large ATRX aggregates (Supplemental Figure 3.1B-C). Similar ATRX aggregates had been observed in GFP-tagged ATRX proteins with a mutation (D217A) in the H3K4me0 binding pocket (Dhayalan et al., 2011). During infection with an ICP0-null HSV, rather than forming aggregates, ATRX localizes to prereplication compartments at 4 hpi (Supplemental Figure 3.1D). Because of the effects ICP0 exerts on ATRX, we conducted the following experiments with HSV-1 7134 (7134) that is ICP0-null.

We showed recently that despite its ability to restrict HSV gene expression and replication, ATRX is not strictly required for the initial deposition of H3 to incoming HSV genomes [Chapter 2; (Cabral et al., 2018)]. To determine if other

nuclear H3 chaperone complexes could also restrict HSV replication, we used siRNA to systematically deplete hTERT-immortalized human foreskin fibroblasts (TERT-HF) of H3 chaperone components (Figure 3.1A-B). At 72 hours after siRNA treatment, we infected cells with 7134 virus at an MOI of 0.1 for 48 hours. Interestingly, ATRX was the only H3 chaperone whose depletion resulted in a significant increase in HSV yields (Figure 3.1 C). While not statistically significant, depletion of DAXX, the binding partner of ATRX, increased viral yield by approximately 5-fold (Figure 3.1C). Depletion of HIRA, another nuclear H3.3 specific chaperone complex that has been implicated in loading H3.3 to HSV genomes, resulted in minor decreases in viral yield. Depletion of CHAF1A, a component of the replication-dependent H3.1/3.2 chaperone complex CAF-1, also resulted in minor increases in viral yield (Figure 3.1C). Likewise, depletion of ASF1A and ASF1B, H3 chaperones that are thought to function in the HIRA/ATRX/DAXX and CAF-1 pathways, respectively, had minor effects on viral yield (Figure 3.1C). Depletion of HIRA in normal human foreskin fibroblasts (HFF) also had little effect on viral yield while depletion of ATRX or DAXX greatly increased vial yield (Supplemental Figure 3.2A). Surprisingly, depletion of SSRP1, a component of the transcriptionally-coupled FACT complex, resulted in decreased viral yields (Figure 3.1C). This observation, combined with a recent report that components of the FACT complex, including SSRP1, associate with input viral DNA throughout the first 6 hours of infection (Dembowski and DeLuca, 2018), suggested that the FACT complex plays a role in promoting viral

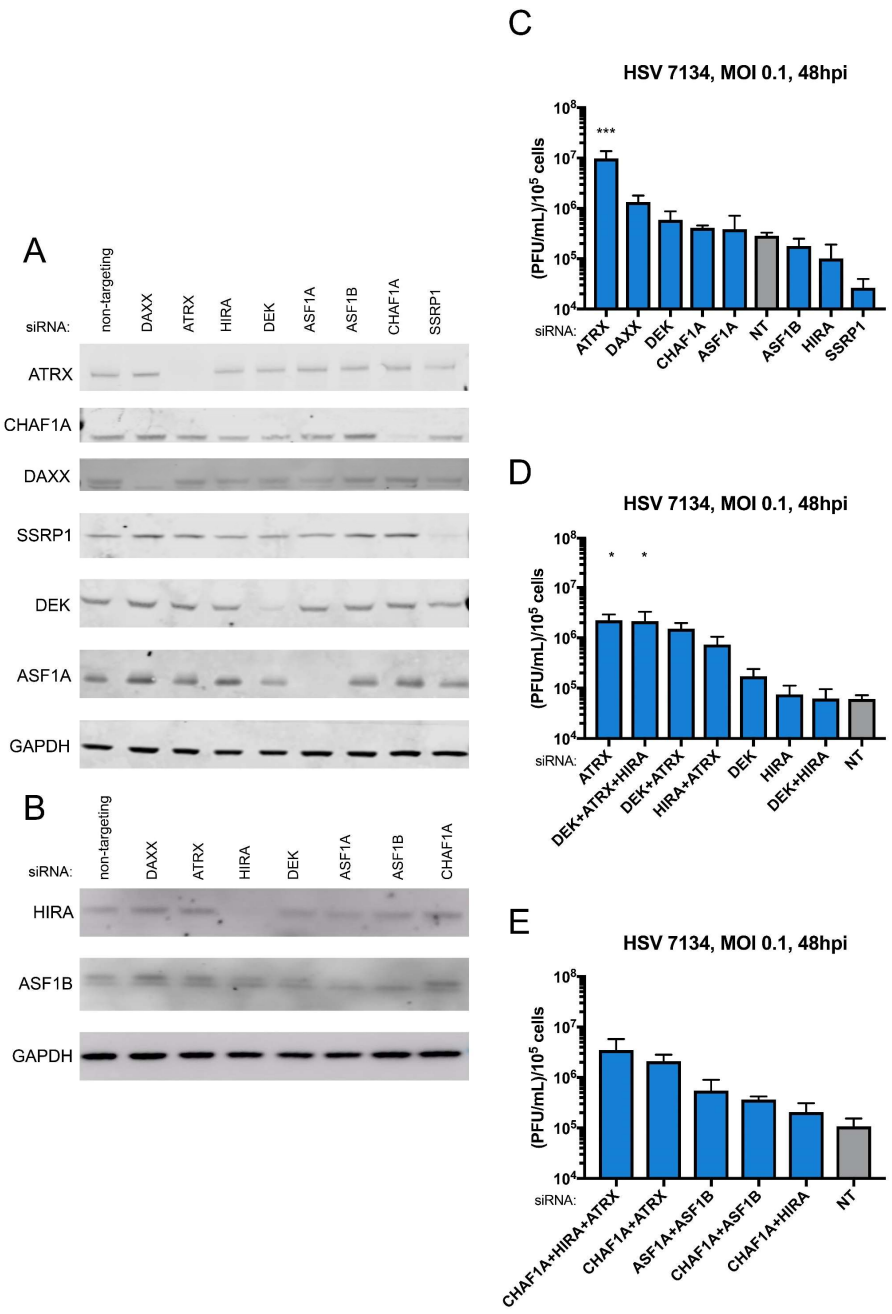

Figure 3.1: ATRX is more restrictive of HSV than other nuclear H3 chaperones.

(A) Immunoblot of lysates from TERT-HF cells treated with siRNA against nuclear H3 chaperones ATRX, CHAF1A, DAXX, SSRP1, DEK, ASF1A using a LiCor Odyssey imager. (B) Immunoblot of nuclear TERT-HF cells treated with siRNA against nuclear H3 chaperones HIRA and ASF1B using x-ray film. Viral yields from TERT-HF cells treated with siRNAs (C) against non-targeting, ATRX,

Figure 3.1 (Continued) CHAF1A, DAXX, SSRP1, DEK, ASF1A, HIRA, and ASF1B or (D) combinatorial siRNA treatments against ATRX, DEK, and HIRA or (E) combinatorial siRNA treatments against CHAF1A, HIRA, ATRX, ASF1A, and ASF1B which were infected with HSV 7134 at an MOI of 0.1. Viral lysates were collected at 48 hpi and titrated on U2OS cells. Yields were normalized to (PFU/mL)/1x10^5 cells. Results were analyzed by One-way ANOVA using Dunnet's multiple comparison correction. Data are reported as the average of 3 independent experiments ± standard error of the mean; $p < 0.05$ (*), $p < 0.01$ (**), $p < 0.001$ (***).

transcription. The same study also observed that DEK associated with the viral genome for most of the first 6 hours of infection. DEK was recently described as a H3.3 chaperone that regulates H3.3 distribution to HIRA and ATRX/DAXX (Ivanauskiene et al., 2014). Despite DEK's association with input HSV genomes, we found that depletion of DEK resulted in a minor increase in viral yield. Combinatorial depletions of nuclear H3 chaperones yielded the large increases in viral yield when ATRX was also depleted (Figure 3.1D-E). Coupled with our previous observation that H3 loading to input viral DNA is ATRX-independent, these results indicated that the ATRX/DAXX complex is more potently restrictive of HSV infection than other nuclear H3 chaperones.

ATRX but not DEK or HIRA is required to maintain viral chromatin during lytic infection.

We next investigated if HIRA or DEK, like ATRX, are required to maintain viral chromatin during lytic infection. We demonstrated recently that ATRX is required to maintain viral chromatin stability during chromatin stress, such as during transcription and DNA replication, but it is not known if other H3 chaperones also contribute to viral chromatin stability. Because it has been reported that H3.3 preferentially associates with HSV DNA during lytic infection (Placek et al., 2009), we depleted TERT-HFs of H3.3 chaperones ATRX, HIRA, and DEK to investigate the effects on viral chromatin and gene expression. Using chromatin

immunoprecipitation-quantitative polymerase chain reaction (ChIP-qPCR) with a pan-histone H3 antibody and cell lysates at 8 hours post infection (hpi) with 7134 virus, we detected a decrease in total H3 only in cells that were depleted for ATRX (Figure 3.2 A-B). Similarly, viral genomes were elevated in ATRX-depleted cells when compared to siNT, siDEK, and siHIRA treated cells (Figure 3.2C). Combinatorial co-depletions of HIRA, DEK, and ATRX resulted in viral H3 decreases that were similar to those observed with ATRX-depletion alone (Figure 3.2A-C). Viral transcript levels from immediate-early (IE), early (E), and late (L) viral genes, as represented by those from the *ICP27*, *ICP8* and *gB*, respectively, increased when ATRX was depleted. Co-depletion of ATRX with DEK and/or HIRA did not greatly enhance viral gene expression beyond ATRX depletion alone (Figure 3.2D-E). Depletion of DEK and HIRA together resulted in elevated *ICP8* transcript levels that were above that of ATRX-depletion (Figure 3.2B). Co-depletion of DEK and HIRA also resulted in a minor increase in *gB* expression but not *ICP27* (Figure 3.2D). Inhibition of viral DNA synthesis with acyclovir, a viral polymerase-specific inhibitor, in conjunction with depletions yielded similar results (Figure 3.2E). Together, these results demonstrated that maintenance of viral chromatin does not require DEK or HIRA, but it does require a unique activity of ATRX that protects viral chromatin stability.

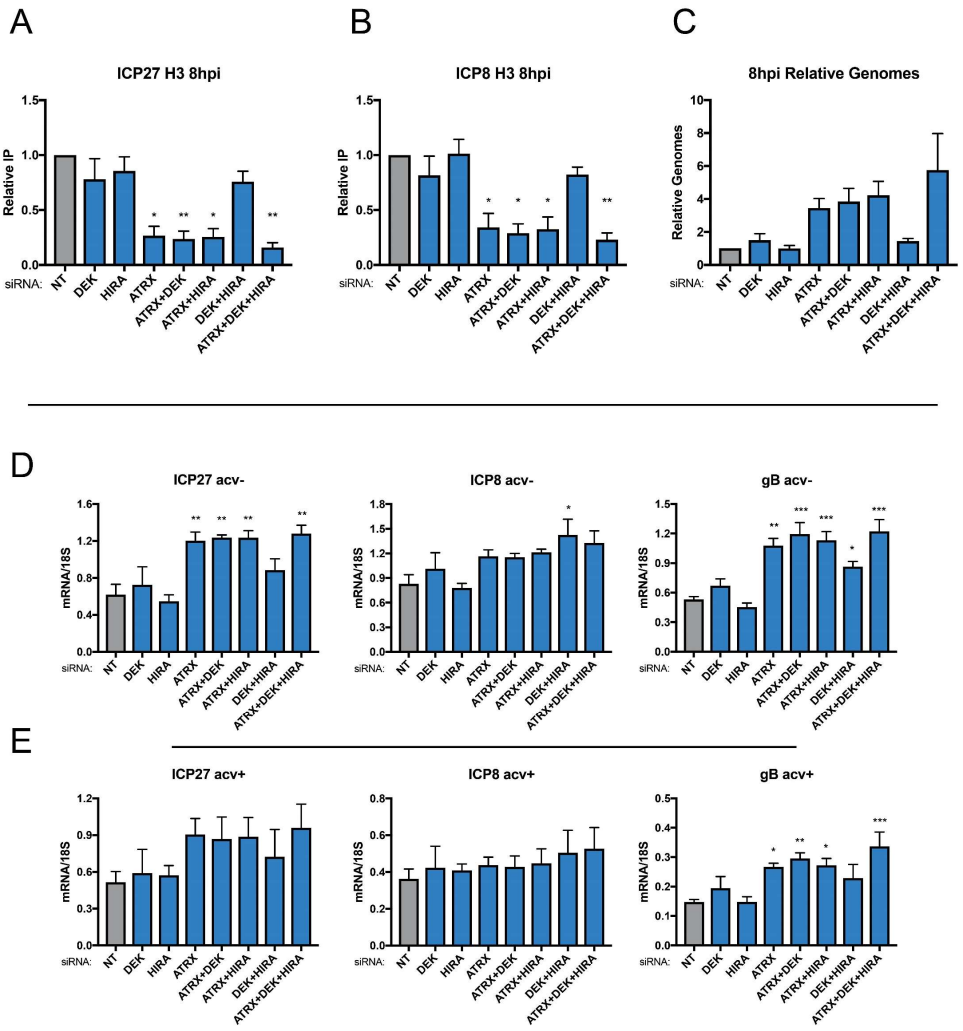

Figure 3.2: ATRX but not DEK or HIRA is required to maintain viral chromatin during lytic infection.

TERT-HF cells were infected with HSV 7134 at an MOI of 3. Infected cells were fixed and harvested 8 hpi. ChIP-qCPR using a pan-H3 antibody and HSV specific primers were used to detect enrichment of H3 at viral gene promoters for (A) *ICP27* and (B) *ICP8*. Results reported as Relative IP (the percent of input immunoprecipitated by each antibody normalized to the 8-hour control sample - set to 1.0 for each replicate). Results were analyzed by one sample T-test. (C) Chromatin input for ICP8 relative to input GAPDH to determine relative viral genome copy numbers. (D) TERT-HFs were treated with siRNAs against non-targeting (NT), ATRX, HIRA, and

Figure 3.2 (Continued) DEK and infected with HSV 7134 at an MOI of 5 in the (D) absence or (E) presence of acyclovir (ACV). Relative viral transcripts for *ICP27*, *ICP8*, or *gB* were quantified by qPCR at 8 hpi. Viral mRNA levels were normalized to cellular 18S transcripts. Results were analyzed by One-way ANOVA using Dunnet's multiple comparison correction. Data are reported as the average of 3 independent experiments ± standard error of the mean; $p < 0.05$ (*), $p < 0.01$ (**), $p < 0.001$ (***).

H3 chaperones exhibit redundant characteristics.

Histone chaperones have been shown to act in a redundant manner in which the loss of one chaperone may be compensated for by the activity of another (Ray-Gallet et al., 2011; Silva et al., 2012). To determine if the initial deposition of H3 to the input viral DNA occurs through a single chaperone or a redundant system of H3 chaperones, we used siRNAs to deplete TERT-HFs of H3 chaperones individually or in combination. Because transcription disturbs chromatin stability (Schwabish and Struhl, 2004), we used the CDK9 inhibitor flavopiridol to inhibit transcription during infection to determine which H3 chaperones may be responsible for *de novo* H3 deposition rather than maintenance. At 4 hpi with 7134 virus, single depletion of H3 chaperones did not result in large decreases in H3 occupation at the *ICP27* or *ICP8* gene promoters (Figure 3.3A-B). Similarly, double depletion of H3 chaperones resulted in minor or no decreases in viral H3. However, triple depletion of HIRA/ASF1A/ATRX consistently resulted in an approximate 30% reduction of viral H3 at both the *ICP27* and *ICP8* gene promoters (Figure 3.3 A-B). This demonstrated that the initial deposition of H3 to incoming viral DNA is not dependent on any one nuclear H3 chaperone. Rather, it suggested that H3 is deposited through redundant mechanisms. Additional H3 chaperones may play a role in redundant H3 deposition, or H3 deposition may also occur through non-canonical pathway such as the one suggested to be mediated by the NAP1-Like proteins (Torigoe et al., 2011; Vlijm et al., 2012).

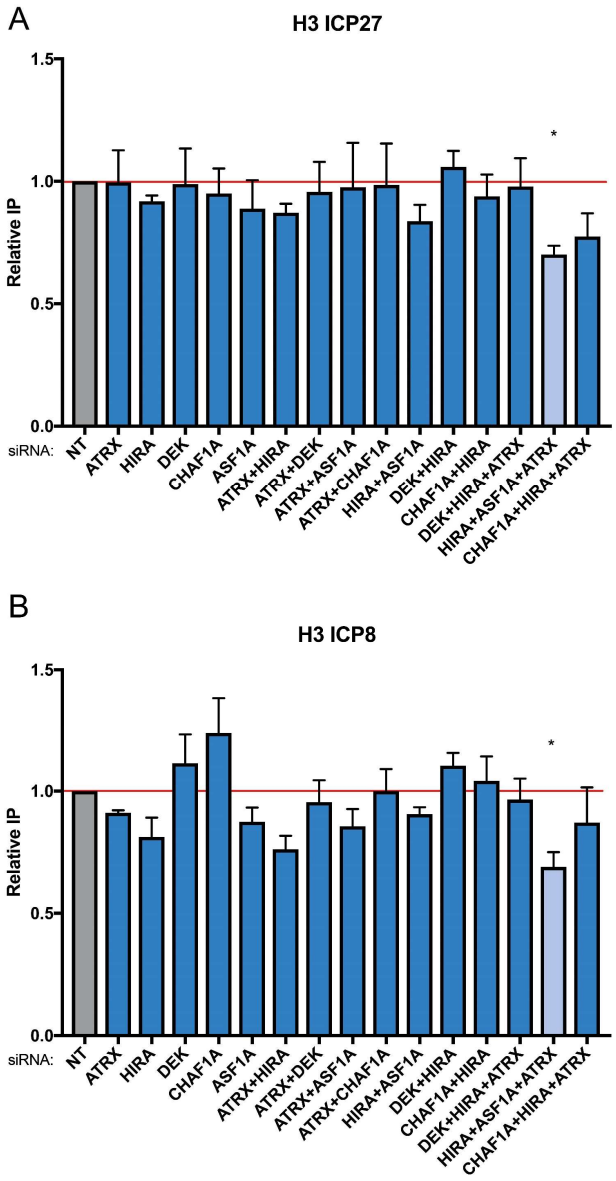

Figure 3.3: H3 chaperones exhibit redundant behavior.

TERT-HF cells were treated with siRNAs against non-targeting (NT), ATRX, HIRA, DAXX, CHAF1A, DEK, and ASF1A. 72 hours post siRNA treatment, cells were infected with HSV 7134 at an MOI of 3 in the presence of flavopiridol. Infected cells were fixed and harvested 8 hpi. ChIP-qCPR using a pan-H3 antibody and HSV specific primers were used to detect enrichment of H3 at viral gene promoters for (A) *ICP27* and (B) *ICP8*. Results reported as Relative IP (the percent of input immunoprecipitated by each antibody normalized to the 8-hour control sample - set to 1.0 for

Figure 3.3 (Continued) each replicate). Results were analyzed by one sample T-test. Data are reported as the average of 3 independent experiments ± standard error of the mean; $p < 0.05$ (*), $p < 0.01$ (**), $p < 0.001$ (***).

ATRX-mediated restriction of HSV does not require H3K9me3 histone lysine methyltransferases.

ATRX and DAXX have been shown to promote H3K9me3 at telomeres and to interact with histone methyltransferases (HMTs) SUV39H1 and SETDB1 (Elsasser et al., 2015; Valle-García et al., 2016). Therefore, we investigated if ATRX restricts HSV infection through either of these HMTs. Depletion of SETDB1 by siRNA was less robust than were depletions of ATRX and SUV39H1, but it did result in diminished protein (Figure 3.4A). While depletion of ATRX-alone resulted in a significant increase in HSV yield, co-depletion with SETDB1 and/or SUV39H1 resulted in minor decreases compared to ATRX-alone (Figure 3.4B). Single depletion of SETDB1 had only a minor effect in viral yield, while depletion of SUV39H1 resulted in a consistent decrease. This was also observed when ATRX-knockout (ATRX-KO) and CAS-9 only control (Control) cells [Chapter 2; (Cabral et al., 2018)] were treated with chaetocin (10nM), an inhibitor of SUV39H1 (Figure 3.4C), indicating the decrease in viral yield was not an off-target effect of siRNA treatment. It is possible that H3K9me2 is sufficient to restrict HSV replication; however, depletion of G9A, an H3K9me2 HMT, had no effect on viral yield (Supplemental Figure 3.3A). SUV39H1 depletion had no effect on viral H3K9me3 levels at 4 hpi. In contrast, depletion of SETDB1 resulted in a modest but significant decrease in H3K9me3 (Figure 3.4D). The poor knockdown of SETDB1 by siRNA may mask the extent to which SETDB1 affects H3K9me3 on the viral

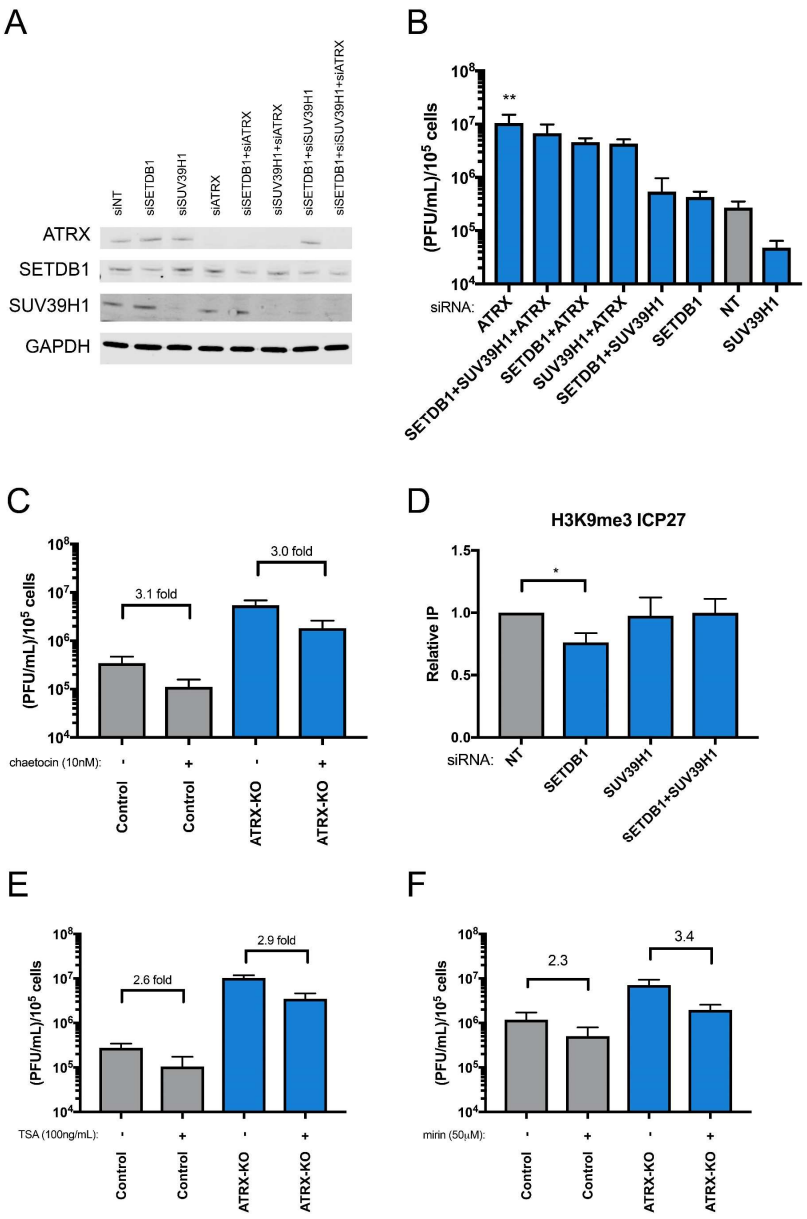

Figure 3.4: Inhibitors of SUV39H1, HDAC class I and II, and MRE11 similarly reduce HSV 7134 viral yields.

(A) Immunoblot of lysates from TERT-HF cells treated with siRNA against non-targeting (NT), ATRX, SUV39H1, and SETDB1. (B) Viral yields from TERT-HF cells treated with siRNAs against non-targeting, ATRX, SUV39H1, and SETDB1 which were infected with HSV 7134 at an MOI of 0.1. Viral lysates were collected at 48 hpi and titrated on U2OS cells. Yields were normalized to

Figure 3.4 (Continued) (PFU/mL)/1x10^5 cells. Results were analyzed by One-way ANOVA using Dunnet's multiple comparison correction. (C) Viral yields from ATRX-KO and Control cells which were infected with HSV 7134 at an MOI of 0.1 in the presence of SUV39H1 inhibitor, chaetocin, following a 1 hour pre-treatment. Viral lysates were collected at 48 hpi and titrated on U2OS cells. Yields were normalized to (PFU/mL)/1x10^5 cells. (D) TERT-HF cells were treated with siRNAs against non-targeting (NT), ATRX, SUV39H1, and SETDB1. 72 hour post siRNA treatment, cells were infected with HSV 7134 at an MOI of 3. Infected cells were fixed and harvested 8 hpi. ChIP-qCPR using a pan-H3 antibody and HSV specific primers were used to detect enrichment of H3 at the viral gene promoter for *ICP27* Results reported as Relative IP (the percent of input immunoprecipitated by each antibody normalized to the 8-hour control sample - set to 1.0 for each replicate). Results were analyzed by one sample T-test. (E and F) (C) Viral yields from ATRX-KO and Control cells which were infected with HSV 7134 at an MOI of 0.1 in the presence of an (E) HDAC class I and II inhibitor, trichostatin A (TSA), or an MRE11 inhibitor, mirin, following a 1 hour pre-treatment. Viral lysates were collected at 48 hpi and titrated on U2OS cells. Yields were normalized to (PFU/mL)/1x10^5 cells. Data are reported as the average of 3 independent experiments ± standard error of the mean; $p < 0.05$ (*), $p < 0.01$ (**), $p < 0.001$ (***).

DNA, warranting further study of this HMT mechanism. Curiously, co-depletion of SETDB1 and SUV39H1 had no effect on viral H3K9me3 levels. Overall, these results suggested that while SETDB1 promoted H3K9me3 on viral chromatin, neither SETDB1 nor SUV39H1 were required for ATRX-mediated restriction of HSV.

ATRX-mediated restriction of HSV is independent of its role in HDAC recruitment and regulation of MRE11 activity.

The ATRX/DAXX complex has numerous roles in regulating chromatin that extend beyond its role as a histone chaperone. DAXX has been shown to regulate gene expression though recruitment of histone deacetylases (HDAC) (Hollenbach et al., 2002; Yao et al., 2014), and it has been proposed that DAXX restricts human cytomegalovirus (HCMV) through recruitment of an HDAC (Saffert and Kalejta, 2006). We infected ATRX-KO and Control cells treated with and without an HDAC inhibitor, trichostatin A (TSA) (100ng/mL). Viral yields were reduced similarly in ATRX-KO and Control cells treated with TSA when compared to cells treated with vehicle only (Figure 3.4E). The reduction of viral yield during TSA treatment was surprising and conflicts with a previous report that TSA treatment can enhance ICP0-null HSV gene expression (Poon et al., 2003). However, a more recent study described a reduction in the number of HSV genomes initiating expression in TSA treated cells (Shapira et al., 2016). While the effects of HDAC inhibitors on HSV yields requires further study to clarify conflicting reports, in either case, the HSV

replication was not differentially affected in ATRX-KO cells versus control cells during TSA treatment. Thus, it is unlikely ATRX requires HDAC activity to restrict HSV.

Several groups reported recently that ATRX can inhibit the activity of MRE11 during double-strand break repair (Clynes et al., 2015; Huh et al., 2016). It has also been reported that MRE11 supports HSV replication (Lilley et al., 2005). While MRE11 and ATRX do not colocalize at 1 hpi (Supplemental Figure 3.4A), both ATRX and MRE11 localize to replication compartments, as marked by ICP8, by 6 hours post infection with HSV 7134 (Supplemental Figure 3.4B). Although MRE11 and ATRX colocalized at 6 hpi, inhibition of MRE11 activity by treatment with mirin (50μM) resulted in similar reductions in viral yield in both ATRX-KO and Control cells compared to untreated cells (Figure 3.4F). This finding argued that ATRX does not restrict HSV through the inhibition of MRE11 activity.

Loss of ATRX enhances viral gene expression but has little effect on cellular gene expression.

Because ATRX-mediated viral restriction did not appear to be through *de novo* histone deposition, HMT or HDAC recruitment, or MRE11 inhibition, we next investigated if loss of ATRX induced changes in cellular gene expression that could account for the ATRX-mediated restriction of HSV. Using ATRX-KO and Control cells, we performed RNA-sequencing (RNA-seq) analysis using poly(A)-enriched RNA harvested from infected and uninfected cells. We infected control

cells that only express Cas9 (Control) with wild-type HSV (WT) as a control. Validating our RNA-seq data, the expression pattern of HSV genes observed from WT infected cells at 8 hpi (Figure 3.5A) closely resembled the gene expression pattern described for this virus at this time point (Harkness et al., 2014). As observed during our qPCR-based experiments, HSV gene expression was enhanced in ATRX-KO cells (Figure 3.5A-C). At 8 hours post infection, HSV reads constituted 22%, 38.2%, and 59% of all mapped reads (human + HSV) in Control cells infected with 7134, ATRX-KO cells infected with 7134, and Control cells infected with KOS, respectively (Figure 3.5B). All HSV genes showed enhanced gene expression in ATRX-KO when compared to HSV expression in Control cells at 8 hpi (Figure 3.5C). These findings validated our previous results and revealed that ATRX affects HSV gene expression globally.

We next investigated the effects that ATRX depletion has on cellular gene expression. Surprisingly, cellular gene expression in ATRX-KO cells was remarkably similar to Control cells (Figure 3.5D). Only 63 genes were upregulated by >2-fold, and only 48 genes were down regulated by >2-fold in ATRX-KO cells (Supplemental table 3.1). No known HSV restriction factors were comparatively down regulated in ATRX-KO cells. Changes in cellular gene expression during 7134 infection were also similar between Control and ATRX-KO cells (Figure 3.5E and F). Even at 8 hpi, the cellular gene expression of Control and ATRX-KO cells was very similar and included relative upregulation of several heat shock-related

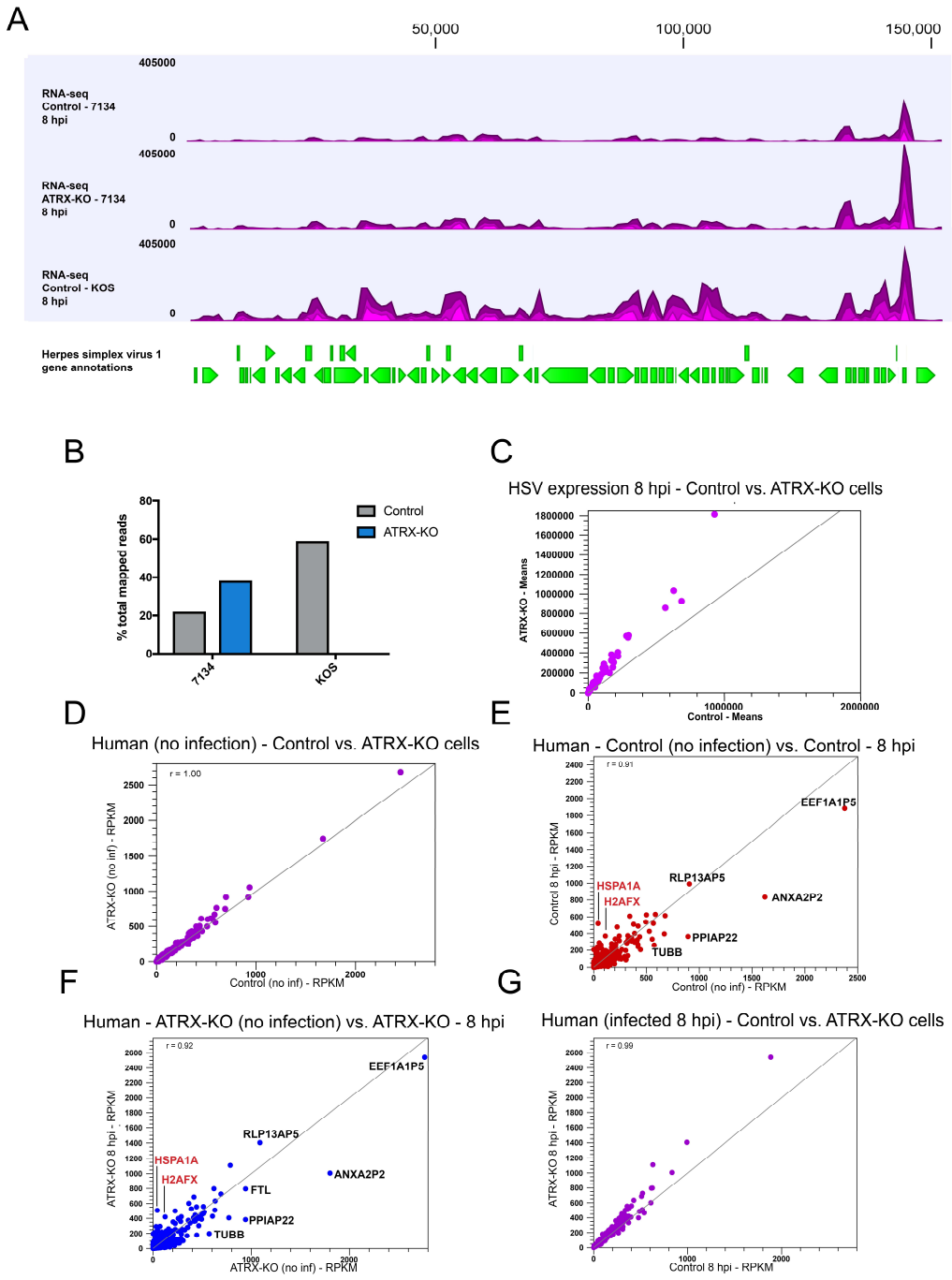

Figure 3.5: Loss of ATRX enhances viral gene expression but does not greatly alter cellular gene expression.

(A) RNA-seq read coverage of the HSV genome from poly(A) enriched RNA harvested at 8 hpi from ATRX-KO and Control cells were infected with either KOS or 7134 HSV strains at an MOI of

Figure 3.5 (continued) 5. HSV reads were normalized to mapped human reads. (B) Reads mapped to the HSV genome as a percentage of total mapped reads (HSV+human) per sample. (C) Differential read count of normalized reads mapped to the HSV genome in ATRX-KO cells/Control cells at 8 hpi with 7134. (D-G) Differential gene expression in reads per kilobase of transcript, per million mapped reads (RPKM) for human genes in (D) uninfected ATRX-KO cells/uninfected Control cells, (E) 7134 infected Control cells 8 hpi/uninfected Control cells, (F) 7134 infected ATRX-KO cells at 8 hpi/uninfected ATRX-KO cells, and (G) 7134 infected ATRX-KO cells 8 hpi/7134 infected Control cells 8 hpi.

proteins (Figure 3.5G, Supplemental Table 3.2). The gene that stands out as differentially expressed between ATRX-KO and Control cells, both before and during infection, is TERT. Transcription is likely driven by changes in the regulation of the hTERT transgene used to immortalize these fibroblasts (Bresnahan et al., 2000). ATRX and DAXX have been shown to regulate expression from a CMV promoter-driven transgene array (Newhart et al., 2012) which may explain the increased expression in ATRX-KO cells in uninfected cells. However, ATRX is also restrictive in HFFs which are telomerase-deficient (Supplemental Figure 3.2A), so it is unlikely that the restrictive effects of ATRX are due to the increase in TERT expression. The similarities in cellular gene expression between ATRX-KO and Control cells both before and during HSV infection argued that the ATRX-mediated restriction of HSV is likely the result of a direct rather than indirect effect.

ATRX limits HSV genome accessibility during early lytic infection.

We next investigated the effects of ATRX on HSV DNA accessibility using Assay for Transposase-Accessible Chromatin using sequencing (ATAC-seq). ATRX has been shown to play a major role in chromatin stability during replication and DNA repair (Huh et al., 2016; Huh et al., 2012; Juhasz et al., 2018; Koschmann et al., 2016; Udugama et al., 2018). ATRX has also been reported to affect chromatin susceptibility to micrococcal nuclease (MNase) digestion (Sadic et al., 2015). To test if ATRX likewise affects HSV DNA accessibility, we infected Control and ATRX-KO cells with 7134 and performed ATAC-seq at 4 and 8 hpi. The HSV

genome was more susceptible to the TN5 transposase in ATRX-KO at both 4 and 8 hpi (Figure 3.6A). The ATAC-seq reads were distributed across the entire HSV genome at both 4 and 8 hpi, indicating a high level of accessibility. Validating the mapping of reads to the HSV genome, little or no read coverage was observed at either ICP0 gene locus as ICP0 is deleted from the 7134 genome (Figure 3.6A). Despite having similar copy numbers at 4 hpi (Figure 3.6B), HSV DNA accounted for 10.9% of all mapped reads (human + HSV) at 4 hpi in ATRX-KO cells while HSV DNA accounted for 1.3% in Control cells (Figure 3.6C). By 8 hpi, these numbers increased to 16.4% and 27.5% in Control and ATRX-KO cells, respectively. The large increases in HSV accessibility from 4 to 8 hpi in both cell lines may reflect newly replicated HSV genomes that are almost entirely unprotected. In support of this, while the total number of reads mapping to the HSV genome is different at 8 hpi in ATRX-KO and Control cells, the distribution pattern is remarkably similar (Figure 3.6A). A possible interpretation of this observation is that the nascently replicated HSV genomes are almost entirely accessible to the Tn5 transpose. The signal from these genomes may obscure signal from input HSV genomes.

The distribution of sequenced fragment lengths in both ATRX-KO and Control cells revealed a bimodal distribution of fragment lengths that mapped to the human genome, with peaks at 200 bp and 400 bp that indicate enrichment for DNA fragment that correspond to mono- and di-nucleosome protected DNA (Figure 3.6D). Unlike cellular reads, the distribution of HSV reads was not bimodal

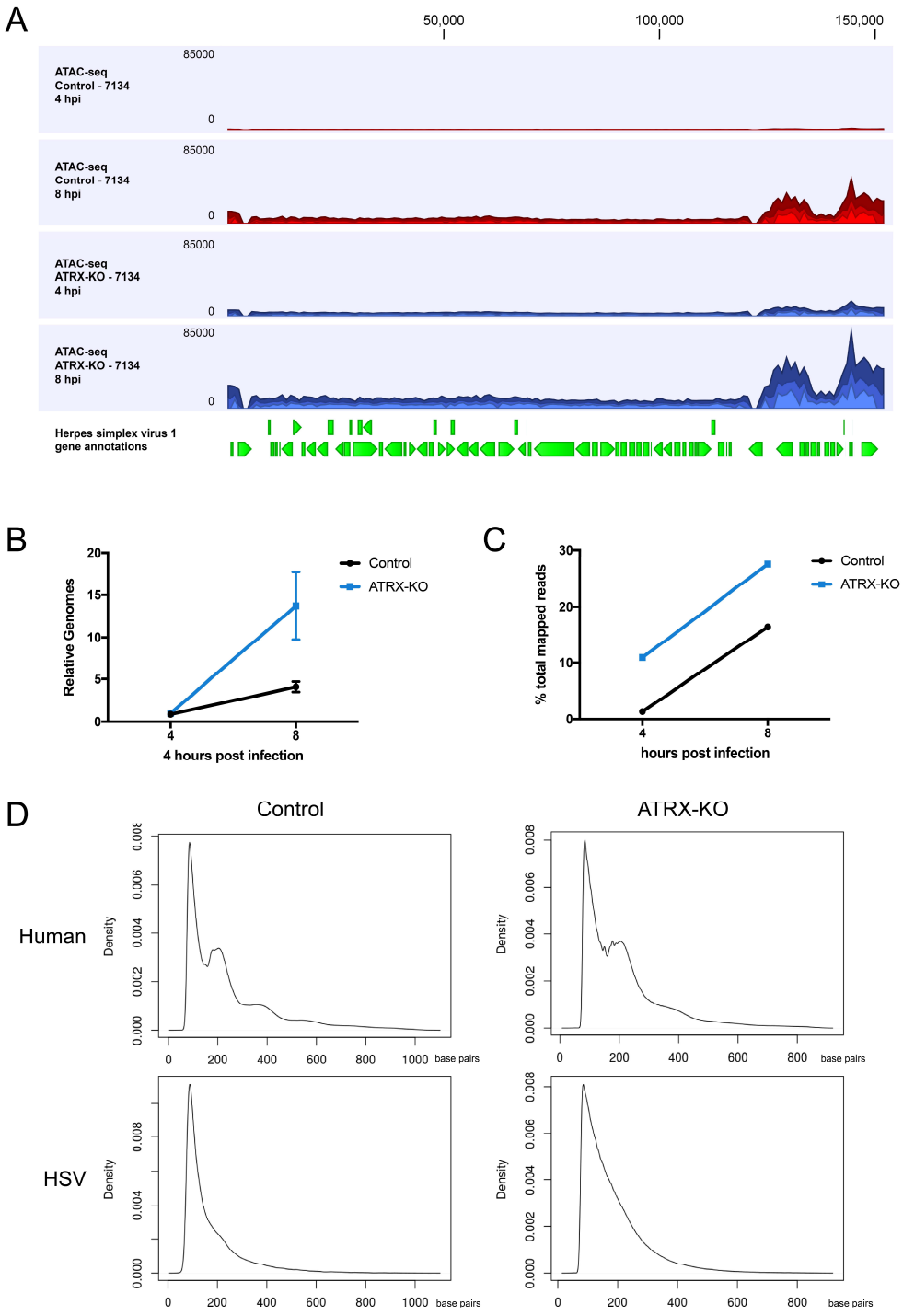

Figure 3.6: ATRX limits HSV genome accessibility.

(A) ATAC-seq read coverage of mapped HSV reads normalized to total mapped human reads from (blue) ATRX-KO or (red) Control cells at 4 and 8 hi with 7134. (B) Relative HSV genome

Figure 3.6 (Continued) quantification by qPCR analysis of *ICP8/GAPDH* signals in TN5 treated ATRX-KO and Control samples at 4 and 8 hpi with 7134. (C) ATAC-seq reads mapped to the HSV genome as a percentage of total mapped reads (HSV+human) in ATRX-KO and Control cells at 4 and 8 hpi. (D) Sequenced fragment length distribution for ATAC-seq reads mapped to the human and HSV genomes in Control and ATRX-KO cells 4 hpi with 7134.

and did not show enrichment for ~200 bp (Figure 3.6D). However, the 4 hpi Control sample did show a flattening of the sequenced fragment length histogram at around 200 bp. This may indicate that a minor subpopulation of HSV DNA fragments were protected in nucleosomes in the presence of ATRX. High levels of H3 were detected by chromatin immunoprecipitation sequencing (ChIP-seq) across the whole HSV genome by 4 hpi, and H3 levels continued to increase through 8 hpi in both ATRX-KO and Control cells (Figure 3.7A). Despite having equal numbers of genomes at 4 hpi and more genomes than Control at 8 hpi (Figure 3.7B), the levels of HSV-associated H3 were lower in ATRX-KO cells than Control at both timepoints (Figure 3.7C). To avoid normalization issues arising from differences in genome copy number due to active viral DNA synthesis, we normalized HSV reads to the mapped human reads rather than an input signal. ChIP-qPCR studies have shown that H3 is reduced over time on replicating HSV genomes in the presence of ICP0 (Cliffe and Knipe, 2008; Lee et al., 2016). We showed recently that a reduction in H3 signal/input signal on ICP0-null HSV genomes was blocked by treatment with a viral polymerase-specific inhibitor, phosphonoacetic acid (PAA) [Chapter 2; (Cabral et al., 2018)]. Taken together with these studies, the H3 ChIP-seq results supported a model in which ATRX promotes the continued accumulation of H3 on the ICP0-null HSV genome over time and that progeny DNA is not loaded with as high of levels of H3 as are the parental genomes. In conjunction with ATAC-seq analysis, the results argued that

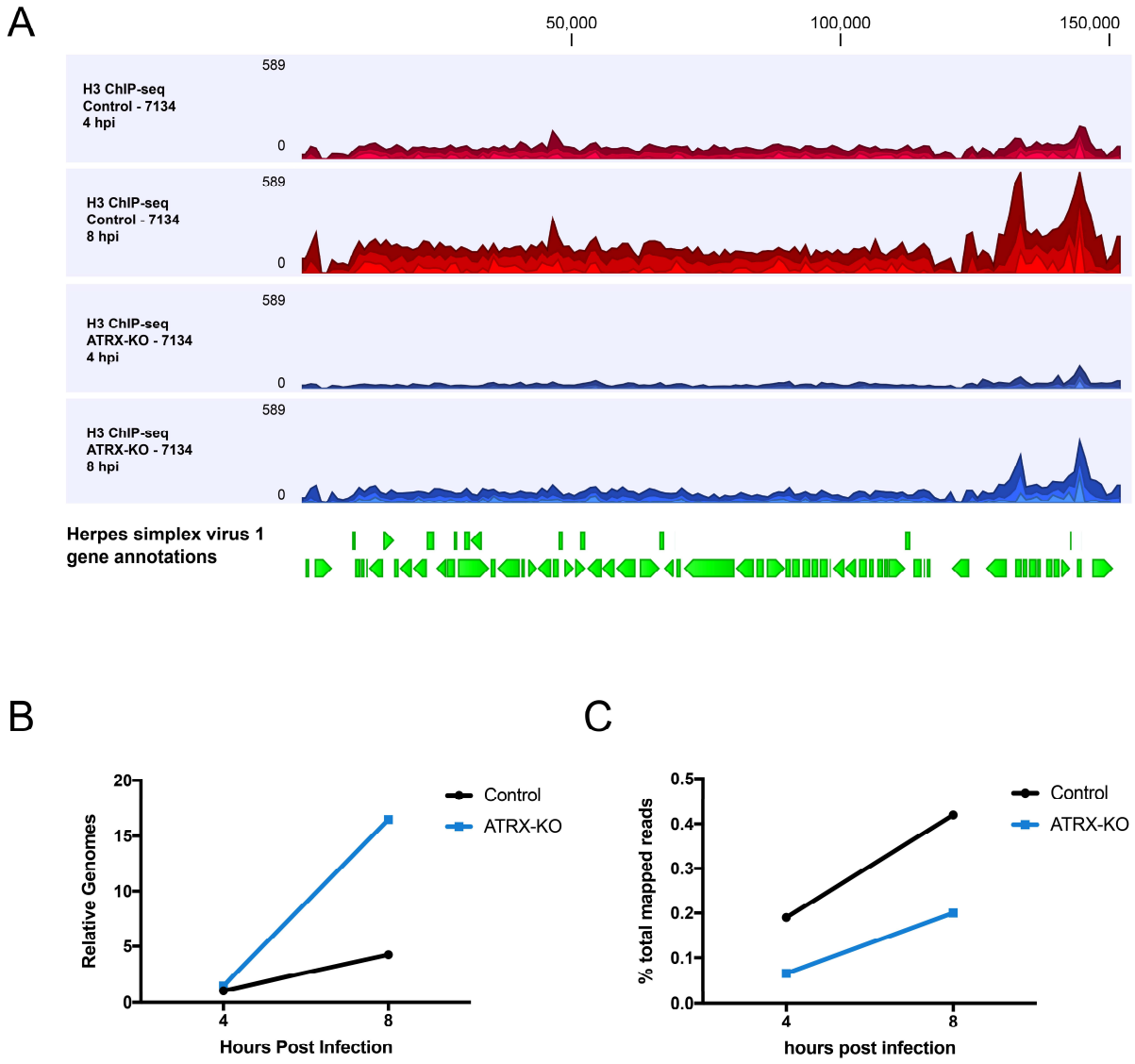

Figure 3.7: ATRX promotes H3 enrichment on the HSV genome during lytic infection.

(A) Total H3 ChIP-seq coverage for mapped HSV reads normalized to total mapped human reads from (blue) ATRX-KO or (red) Control cells at 4 and 8 hi with 7134. (B) Relative HSV genome quantification by qPCR analysis of *ICP8/GAPDH* signals in total H3 ChIP-seq ATRX-KO and Control samples at 4 and 8 hpi with 7134. (C) ChIP-seq reads for total H3 that mapped to the HSV genome as a percentage of total mapped reads (HSV+human) in ATRX-KO and Control cells at 4 and 8 hpi.

HSV genomes are not generally organized into proper nucleosomes after nuclear entry despite high levels of H3 across the genome. These observations revealed that ATRX exerts its restrictive effects on HSV globally rather than through a site-specific activity, possibly through enhanced H3 retention and reduced accessibility to input HSV genomes.

HSV actively induces a cellular stress response that globally upregulates histone gene expression.

It was reported recently that infection with wild type HSV induces a salt- and heat shock-like disruption of host transcription termination (DoTT), transcription downstream of genes (DoG), and results in an increase of open chromatin regions (OCRs), especially downstream of poly(A) sites (Hennig et al., 2018; Rutkowski et al., 2015). To validate our data, we used our ATAC-seq and RNA-seq data sets to verify the Hennig et al. observation that SLC12A2 and the region downstream of the gene were enriched for OCRs and showed evidence of DoTT by 8 hpi (Supplemental Figure 3.5A). Further analysis of ATAC-seq results revealed that over 600 cellular genes exhibited increased OCRs in ATRX-KO versus Control cells at 4 hpi with 7134, including heat shock-related proteins such as HSP70 and HSP40 (Figure 3.8A). Gene ontology (GO) term enrichment analysis of genes exhibiting increased OCRs found that terms related to translation, including ribosomal subunits and elongation initiation factors, were particularly enriched (Figure 3.8B). We also found that several housekeeping genes commonly used for

normalization, such as GAPDH, showed changes in accessibility during infection (Supplemental Figure 3.5B).

Genes with increased OCRs, were particularly enriched for histone genes (Figure 3.8C-D). Histone genes were also enriched for elevated relative transcript levels (Supplemental Table 3.3). The H2AFX gene, which encodes a histone protein involved in the DNA damage response, had a 3.2-fold increase in ATAC-seq reads in ATRX-KO cells at 4 hpi as compared to Control cells, but by 8 hpi, ATRX-KO and Control cells both exhibited increased open chromatin (Figure 3.8E). Using publicly available UCSC genome browser sessions for ATAC-seq data from WT infected HFFs [http://www.bio.ifi.lmu.de/HSV-1 (Hennig et al., 2018)], we validated our observation that the H2AFX gene locus accumulates OCRs and that this does not occur during salt or heat shock. The increase in open chromatin signal at H2AFX was not accompanied by reduced histone occupancy through the body of the gene (Figure 3.8F). We noted that the H3 signal was generally lower in ATRX-KO cells at both time points as compared with Control cells. The H3 signal decreased slightly both upstream and downstream of the gene from 4 to 8 hpi in both ATRX-KO and Control cells, but the H3 signal slightly increased through the body of the gene (Figure 3.8F). This suggested that chemical modifications of histones or changes in nucleosome composition may play a larger role in opening these sites than does histone eviction or repositioning. Unlike H3, the increase in open chromatin was accompanied by a 3.4-fold increase in relative transcript accumulation from H2AFX from 4-8 hpi in

both ATRX-KO and Control cells (Figure 3.8G). While the increase in OCRs extended into the neighboring gene, increased transcript accumulation, as detectable by poly(A) enrichment, was limited to the boundaries of the H2AFX gene. The increase in OCRs observed in ATRX-KO cells occurred by 4 hpi, while the same increase in OCRs was not observed in Control cells until 8 hpi (Figure 3.8E). This demonstrated that the OCR formation progressed faster in ATRX-KO cells. It also argued that the HSV induced stress response is triggered by the activity of a *de novo* expressed viral protein. As this response can be observed during 7134 infection, the response is ICP0-independent.

Figure 3.8: Loss of ATRX accelerates the progression of HSV infection.

(A) Differential ATAC-seq coverage of human genes in 4134 infected ATRX-KO cells 4hpi/7134 infected Control cells 4 hpi. Dots in red represent gene annotations that have a 2-fold enriched in ATRX-KO samples with at least 20 reads per gene annotation. Gene annotations in red are considered to have higher accumulation of open chromatin regions (OCRs). (B) Gene ontology-(GO) term enrichment analysis of gene annotations identified as having elevated levels of OCRs in Figure 3.8A. (C) GO-term enrichment analysis for genes with elevate OCRs and upregulate gene expression from analysis of normalized reads mapped to the human genome. (D) GO-term enrichment of histone related genes in genes with elevate OCRs and upregulate gene expression from analysis of normalized reads mapped to the human genome. (E) ATAC-seq read coverage of mapped H2AFX gene annotation reads normalized to total mapped human reads from (blue) ATRX-KO or (red) Control cells at 4 and 8 hi with 7134. (F) Total H3 ChIP-seq coverage for mapped H2AFX gene annotations reads normalized to total mapped human reads from (blue) ATRX-KO or (red) Control cells at 4 and 8 hi with 7134. (G) RNA-seq coverage for mapped H2AFX gene annotations reads normalized to total mapped human reads from (blue) ATRX-KO or (red) Control cells at 4 and 8 hi with 7134

Figure 3.8 (Continued)

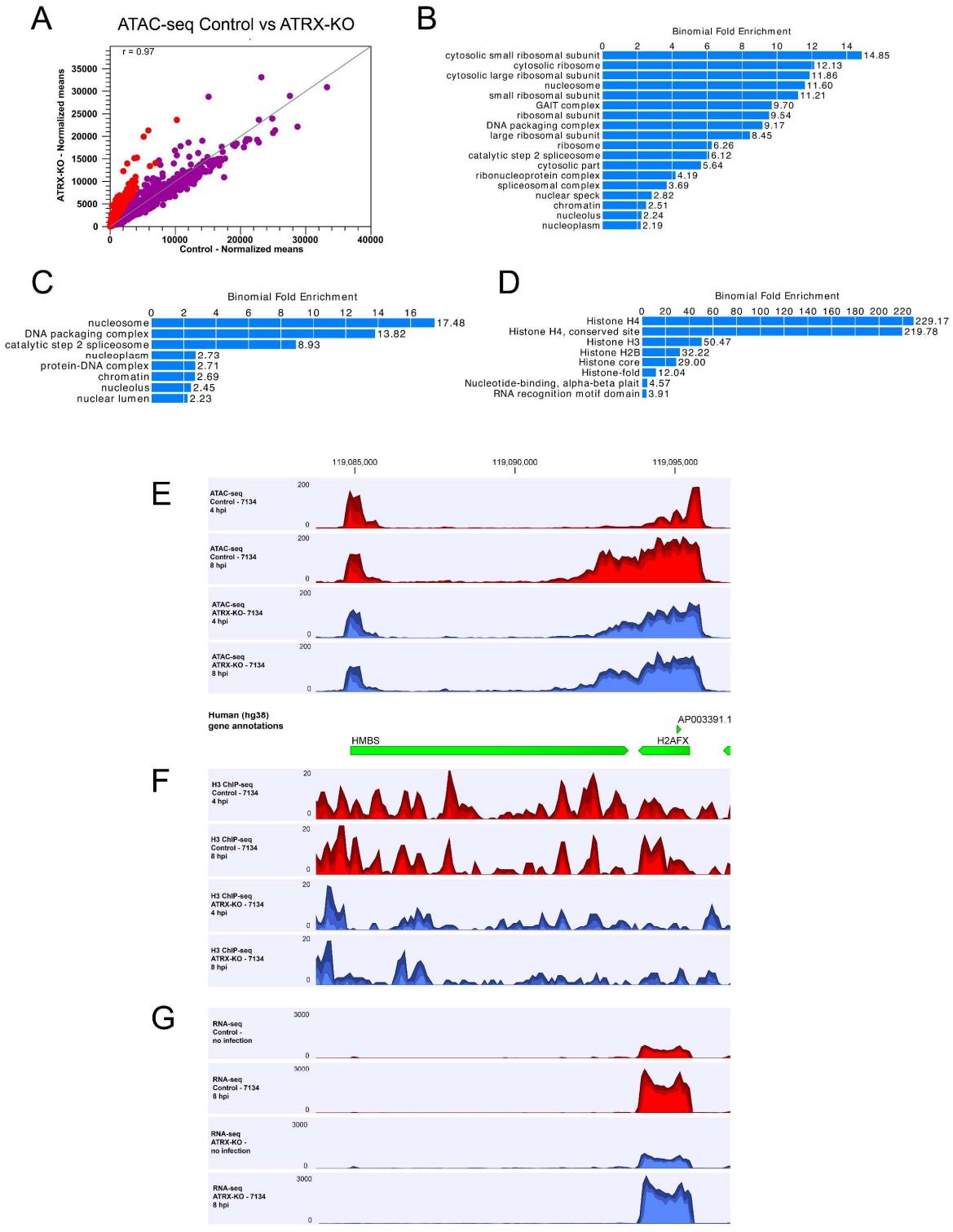

Discussion

Preventing the expression of foreign gene products is paramount in the cellular effort to defend against intracellular pathogens. Once viral proteins are expressed, they disrupt normal cellular function and hijack cellular pathways for the purpose of viral propagation, a process that often results in injury to or death of the infected cell. To prevent such hostile takeovers, cells mobilize factors, including chromatin-modifying proteins, to restrict gene expression and replication of invading DNA viruses. In this study, we demonstrate that the ATRX/DAXX complex is has a higher capacity to restrict ICP0-null HSV gene expression and replication than other nuclear H3 chaperones. The *de novo* deposition of H3 to viral genomes happens through redundant pathways, and histone H3 does not largely organize into fully formed nucleosomes on the HSV genome during lytic infection. ATRX enhances H3 retention across the entire HSV genome and limits accessibility of HSV DNA to Tn5 transpose activity during ATAC-seq, suggesting a possible mechanism for viral restriction. Loss of ATRX results in an accelerated viral lifecycle and early activation of a stress response that appears to be induced by a *de novo* expressed viral protein. These observations support a model in which ATRX supports cellular efforts to chromatinize invading viral DNA and delay viral gene expression and replication through enhanced H3 retention and limiting viral DNA accessibility.

H3 chaperone redundancy.

While histone chaperones fulfill specialty functions, the roles they play in true *de novo* chromatin formation in living cells are not well understood. HSV infection has proven to be a uniquely suited tool for investigating this process. In the absence of transcription, we found that no single nuclear H3 chaperone was required for *de novo* deposition of histone H3 on viral DNA. Even dual depletions of H3 chaperones had only minor effects on H3 occupation at HSV gene promoters. Only triple-depletion of HIRA, ATRX, and ASF1A resulted in a significant reduction in H3 loading by 4 hpi. This argues that the pathways for *de novo* H3 deposition on naked DNA act in a redundant manner.

Previous studies have reported that HIRA and ASF1A promote H3.3 and total H3 occupation on the HSV during early lytic infection, respectively (Oh et al., 2012; Placek et al., 2009). Here we show that neither HIRA nor ASF1A is strictly required for *de novo* loading of H3 to the HSV genome. This discrepancy may be accounted for by the fact that the HIRA and ASF1A studies were performed in transformed HeLa cells that have altered chromatin stability, as evidenced by their hyperploidy. Another plausible explanation might be a difference in HSV strains. While these studies used wild-type virus, here we employ an ICP0-null HSV to investigate the cellular mechanisms that might be disrupted by the activity of ICP0. The presence of ICP0 effectively renders depletion of any other histone chaperone a double depletion because the activity of the ATRX/DAXX complex is disrupted by ICP0. While we show that a triple depletion ASF1A/ATRX/HIRA was necessary

for significant reduction in total H3 in the absence of transcription, a depletion of ATRX by ICP0 combined with depletion of another H3 chaperone may be sufficient to significantly reduce H3 on the HSV genome.

Chromatin state is normally informed by the surrounding chromatin features. Newly replicated eukaryotic DNA is loaded with parental histones which are used to re-establish the parental epigenetic state [reviewed in (Moazed, 2011)]. Recycling of parental histones can reproduce positional information of histone post-translational modifications (PTMs) on newly synthesized DNA (Reverón-Gómez et al., 2018). Nuclear naked DNA is likely rarely encountered by cells outside of the context of cell death or viral infection. Thus, naked DNA in the nucleus represents a danger signal to cells and may elicit an “all-hands-on-deck” response to which any histone chaperone capable of loading histones is recruited. It is also possible that proteins, such as NAP1L1, can load H3-containing nucleosome like structures as has been observed *in vitro* (Torigoe et al., 2011). Further studies will be required to map the required proteins and pathways for *de novo* histone deposition. HSV will continue to be a unique and useful tool to investigate these pathways with high temporal resolution.

Restriction of HSV is likely mediated by a direct effect of ATRX.

The ATRX/DAXX complex is the only nuclear H3 chaperone complex that exhibited the capacity to restrict HSV. Like the other H3 chaperones, ATRX is not strictly required for H3 deposition to the HSV genome in the absence of

transcription. We recently proposed a model in which epigenetic restriction of HSV occurs in a biphasic manner: H3 is loaded on the HSV genome, and then a second maintenance phase, mediated by ATRX, acts to restrict the virus. Our findings that H3 deposition occurs in a redundant process and that only the ATRX/DAXX complex is restrictive of HSV support this model and argued that ATRX possesses a unique activity by which it restricts DNA viruses. They also suggest that H3 may not be inherently restrictive and may require the activity of additional host factors to restrict viral gene expression.

ATRX has numerous functions in regulating cellular processes that extend beyond its function as a histone chaperone. The ATRX/DAXX complex is known to recruit both HDACs and HMTs to modulate histone PTMs and regulate chromatin stability and gene expression (Elsasser et al., 2015; Sadic et al., 2015; Yao et al., 2014). ATRX also has functions in DNA damage response pathways where it is thought to facilitate repair, inhibits over-resection by MRE11, and promotes restart and repair of stalled replication forks (Clynes et al., 2015; Clynes et al., 2014; Huh et al., 2016; Juhasz et al., 2018). However, when we perturbed several of these pathways, we could find no difference in the effects on ATRX-KO versus Control cells. Remarkably similar gene expression profiles between Control and ATRX-KO argue that this restriction is likely a direct rather than indirect effect of ATRX depletion. This argument is supported by the numerous virally encoded mechanisms that disrupt or manipulate the ATRX/DAXX complex. HSV, HCMV, and AdV encode viral proteins that drive the degradation of either ATRX or DAXX

(Jurak et al., 2012; Saffert and Kalejta, 2006; Schreiner et al., 2013) while EBV and human papilloma viruses (HPVs) encode proteins that bind DAXX, displace ATRX, and manipulate DAXX function (Kivipõld et al., 2015; Tsai et al., 2011). The evolution of many viral mechanisms aimed at disarming ATRX restriction provide strong support for its important role as a generalized restriction factor against DNA viruses.

ATRX delays the HSV lifecycle by limiting viral DNA accessibility.

The ATRX -interacting domain of DAXX is required for ATRX and DAXX-mediated restriction of HSV (Lukashchuk and Everett, 2010). This argues that ATRX and DAXX restrict HSV while in complex with one another. In support of this finding, we showed recently that depletion of DAXX in ATRX-KO cells is not additive to ATRX depletion in terms of HSV yield [Chapter 2; (Cabral et al., 2018)]. However, we also showed that ATRX is not strictly required for H3 deposition to viral DNA and that ATRX restriction is not mediated through several of its other described functions. Taking these observations into account, we hypothesized that the ATRX/DAXX complex may inhibit DNA viruses by reducing H3 turnover and limiting viral DNA accessibility [Chapter 2; (Cabral et al., 2018)].

In this study, we provide evidence to support this model. We showed that ATRX-KO resulted in reduced H3 retention from 4-8hpi across the entire HSV genome, and this was mirrored by an increase in accessibility of HSV DNA in ATRX-KO cells as shown in ATAC-seq studies. ATAC-seq also revealed that the

HSV genome is not organized into nucleosome during the early stages of lytic infection. HSV DNA is thought to be organized into nucleosome-wrapped chromatin during latent infection (Deshmane and Fraser, 1989). Whether nucleosomes are associated with the HSV genome during lytic infection has been a more controversial topic.

Despite the rapid deposition of histones on viral DNA upon nuclear entry, studies investigating the organization of viral chromatin with the use of nuclease digestion suggest that viral DNA is not organized into ordered nucleosomes. DNase digestion of DNA from cells during lytic HSV infection largely yielded smeared DNA staining when probed for HSV DNA (Kent et al., 2004; Lacasse and Schang, 2010; Muggeridge and Fraser, 1986). However, these same studies have also shown that increasing the concentration of DNase could yield a single band of approximately 150 bp, the size of a DNA fragment protected by nucleosomes, suggesting that only a small fraction of viral DNA yielded fragments consistent with nucleosome protection (Leinbach and Summers, 1980; Muggeridge and Fraser, 1986). Another study suggested that while nucleosome-like structures associate with some fraction of viral DNA, they do not do so in a regular repeating structure (Kent et al., 2004). A recent study suggested that nucleosome-like structures associate only loosely with HSV genomes and that the susceptibility of HSV DNA to nuclease digestion changed during the course of infection (Lacasse and Schang, 2010). The fragmentation of HSV DNA by the Tn5 nuclease during ATAC-seq showed little evidence for nucleosome-mediated protection of viral DNA

in ATRX-KO cells at 4 and 8 hpi. However, the distribution curve of sequenced fragment lengths flattens slightly at 200 bp in reads for HSV DNA in Control cells. This may be indicative of protection from Tn5 activity by nucleosomes or nucleosome-like structures that are enhanced in the presence of ATRX. These results also agree with previous reports of a minor population of nucleosome-bound HSV DNA during lytic infection and support a model in which HSV is only loosely bound in unstable nucleosomes or nucleosome-like structures . By 8 hpi, the distribution of read lengths in Control cells more closely resembles the curve in ATRX-KO cells. We hypothesize that ATRX is mediating histone retention on HSV DNA, thereby reducing histone turnover and accessibility for viral transcription and replication factors. ATRX may also be promoting the formation of nucleosomes or nucleosome-like structures during very early stages of infection which are likely destabilized by transcription of viral genes.

By limiting HSV genome accessibility, ATRX effectively limits the kinetics of viral infection. Heat shock-associated proteins have long been known to be induced during HSV infection (Kobayashi et al., 1994; LaThangue et al., 1984) and to promote productive viral gene expression and replication (Bringhurst and Schaffer, 2006; Li et al., 2004; Preston and Nicholl, 2008). More recently, HSV has been described to induce DoTT (Hennig et al., 2018) and antisense transcription at cellular genes (Wyler et al., 2017). This may contribute to double-stranded RNAs (dsRNAs) that are detectable during HSV infection (Weber et al., 2006). Induction of DoTT, antisense transcription, and dsRNA foci were recently reported

as part of the heat shock response of *C. elegans* (Melnick et al., 2019). Melnick et al. reported an enrichment of translation-related RNA recovered from dsRNA foci. We showed that HSV infection induces OCRs at translation-related genes. Coupled with our observation that the presence of ATRX delays the onset of OCR enrichment, these observations argue that HSV induces a stress response though the activity of a nascent viral protein. Given that HSP40 and HSP70 are have been reported to increase the affinity of HSV origin-binding protein, UL9, for the S segment origin (Tanguy Le Gac and Boehmer, 2002), induction of a stress response may serve as a marker for transition of the viral genomes to a replication-ready state. Supporting this hypothesis, we have shown in this study that the loss of ATRX results in earlier detection of stress-related OCRs and enhances the kinetics of viral replication (Figure 3.7B). When we validated our observations using publicly available ATAC-seq data comparing the effects of heat shock, salt shock, and HSV infection in HFFs [http://www.bio.ifi.lmu.de/HSV-1 (Hennig et al., 2018)], we noted that H2AFX and GAPDH do not accumulate OCRs during salt shock or heat shock. Additionally, the HSPA1A gene, encoding an HSP70 family protein, accumulated OCRs during heat shock and HSV infection, but not salt shock. This raises the intriguing possibility that the HSV induced stress response and accumulation of OCRs at some genes may be unique to HSV or related to activation of DNA damage responses. Further studies will be required to elucidate the mechanism of viral induction of a unique stress

response and explore it as a possible therapeutic target for both productive and latent infections.

Materials and Methods

Cell culture, viruses, and infections

HFF cells were obtained from the American Type Culture Collection (Manassas, VA). TERT-HF immortalized fibroblasts were a kind gift from Robert Kalejta. All cells are regularly tested for the presence of mycoplasma contamination. Cells used in this study were mycoplasma-free.

All fibroblast cells were maintained in Dulbecco's Modified Eagle's medium (DMEM; Corning, Corning NY) supplemented with 10% (v/v) fetal bovine serum (FBS) in humidified 5% CO_2 incubators at 37ºC. Cells were serially passaged by trypsin-EDTA (0.05%; Corning) treatment and transfer to fresh media. ATRXKO and Control cells were maintained under 4 μg/ml puromycin.

HSV-1 KOS was used as the wild type virus in this study. HSV-1 7134 (Cai and Schaffer, 1992) was used for experiments requiring an ICP0-null HSV. Cells were infected with viruses at the indicated MOI in PBS containing 1% (w/v) glucose and 1% (v/v) bovine calf serum (BCS). Infections were carried out at 37ºC with constant agitation with a 1 h adsorption time. After 1 h, the inoculum was removed and replaced with DMEM supplemented with 1% BCS (DMEV) and then incubated at 37ºC until times indicated. ICP0-null viral yields were determined by infecting U2OS cells with serial dilutions of viral lysates collected at indicated times. Flavopiridol (1 μM; Selleck Chemicals, Houston, TX) was added to cells at 1 h prior to infection and maintained until time of harvest.

Preparation of EdC-labeled HSV-1 stocks

EdC-labeled HSV-1 was prepared as described previously [Chapter 2; (Cabral et al., 2018)].

Protein Depletions

To deplete cells of endogenous proteins, siRNAs were transfected into $1x10^5$ cells plated in a 12-well dish using Lipofectamine RNAiMAX Reagent (Invitrogen). At 48 h post transfection, cells were re-seeded into assay-appropriate dishes and infected 24 h later.

siRNAs used in this study:

siNT: Dharmacon ON-TARGETplus Non-targeting pool

siATRX: Dharmacon ON-TARGETplus ATRX pool

siDAXX: Dharmacon ON-TARGETplus DAXX pool

siHIRA: Dharmacon ON-TARGETplus HIRA pool

siCHAF1A: Dharmacon ON-TARGETplus CHAF1A pool

siASF1A: Dharmacon ON-TARGETplus ASF1A pool

siASF1B: Dharmacon ON-TARGETplus ASF1B pool

siDEK: Dharmacon ON-TARGETplus DEK pool

siSSRP1: Dharmacon ON-TARGETplus SSRP1 pool

siSUV39H1: Dharmacon ON-TARGETplus SUV39H1 pool

siSETDB1: Dharmacon ON-TARGETplus SETDB1 pool

siG9A: Dharmacon ON-TARGETplus G9A pool

Antibodies

The following antibodies were used in this study:

DAXX Sigma D7810

GAPDH Abcam ab8245

ICP8 (Knipe et al., 1987)

ICP4 (Showalter et al., 1981)

ICP0 East Coast Bio H1A207

ATRX Abcam 97508

H3 Abcam ab1791

H3K9me3 Abcam ab8898

Negative control rabbit IgG Millipore NG1893918 (ChIP)

HIRA Millipore 04-1488

SETDB1 Proteintech 11231-1-AP

SUV39H1 Cell Signaling 8729S

CHAF1A Cell Signaling 54805

SSRP1 Biolegend 609702

ASF1A Cell Signaling 2990S

ASF1B Cell Signaling 2769S

DEK Proteintech 16448-1-AP

MRE11 Novus NB100-142

Immunoblots

Cells were harvested at the times indicated in lithium dodecyl sulfate (LDS) sample buffer and incubated at 95ºC for 10 min. Protein samples were run on NuPAGE 4-12% bis-Tris gels (Invitrogen). Proteins were transferred from the gel to a nitrocellulose membrane. Membranes were blocked in LI-COR blocking solution for 1 h. Membranes were incubated with primary antibody overnight at 4ºC. Membranes were washed 3 times with PBST, incubated in secondary antibody for 1 h at room temperature (IRDye 800CW Goat anti-Mouse IgG and IRDye 800CW Goat anti-Rabbit IgG for LI-COR; α-mouse IgG^{+}HRP and α-Rabbit IgG^{+}HRP, Cell Signaling 7076s and 7074s, respectively for film). Membranes were washed 3 times in PBST. Membranes were imaged with a LI-COR Odyssey imager (Lincoln, NE) or were incubated with SuperSignal West Pico chemiluminescent substrate (Thermo Scientific) and imaged with a chemiluminescence imager.

Immunofluorescence and detection of EdC-labeled HSV-1 genomes

Staining of samples was performed as previously described [Chapter 2; (Cabral et al., 2018)]. All antibodies were used at 1:500 dilution. Images were captured with a Zeiss Axioplan widefield microscope using a 100x oil immersion objective lens. Image J (FIJI) was used to minimally adjust contrast of exported images.

RT-qPCR quantification of viral transcripts

Total RNA was isolated using the Qiagen RNeasy kit per manufacturer's instructions. Resulting RNA was quantified, treated with DNAse (DNAfree Kit, Ambion), and reverse transcribed (High Capacity cDNA RT Kit, Applied Biosystems) to produce cDNA. Quantitative PCR was performed using Fast SYBR Green reagents (ThermoFisher) on a StepOnePlus from Applied Biosystems (ThermoFisher). Oligos for qPCR reactions are as follows:

ICP27 (mRNA) for GCATCCTTCGTGTTTGTCATT

ICP27 (mRNA) rev GCATCTTCTCTCCGACCCCG

ICP8 (mRNA) for GTCGTTACCGAGGGCTTCAA

ICP8 (mRNA) rev GTTACCTTGTCCGAGCCTCC

gB (mRNA) for TGTGTACATGTCCCCGTTTTACG

gB (mRNA) rev GCGTAGAAGCCGTCAACCT

18S (mRNA) for GCCGCTAGAGGTGAAATTCTTG

18S (mRNA) rev CTTTCGCTCTGGTCCGTCTT

Chromatin Immunoprecipitation

ChIP experiments were carried out as described previously in detail (Lee et al., 2016) with minor changes. Briefly, infected cell monolayers were fixed in 1% formaldehyde (Sigma-Aldrich) at 37ºC for 15 min. Fixation was quenched with glycine at a final concentration of 125 mM for 3 min. Cells were washed 3 times in

ice-cold PBS supplemented with 1 mM phenylmethanesulfonylfluoride (PMSF), collected in PBS + PMSF, and pelleted at 2000 rpm for 5 min at 4ºC. Cell pellets were re-suspended in 1 mL lysis buffer (1% SDS, 10 mM EDTA, 50 mM Tris, pH 8.1), transferred to 15 mL polystyrene tubes and sonicated at 4ºC in a Diagenode Biorupter on the high setting for 9 cycles of 5 min each (30 sec ON, 30 sec OFF). An aliquot of recovered chromatin was used for each IP reaction in 1 ml IP dilution buffer (150 mM NaCl, 10 mM Na_2HPO_4, 2 mM EDTA, 1.1% Triton, 0.1% SDS). An aliquot of a no antibody IP reaction was retained as 10% input sample. IPs were performed with 2.5 µg (6.0 µg for ATRX ab) of ChIP grade antibody (see Antibodies) per reaction and incubated overnight at 4ºC. 20 µl of MagnaChIP protein A magnetic beads (Millipore) were added for 2.5-3 hrs at 4ºC with rotation, washed 3 times with a cold low-salt buffer (150 mM NaCl, 20 mM Tris·HCl, pH 8.1, 2 mM EDTA, 1% Triton X-100, and 0.1% SDS, 1 mM PMSF) and 3 times with cold LiCl wash buffer (50 mM HEPES pH 7.5, 250 mM lithium chloride, 1 mM EDTA, 1% NP-40, 0.7% sodium deoxycholate, 1 mM PMSF), and washed once with cold Tris-EDTA buffer (10 mM Tris-HCl, pH 8, 1 mM EDTA). DNA-protein complexes were eluted in 100 µl of elution buffer (1% SDS, 0.1 M $NaHCO_3$) at 65ºC for 20 min. Protein-DNA crosslinks were reversed by adding NaCl (0.2 M final concentration) and incubating at 95ºC for 30 min followed by 1 h RNase A (Ambion) treatment at 37ºC and Proteinase K treatment (Roche) at 45ºC for 2 h. DNA was purified using a QIAquick PCR purification kit (Qiagen) end eluted twice with 50 µl buffer EB for a final volume of 100 µl.

Quantitative-PCR was performed to quantify DNA using Fast SYBR Green reagents (ThermoFisher) on a StepOnePlus from Applied Biosystems (ThermoFisher). Oligos for qPCR reactions are as follows:

ICP27 Promoter (genomic)

FWD ACCCAGCCAGCGTATCCACC

REV ACACCATAAGTACGTGGC

ICP8 promoter (genomic)

FWD GAGACCGGGGTTGGGGAATGAATC

REV CCCCGGGGGTTGTCTGTGAAGG

GAPDH promoter (genomic)

FWD CAGGCGCCCAATACGACCAAAATC

REV TTCGACAGTCAGTCAGCCGCATCTTCTT

RNA-seq

For RNA-seq, $2x10^6$ cells were plated into 10cm dishes. Cells were infected at an MOI of 5 and harvested at 8 hour post infection. Total RNA was isolated using the RNAqueous Total RNA Isolation Kit (Thermo) per the manufacturer's instructions. The NEBNext Poly(A) mRNA Magnetic Isolation Module (NEB) was used to enrich mRNA from 1µg of the isolated total RNA samples. Poly(A) enriched RNA was used as input for generating RNA-seq libraries using NEBNext Ultra™ II Directional RNA Library Prep Kit for Illumina (NEB) per the manufacturer's

instructions. Libraries were sent to the Bauer Core Facility at Harvard University for 2x75 paired end sequencing on an Illumina HiSeq 2500. Reads were aligned to the HSV genome (HSV-1 KOS strain, GenBank accession number KT899744) (Colgrove et al., 2016) and to the human genome (GRCh38) and analyzed using CLC Genomics Workbench Software (Qiagen).

ATAC-seq

For Omni-ATAC-seq, $1x10^5$ TERT-HF cells were plated into 12 well plates. Cells were infected at an MOI of 5 and harvested at the times indicated. Omni-ATAC-seq was performed as described (Corces et al., 2017) with the addition of an solid phase reversible immobilization (SPRI) size selection on the final library to isolate fragments between 200-1000 bp. Libraries were sent to the Bauer Core Facility at Harvard University for 2x75 paired end sequencing on an Illumina HiSeq 2500. Reads were aligned to the HSV genome (HSV-1 KOS strain, GenBank accession number KT899744) (Colgrove et al., 2016) and to the human genome (GRCh38) and analyzed using CLC Genomics Workbench Software (Qiagen).

ChIP-seq

For ChIP-seq, $1.4x10^7$ TERT-HF cells were plated into 2x150mm dishes and were infected at an MOI of 3. Chromatin immunoprecipitation was performed as described above with the following modifications: after sonication, 300uL of sonicated sample was added to 900uL of IP dilution buffer. 50uL of sonicated

sample was retained for input. 6µL of pan-histone H3 antibody (Abcam ab1791) was added and incubated at 4°C overnight. Samples were washed as described, then eluted for 60 minutes at 65°C. The eluate was transferred to a new tube, and the eluate was incubated at 65°C to reverse crosslinking. Samples were then treated with RNase A (Ambion) for 1hr at 37ºC and Proteinase K treatment (Roche) at 45ºC for 2 h. DNA was purified using a QIAquick PCR purification kit (Qiagen) end eluted with 50 µl buffer EB. 10ng of recovered ChIP DNA was used to prepare a library with the TruSeq ChIP Library Preparation Kit (Illumina) per the manufacturer's instructions. Libraries were sent to the Bauer Core Facility at Harvard University for 2x75 paired end sequencing on an Illumina HiSeq 2500. Reads were aligned to the HSV genome (HSV-1 KOS strain, GenBank accession number KT899744) (Colgrove et al., 2016) and to the human genome (GRCh38) and analyzed using CLC Genomics Workbench Software (Qiagen).

Chapter 4: Dissertation Perspective

4.1 Summary of Results

These studies were designed and conducted to investigate the mechanism by which ATRX restricts herpes simplex virus and how that restriction relates to the formation of viral chromatin during lytic infection. Prior to the work presented in this dissertation, ATRX was known to restrict DNA virus infection, but the mechanism was poorly understood. Evidence exists that the ATRX/DAXX complex plays a role in histone occupation of viral genomes at later times post infection, so we hypothesized that ATRX was mediating the loading of histones to the viral genome upon its nuclear entry. Early experiments designed to quantify the kinetics of viral entry and restriction factor recruitment revealed that ATRX and HSV DNA colocalized almost immediately after viral genomes were detectable in the nucleus, 15 minutes post infection. We also found that ATRX restricted viral mRNA accumulation from genes of all kinetic classes during ICP0-null HSV infection. Surprisingly, we found that ATRX was not required for deposition of H3 or histone post-translational modifications (PTMs) from 2-4 hpi. However, we observed that depletion of ATRX resulted in early viral DNA replication and reduced H3 and PTMs from 4-8 hpi.

We then hypothesized that ATRX acts to stabilize chromatin in the face of chromatin stresses, such as transcription and replication. In support of this hypothesis, in the presence of a viral polymerase inhibitor, accumulation of histones and PTMs on ICP0-null HSV genomes was impaired from 4-8 hpi in ATRX-KO cells. We also found that inhibition of transcription rescued the

accumulation of viral chromatin from 4 to 8 hpi in ATRX-KO cells. These results argued for a model in which chromatin is loaded onto viral DNA by other histone chaperones, and ATRX subsequently stabilizes viral chromatin during challenges to chromatin stability. ATRX-mediated stabilization of viral chromatin could limit the access of transcription and replication factors to viral genomes.

In chapter 3, we tested our model in which other nuclear H3 chaperones mediate *de novo* H3 deposition to viral DNA prior to ATRX stabilization of viral chromatin. We investigated the restrictive capacity of the major nuclear histone chaperone complexes through a series of siRNA depletion studies. We found that only the ATRX/DAXX complex was significantly restrictive of HSV infection. We also found that *de novo* H3 deposition to HSV genomes did not require any single nuclear H3 chaperone complex. Only a triple depletion of ATRX, HIRA, and ASF1A resulted in a partial but significant decrease in H3 occupation at viral gene promoters. These results argued that ATRX possesses a unique restrictive function among nuclear H3 chaperones and that deposition of H3 to viral genomes occurs through redundant pathways. However, ATRX did not appear to restrict HSV through its functions in recruiting HDACs, H3K9me3 HMTs, or restricting MRE11 activity during DNA repair.

Having established that *de novo* H3 deposition to viral DNA occurs through redundant pathways, we then tested the aspect of our model in which ATRX mediates restriction of ICP0-null HSV through the stabilization of viral chromatin. RNA-seq showed that the gene expression in uninfected ATRX-KO cells and

Control cells was very similar and likely did not account for ATRX-mediated restriction of HSV, arguing that the restrictive effects of ATRX are likely direct rather than indirect. ATAC-seq revealed that HSV DNA was nearly 10-fold more accessible to TN5 transposase activity in ATRX-KO cells as compared to Control cells at 4 hpi with 7134, and HSV showed signs of weak nucleosome association in Control cells but not in ATRX-KO cells. This was accompanied by a global defect in H3 accumulation on viral DNA from 4 to 8 hours in ATRX-KO versus Control cells. We also found that infection with an ICP0-null HSV could induce a unique stress response that resulted in open chromatin at over 600 human genes, and the opening of chromatin occurred earlier in ATRX-KO cells. We conclude that ATRX likely restricts HSV infection by stabilizing viral chromatin through enhanced H3 retention and reduced accessibility to viral DNA, resulting in delayed viral gene expression and replication.

4.2 Discussion

Recruitment of PML-NB proteins to HSV genomes

A long-standing question in the herpesvirus field is whether PML-NB proteins and other restriction factors, such as IFI16, are recruited to viral DNA upon nuclear entry or if viral DNA is trafficked to sites where these proteins are already in nuclear bodies. Answering this question is important for the understanding of nuclear DNA sensing and the rapidity of the host cell response to foreign DNA. Evidence exists for the formation of transient punctate IFI16 structures at the nuclear periphery at early times post infection. Two studies have reported observing this phenomenon using fluorescently-tagged IFI16 proteins in conjunction with live cell imaging (Diner et al., 2016; Everett, 2016). One of the studies also observed PML-NB proteins PML and DAXX forming similar punctate structures in response to HSV infection (Everett, 2016). However, due to technical limitations, neither of these studies were able to show punctate structure formation of restriction factors in the context of viral DNA. In addition, our study of ATRX and IFI16 colocalization with HSV DNA and other recent reports suggest that recruitment of IFI16 and PML-NB proteins are not co-dependent (Alandijany et al., 2018; Cabral et al., 2018; Orzalli et al., 2013). However, the order of recruitment and whether PML-NB proteins are involved in displacing IFI16 from HSV DNA shortly after focus formation has yet to be defined.

To follow up on our viral entry and host restriction factor recruitment kinetic studies, we have worked to design an experimental system to investigate whether

host restriction factors are recruited to viral DNA or vice-versa. In collaboration with NEOVIRTECH, we engineered two autofluorescent HSVs, one derived from WT and one derived ICP0-null 7134, in which we have inserted an ANCHOR™ (NEOVIRTECH) cassette (HSV-ANCHOR, 7134-ANCHOR). The commercialized ANCHOR™ technology consists of a series of non-repetitive ANCH sequences that act as nucleation sites for a fluorescently-labeled OR protein that is also encoded on the cassette (Komatsu et al., 2018; Mariamé et al., 2018). While these viruses produce OR-GFP protein during infection, detection of viral entry will require engineering a cell line that stably expresses high levels of OR protein so it can nucleate on the viral DNA upon ejection from the capsid. The cell line would also need to express a fluorescently-tagged protein of interest, such as ATRX, PML, or IFI16. With this system, we would be able to investigate recruitment of PML-NB proteins and IFI16 in the context of viral DNA using live-cell microscopy and gain further insight into the spatiotemporal dynamics of nuclear DNA sensing. Based on previous live cell imaging studies of restriction factor behavior, we expect that ATRX, PML, and IFI16 are recruited to incoming HSV genomes with similar kinetics. This would support the hypothesis we put forward in Chapter 2 that PML-NBs and IFI16 represent independent nuclear DNA sensing pathways that operate concurrently.

The HSV-ANCHOR system would also allow us to ask questions about the timing and positioning of replication compartment formation in relation to input viral genomes, ATRX and DNA damage protein recruitment to replication

compartments, and IFI16 filament formation (Merkl and Knipe, 2019) in the context of replication compartments and actively replicating viral DNA.

ATRX and DAXX domain requirement for HSV restriction.

ATRX is a large, multifunctional protein with a plant homeodomain (PHD) containing an ADD domain and an ATPase/helicase domain, and it is known to interact with a variety of chromatin-related nuclear proteins. Engneering amino acid changes in the ATRX binding domain of DAXX impairs the ability of both DAXX and ATRX to restrict ICP0-null HSV (Lukashchuk and Everett, 2010). However, it is currently unknown if other domains of either protein are also required to restrict DNA viruses. It has been reported that expression of a mutant form of DAXX with impaired H3.3 interaction could rescue ATRX-mediated repression of a retrotransposon reporter element in DAXX-KO cells (Sadic et al., 2015). This argued that the ATRX/DAXX complex can mediate gene silencing without H3.3 chaperone functionality. ATRX is also a histone PTM reader capable of binding H3K9me3 in the context of H3k4me0 with its ADD domain (Dhayalan et al., 2011). ATRX has also been reported to recruit HP1 and HMT SETDB1 to mediate heterochromatin formation and maintenance (Lechner et al., 2005; Sadic et al., 2015).

Investigating the required domains of ATRX and DAXX could provide significant insights into the specific interactions and mechanisms that are required for HSV restriction. We observed that the restrictive effects of ATRX and DAXX

are not additive, supporting the observation that DAXX requires its interaction with ATRX to restrict ICP0-null HSV (Lukashchuk and Everett, 2010). A series of previously described point mutations that affect functional and interaction domains (Berube et al., 2000; Lechner et al., 2005; Li et al., 2017; Nan et al., 2007) of ATRX could be introduced to investigate if the HP1 binding domain, ADD domain histone reader function, or ATPase/helicase domains play significant roles in ATRX-mediated viral restriction. Likewise, engineering a DAXX-KO cell line then adding back DAXX with point mutations in the H3.3 binding domain that diminishes affinity for H3.3 could be used to test the necessity of H3.3 chaperone activity in restricting HSV. Due to our observations that ATRX affects H3 occupation and chromatin stability on the HSV genome, we hypothesize that ATRX-mediated restriction will require chaperone or histone tail binding activity. However, it is possible that recruitment of HP1 or the activity of the ATPase/helicase domain confer restrictive activity to ATRX. As a member of the SNF2 family of ATPases/helicases, it is possible that the ATPase/helicase domain of ATRX promotes the conversion of nucleosome-like structures into more stable nucleosomes as has been described for other members of the SNF2 family (Torigoe et al., 2011). Point mutations introduced to the ATPase/Helicase domain of ATRX in conjunction with DNase digestion and ATAC-seq assays of viral chromatin could potentially define the role that ATRX plays in converting HSV occupying histone into nucleosomes.

Disruption of Nucleosome formation during lytic HSV infection.

As discussed in the Introduction and in Chapter 3, the HSV genome is not associated with histones while in the viral particle (Oh and Fraser, 2008; Pignatti and Cassai, 1980). However, this study and numerous others showed that HSV genomes, upon nuclear entry, are rapidly loaded with histones that are enriched for histone modifications such as H3K9me3 and H3K27me3 (Cabral et al., 2018; Cliffe and Knipe, 2008; Kent et al., 2004; Lee et al., 2016; Oh and Fraser, 2008). Digestion of infected cell DNA by treatment with DNase has been reported to yield smear patterns that are typical of non-nucleosome DNA (Kent et al., 2004; Lacasse and Schang, 2010; Muggeridge and Fraser, 1986). However, after digesting HSV DNA with higher concentrations of DNase, a weak band of DNA could be detected at 150 bp, suggesting that some fraction of HSV DNA was wrapped around infrequent and irregularly spaced nucleosomes (Kent et al., 2004; Lacasse and Schang, 2010; Muggeridge and Fraser, 1986).

In Chapter 3 we show that the presence of ATRX results in reduced HSV chromatin accessibility and enhanced retention of H3 on viral DNA. In ATAC-seq samples from HSV 7134 infected Control cells, we detected a slight flattening of the sequenced fragment length histogram that corresponded to approximately 200 bp. This is the known peak size of mono-nucleosome protected DNA fragments in ATAC-seq assays (Buenrostro et al., 2015), which was clearly detected in sequenced fragment length distribution histograms for reads aligned to the human genome. We did not detect enrichment of 200 bp fragment lengths in HSV aligned

samples from Control cells at 8 hpi or ATRX-KO cells at 4 and 8 hpi. This result agrees with previous observations that a subfraction of HSV DNA fragments were protected from DNase treatment by nucleosomes and suggests that ATRX may play a role in promoting nucleosome formation at early times post infection. This could account for the reduced accessibility observed in Control cells as compared to ATRX-KO cells. However, it is also possible that the high ATAC-seq signals from ATRX-KO 4 and 8 hpi and Control 8 hpi samples mask the signal from the minor population of fragments. Further ATAC-seq and DNase digestion studies using samples from HSV infected ATRX-KO and Control cells harvested at earlier time points would further our understanding of nucleosome formation kinetics and the role ATRX plays in promoting nucleosome formation. Additionally, inhibition of transcription and viral DNA synthesis using flavopiridol and phosphonoacetic acid, respectively, could aid in further resolving the role these processes play in destabilizing nucleosomes and viral chromatin.

A possible mechanism by which ATRX could mediate HSV DNA stability accessibility is through reducing the rate of histone turnover. ATRX is required for heterochromatin maintenance at pericentric heterochromatin and telomeres (Goldberg et al., 2010; Lewis et al., 2010; McDowell et al., 1999). It has also been observed that pericentric heterochromatin and telomeres exhibit high levels of chromatin stability with very low histone turnover (Kraushaar et al., 2013). It is possible that ATRX acts to stabilize chromatin in these regions, and perceived loss of histone occupation during ATRX-depletion is the result of destabilized chromatin

and increased histone turnover rather than a defect in histone loading. Applying this model to HSV, we hypothesize that the observed stability of viral chromatin in the presence of ATRX is due to reduced histone turnover. Reduced histone turnover would facilitate the retention not only of H3 but also the repressive histone PTMs H3K9me3 and H3K27me3 that we and others have observed to accumulate on HSV DNA during infection. Testing this hypothesis will be technically challenging. However, a recently described pulse-chase technique known as time-ChIP in which a pulsed small molecule can drive auto-biotinylation of ectopically expressed SNAP-tagged histones (Deaton et al., 2016; Siwek et al., 2018). During the chase period, samples can be harvested for ChIP-qPCR or ChIP-seq at short intervals to monitor the loss of tagged H3 with high temporal resolution. This technique can be used to examine histone variant turnover during lytic HSV infection in the presence or absence of ATRX and define its role in histone turnover.

Possible roles for ATRX in the maintenance of latent HSV chromatin.

In contrast to lytic infection, latent HSV genomes are thought to be organized into chromatin domains that include regularly spaced nucleosomes bearing repressive heterochromatin modifications (Cliffe et al., 2009; Deshmane and Fraser, 1989; Lee et al., 2018b). The ATRX/DAXX complex has been reported to play a role in maintaining latency of EBV as depletion of either DAXX or ATRX results in reactivation of EBV lytic gene expression (Tsai et al., 2011). The complex has also

been implicated in promoting H3 occupation of quiescent HSV genomes in primary human fibroblasts (Cohen et al., 2018). ATRX and other PML-NB proteins have been reported to form foci adjacent to latent HSV genomes in murine neurons (Catez et al., 2012). We hypothesize that ATRX plays an active role in maintaining the repressed state of latent HSV genomes by stabilizing and maintaining the integrity of viral chromatin.

HSV has evolved multiple mechanisms with which it can modulate ATRX activity. HSV-1 and HSV-2 code for miR-H1 and miR-H6, respectively. Each miRNA was demonstrated to be capable of depleting endogenous ATRX (Jurak et al., 2012). HSV also encodes the viral E3 ubiquitin ligase, ICP0, which has also been shown to promote the proteasome-dependent degradation of ATRX (Jurak et al., 2012). While ICP0 was required for the degradation of the ATRX protein, an HSV lacking miR-H1 was still capable of degrading ATRX during lytic infect (Jurak et al., 2012). Although miR-H1 was highly expressed during lytic infection, very low levels of miR-H1 were detected by Illumina sequencing in samples from a latent infection (Jurak et al., 2010) making it possible that miR-H1 modulates ATRX levels during latency. However, because the levels of miR-H1 are very low during latency, this may be unlikely.

It has been proposed that reactivation from latency happens in a two-phase process: the first phase is a wave of lytic gene reactivation accompanied by a histone methyl/phopho switch at H3K9me3/pS10 mediated by JNK; the second phase is full reactivation driven by lysine demethylases that remove restrictive

heterochromatin modification from HSV promoters (Cliffe et al., 2015). Interestingly, ATRX was recently shown to tolerate the H3K9me3/pS10 histone methyl/phospho switch and could continue to repress gene expression in postmitotic neurons (Noh et al., 2015a; Noh et al., 2015b). Low levels of miR-H1 may serve to modulate ATRX levels which may reduce the barrier to reactivation. Another model might be that miR-H1 is expressed during the phase I wave of lytic gene expression and drives a reduction in ATRX mRNA while nascently translated ICP0 could drive ATRX loss at the protein level. The loss of ATRX may destabilize viral heterochromatin and contribute to reactivation of HSV. Recent advances in induced pluripotent stem cell-derived neuronal culture systems present a possible system for testing this hypothesis.

The latency associated-transcript (LAT) is an 8.3-9 kbp virus-encoded long noncoding RNA (lncRNA) that has been shown to promote maintenance of HSV latency and the accumulation of restrictive heterochromatin on the latent viral genome (Cliffe et al., 2009; Wang et al., 2005). The mechanism by which LAT promotes latency is not well defined. Interestingly, several recent studies have shown that ATRX activity is modulated by cellular lncRNAs. ATRX was shown to direct the activity of the Polycomb Repressive Complex 2 (PRC2) through an interaction with and possible remodeling of the Xist RNA which resulted in accumulation of H3K27me3 on the X chromosome (Sarma et al., 2014). ATRX activity was also found to be modulated by the telomere-encoded TERRA RNA that competed ATRX away from target loci (Chu et al., 2017) and by a muscle-

specific lncRNA, ChRO1, which promoted H3.3 deposition at chromocenters (Lee et al., 2018a). It is possible that the LAT RNA modulates ATRX activity. It may act to compete with ATRX for binding on the HSV genome as TERRA does at human loci, thereby alleviating ATRX-mediated chromatin stability or biasing chromatin towards a particular state or histone PTM. LAT could also be used to target PRC2 to the HSV genome through ATRX. PRC2 directs the addition of H3K27me3 to H3 histones. LAT is thought to promote H3K27me3 enrichment on the latent HSV genome and establish a latent state that is poised for reactivation(Cliffe et al., 2009; Deshmane and Fraser, 1989; Lee et al., 2018b). A pull-down of LAT RNA followed by mass spectrometry could define the interactome of LAT and provide insights into its mechanism of action such as a possible interaction with ATRX.

HSV-induced stress response.

In Chapter 3 we showed that ATRX-KO cells infected with an ICP0-null HSV experienced an induction of open chromatin regions (OCRs) at translation, heat shock, and histone related genes earlier during infection than did infected Control cells. An increase in OCRs downstream of genes was recently reported during wild type HSV infection (Hennig et al., 2018). HSV infection was also shown to induce disruption of transcriptional termination (DoTT) (Rutkowski et al., 2015), which was very similar to DoTT induced during salt and heat shock responses (Hennig et al., 2018; Rutkowski et al., 2015). DoTT was also reported to occur in *C. elegans* after heat shock and was accompanied by the accumulation of double

stranded RNA (dsRNA) foci that were enriched for antisense transcripts from translation-related genes (Melnick et al., 2019). Similarly, dsRNA accumulation has also been reported during HSV infection (Weber et al., 2006). The induction of OCRs at stress response related genes during HSV infection argues that HSV induces a stress-like response. Indeed, higher levels of OCRs are detected at these genes in infected ATRX-KO cells at 4 hpi than Control cells, arguing that *de novo* expression of viral genes is required. Our observation that H2AFX accumulates OCRs during HSV infection was validated using published ATAC-seq data that compared the effects of heat shock, salt shock, and HSV infection [http://www.bio.ifi.lmu.de/HSV-1 (Hennig et al., 2018)]. H2AFX did not accumulate OCRs during heat shock and salt shock, arguing that accumulation of some OCRs may be unique to HSV infection. This was also true for GAPDH. It is tempting to speculate that HSV induces a stress-like response as a way to activate heat shock proteins that have been well described to increase the efficiency of HSV replication through a number of different mechanisms (Bringhurst and Schaffer, 2006; Kobayashi et al., 1994; LaThangue et al., 1984; Liu et al., 2018; Preston and Nicholl, 2008; Tanguy Le Gac and Boehmer, 2002). In support of the virus inducing a heat shock-like stress response, it was shown that heat shocking cells before infection could enhance replication of an ICP0-null HSV (Bringhurst and Schaffer, 2006). HSV even encodes a viral protein, UL14, that exhibits heat shock protein-like functions and contains a conserved sequence that is similar to one found in a substrate-binding region of HSP70 (Ohta et al., 2011).

It will be important to determine how HSV triggers the stress response and if it plays a role in the transition between phases of the viral life cycle. It was reported previously that early protein synthesis but not viral replication was required for HSV-induced upregulation of HSP70 (Kobayashi et al., 1994). Infection with HSVs that are deficient for expression of various immediate early and early genes, such as *ICP27*, *ICP4*, or *ICP8*, can be used to investigate the requirements of the stress response activation. Translation is globally inhibited during heat shock response, so it is also possible HSV induces a stress response to aid in host cell shutoff. It may be informative to perform a bioinformatics study to determine if there are any features that are shared between genes that increase in OCRs during infection and any HSV genes. It is possible that HSV has adapted to take advantage of a stress response to regulate its own gene expression order and induce open chromatin on the HSV genome and escape host cell shutoff. An increased understanding of how HSV induces a stress response and the full extent of its role in the HSV lifecycle may lead to the identification of new therapeutic targets or strategies.

Appendix

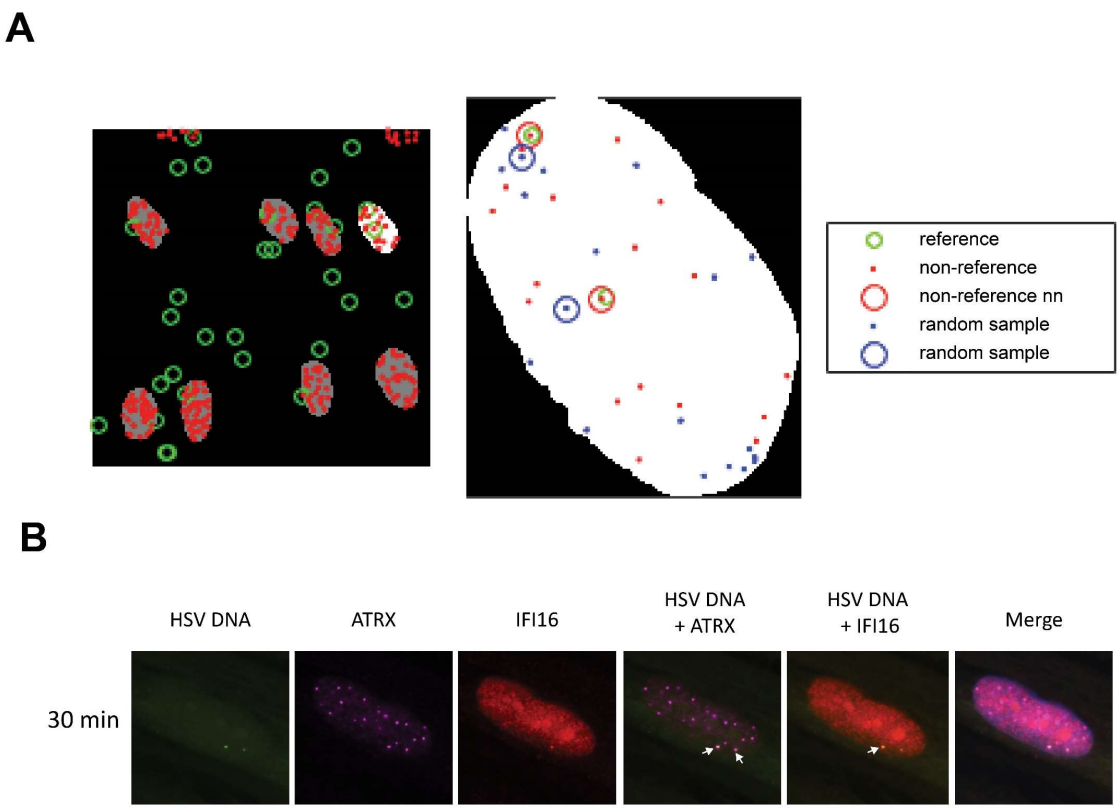

Supplemental Figure 2.1: Foci and colocalization detection.

(A) Screen shot from the frequency distribution script. For each reference channel focus (green) that is detected in a nuclear area (center), the script records the distance between the reference focus and its nearest neighbor (nn) non-reference focus (red). The script also generates random x,y positions within the nuclear mask to simulate the center of a random sample object (blue) and records the distance from the reference channel foci to random sample nn. The script generates a number of random sample points equal to the number of non-reference foci detected within that nuclear area. The script then generates a report of distances from each reference focus to its nearest neighbor in the non-random sample set and the random sample set within a defined radius from the reference focus. (B) Sample image showing ATRX (magenta) and IFI16 (red) colocalization with vDNA (green). White arrows indicate areas of colocalization.

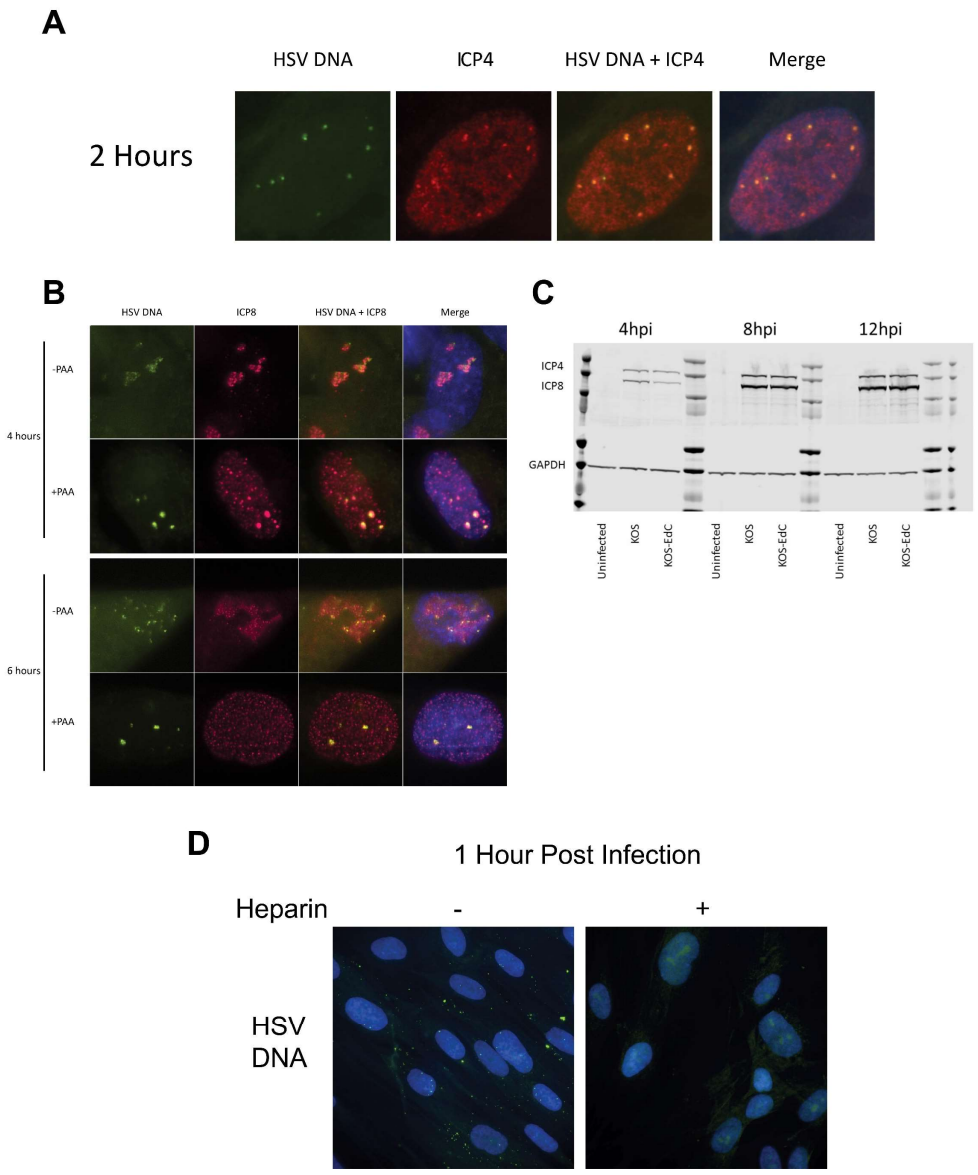

Supplemental Figure 2.2: EdC labeling of KOS HSV.

(A) HFF cells infected with HSV-EdC at an MOI of 5 and fixed at 2 hpi. vDNA is shown in green and viral protein ICP4 in red. (B) HFF cells infected with HSV-EdC at an MOI of 5 in the absence (-) or presence (+) of viral DNA synthesis inhibitor PAA and fixed at 4 and 6 hpi. vDNA is shown in green and viral protein ICP8 in red. (C) Immunoblot comparing ICP4 and ICP8 from HSV and HSV-EdC at 4, 8, and 12 hpi. (D) HFF cells infected with HSV-EdC at an MOI of 5 in the absence (-) or presence (+) heparin at 1 hpi. HSV-EdC genomes in green.

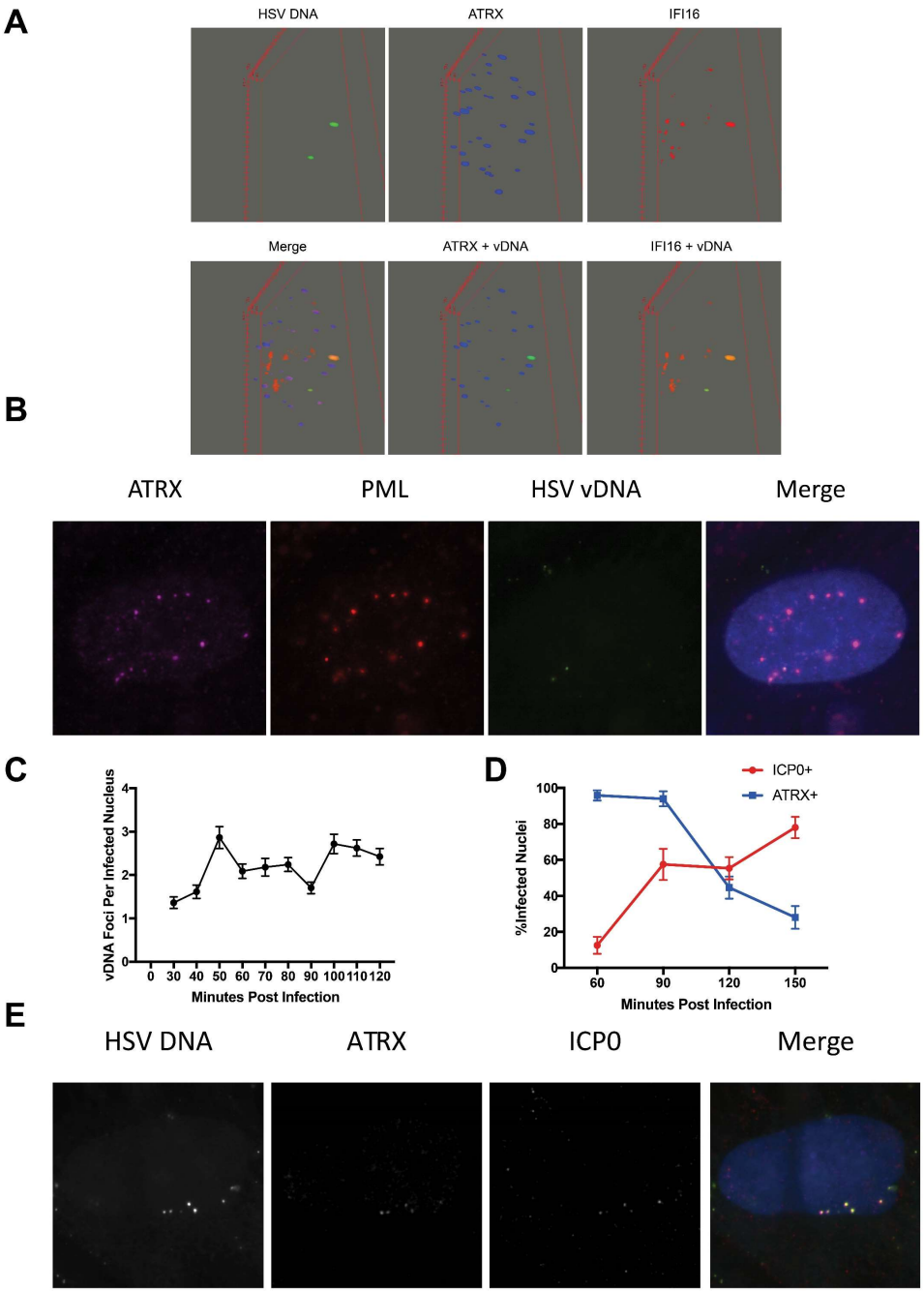

Supplemental Figure 2.3: HSV DNA colocalization with ATRX, IFI16, and PML.

(A) FIJI generated 3D volume projections of ATRX (blue) and IFI16 (red) colocalization with vDNA (green). Red lines define the bounding box of the X, Y, Z area being projected. (B) ATRX (magenta) and PML (red) colocalization with vDNA (green) at 1 hpi with HSV-EdC at an MOI of 5.

Supplemental Figure 2.3 (Continued) (C) The number of viral DNA per infected nucleus form 30-120 mpi after infection with HSV-EdC at an MOI of 5. $n \geq 36$ infected nuclei per time point. (D) Percentage of nuclei that are positive for HSV vDNA plus ATRX staining (ATRX+) or vDNA plus ICP0 staining (ICP0+) form 60-150 mpi. $n \geq 33$ infected nuclei per time point. (E) HFFs infected with HSV-EdC at an MOI of 5. Cells were fixed and stained for HSV DNA, ATRX, and ICP0 at 90 mpi.

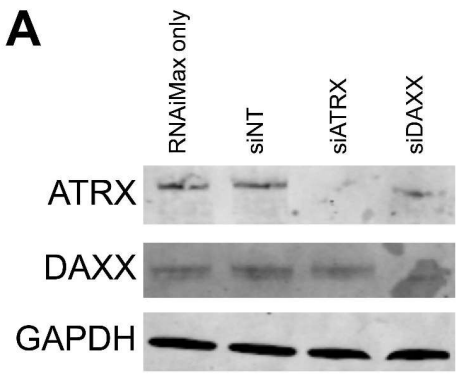

Supplemental Figure 2.4: siRNA depletion of ATRX and DAXX in HFF cells.

(A) Immunoblot detection of ATRX and DAXX from HFF whole cell lysates 72 h after treatment with transfection reagent only (RNAiMax only), siNT, siATRX, siDAXX, or siATRX + siDAXX (siA+D).

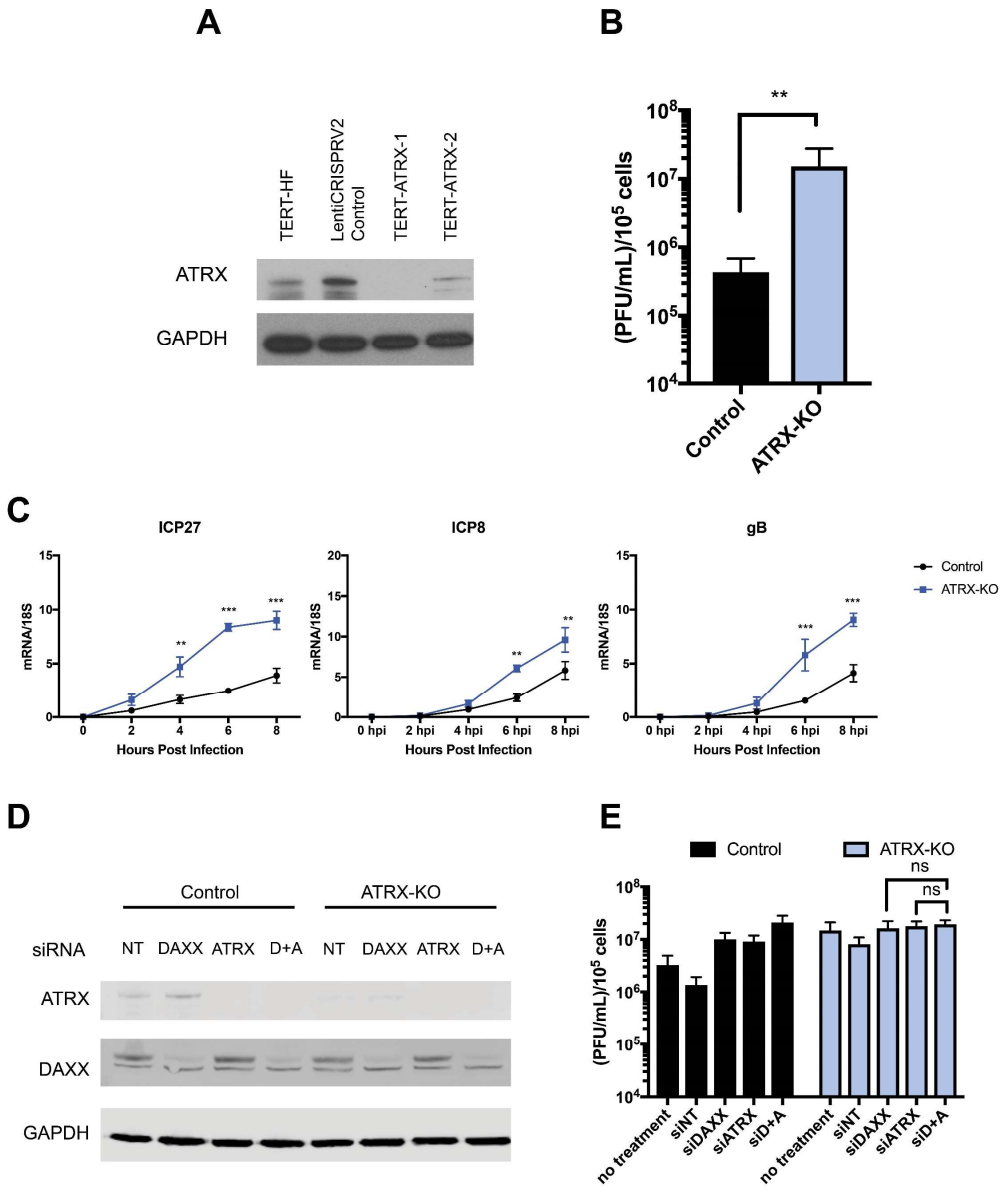

Supplemental Figure 2.5: CRISPR-mediated knockout of ATRX alleviates viral restriction.

(A) Immunoblot of immortalized fibroblasts (TERT-HF) transduced with lentivirus expressing Cas9 alone (LenitCRISPR V2 control), or Cas9 and co-expressing sgRNA against ATRX (TERT-ATRX-1 and TERT-ATRX-2). LenitCRISPR V2 control was used as the Control cell line in this study. TERT-ATRX-1 was used as the ATRX-KO cell line in this study. (B) Viral yields from Control and ATRX-KO cells infected with HSV 7134 at an MOI of 0.1 for 48 h. Viral lysates were collected and

Supplemental Figure 2.5 (Continued) titrated on U2OS cells. Yields were normalized to (PFU/mL)/1x105 cells. Results analyzed by two-tailed t-test. (C) Relative viral transcripts for *ICP27*, *ICP8*, and *gB* detected by qPCR in whole cell lysates collected from ATRX-KO or Control cells treated with siNT, siDAXX, or siATRX for 72 h then infected with HSV 7134 at an MOI of 5. Lysates were collected at 4 and 8 hpi. Results were analyzed by two-way ANOVA. (D) Control and ATRX-KO cells treated with siNT, siDAXX, siATRX, or siATRX+siDAXX (siA+D). (E) Viral yields from ATRX-KO and Control cells treated with siRNAs against non-targeting, ATRX, DAXX, or ATRX + DAXX (siD+A) and infected with HSV 7134 at an MOI of 3 and collected at 24 hpi. Results were analyzed by two-way ANOVA. Panels B, C, and E are reported as the average of 3 independent experiments $\pm$ standard error of the mean; $p < 0.05$ (*), $p < 0.01$ (**), $p < 0.001$ (***).

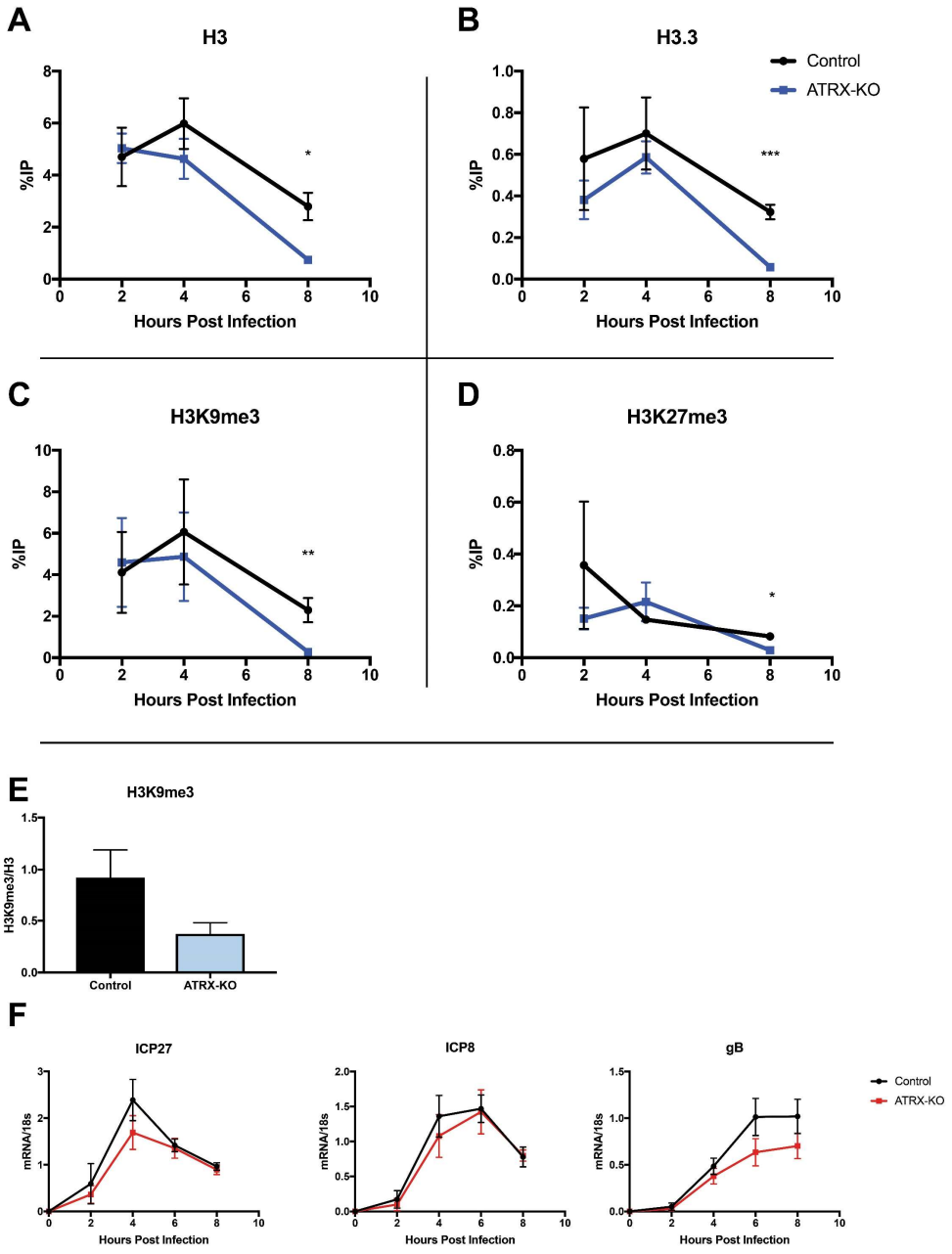

Supplemental Figure 2.6: ATRX depletion enhances removal of heterochromatin from the ICP8 promoter.

ATRX-KO or Control cells were infected with HSV 7134 at an MOI of 3. Infected cells were fixed and harvested 2, 4, and 8 hpi. ChIP-qCPR and HSV specific primers were used to detect chromatin

Supplemental Figure 2.6 (Continued) enrichment of (A) H3, (B) H3.3, (C) H3K9me3, and (D) H3K27me3 at the viral gene promoter for ICP8. Results are reported as the percent of input immunoprecipitated by each antibody. Two-tailed t-tests were used to compare results from ATRX-KO versus Control cells for each antibody and each time point. (E) H3K9me3 enrichment per H3 for the ICP8 promoter. ChIP-PCR experiments in Figure 5 - supplement 1 are reported as the average of 4 independent experiments ± standard error of the mean; $p < 0.05$ (*), $p < 0.01$ (**). (F) Relative viral transcripts for ICP27, ICP8, and gB detected by qPCR in whole cell lysates collected from ATRX-KO or Control cells that were infected with HSV 7134R at an MOI of 5. Lysates were collected at 0, 2, 4, 6, and 8 hpi. Viral mRNA was normalized to cellular 18S transcripts

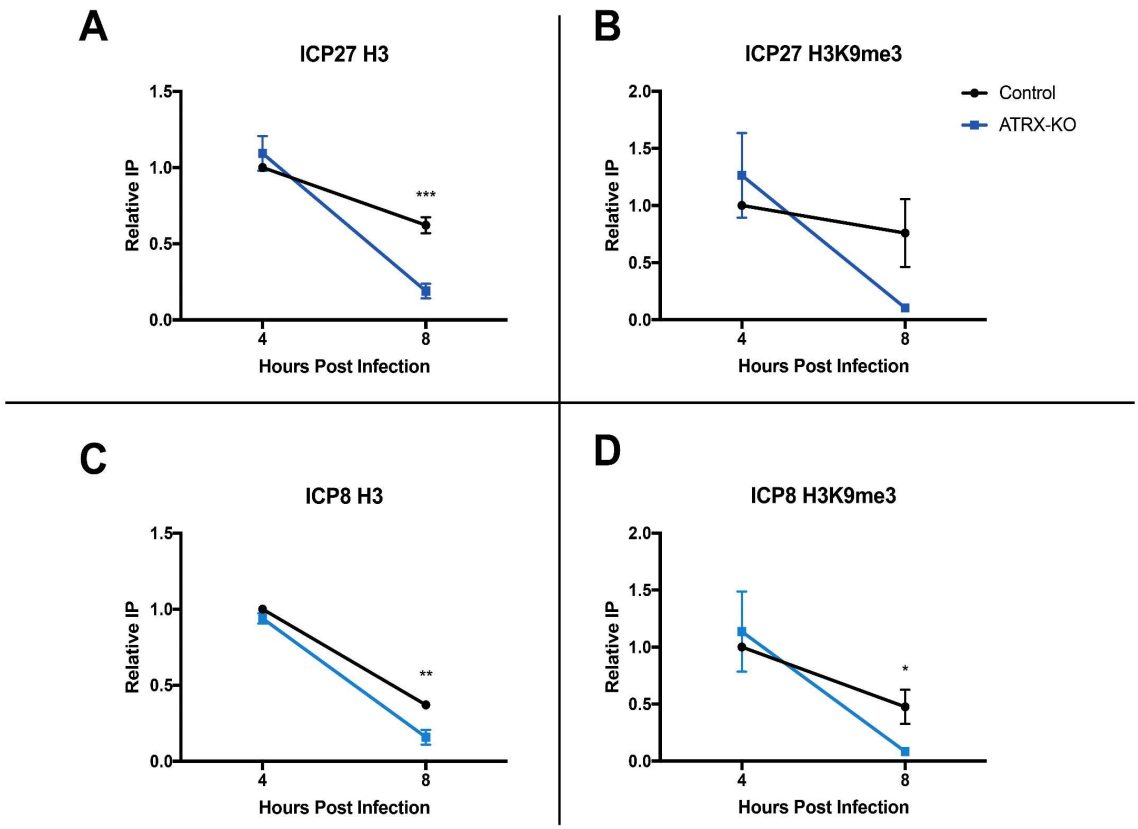

Supplemental Figure 2.7: Untreated controls for ChIP.

ATRX-KO or Control cells were infected with HSV 7134 at an MOI of 3. Infected cells were fixed and harvested 8 hpi. ChIP-qCPR and HSV specific primers were used to detect chromatin enrichment of at the viral gene promoters in the absence (this figure) or presence of PAA (Figure 2.6). Results are reported as "Relative IP" (the percent of input immunoprecipitated by each antibody normalized to the 4-hour control sample set to 1.0 for each replicate). Enrichment of (A) H3 and (B) H3K9me3 at the *ICP27* gene promoter. Enrichment of (C) H3 and (D) H3K9me3 at the *ICP8* gene promoter. Results are reported as the percent of input immunoprecipitated by each antibody. All data for Supplemental Figure 2.7 are reported as the average of 4 independent experiments ± standard error of the mean; two-tailed t-test, $p < 0.05$ (*), $p < 0.01$ (**), $p < 0.001$ (***).

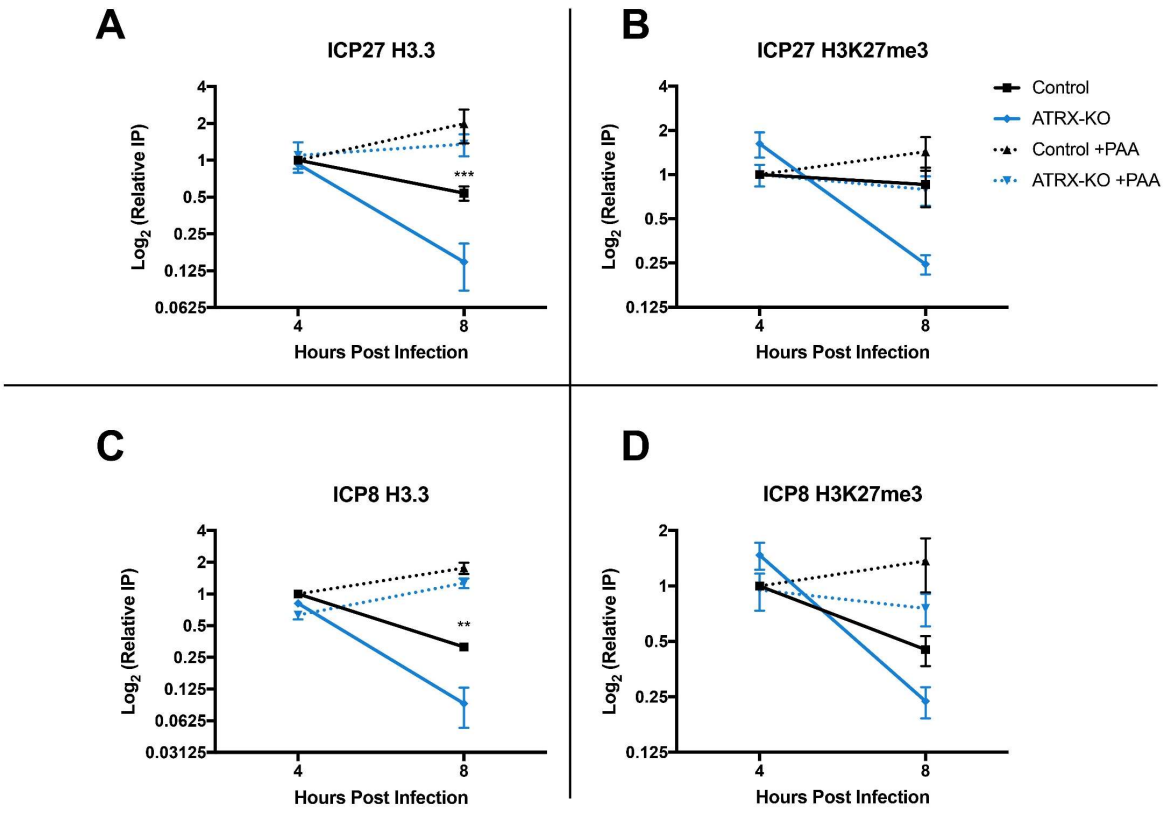

Supplemental Figure 2.8: ATRX promotes maintenance of H3K27me3 and H3.3 on input viral genomes.

ATRX-KO or Control cells were infected with HSV 7134 at an MOI of 3. Infected cells were fixed and harvested 8 hpi. ChIP-qCPR and HSV specific primers were used to detect chromatin enrichment of at the viral gene promoters in the absence (solid lines) or presence (dotted lines) of PAA. Results are reported as "Relative IP" (the percent of input immunoprecipitated by each antibody normalized to the 4-hour control sample set to 1.0 for each replicate). Enrichment of (A) H3.3 and (B) H3K27me3 at the *ICP27* gene promoter. Enrichment of (C) H3.3 and (D) H3K27me3 at the *ICP8* gene promoter. Results are reported as the percent of input immunoprecipitated by each antibody. All data for Supplemental Figure 2.8 are reported as the average of 4 independent experiments ± standard error of the mean; two-tailed t-test, $p < 0.05$ (*), $p < 0.01$ (**), $p < 0.001$ (***).

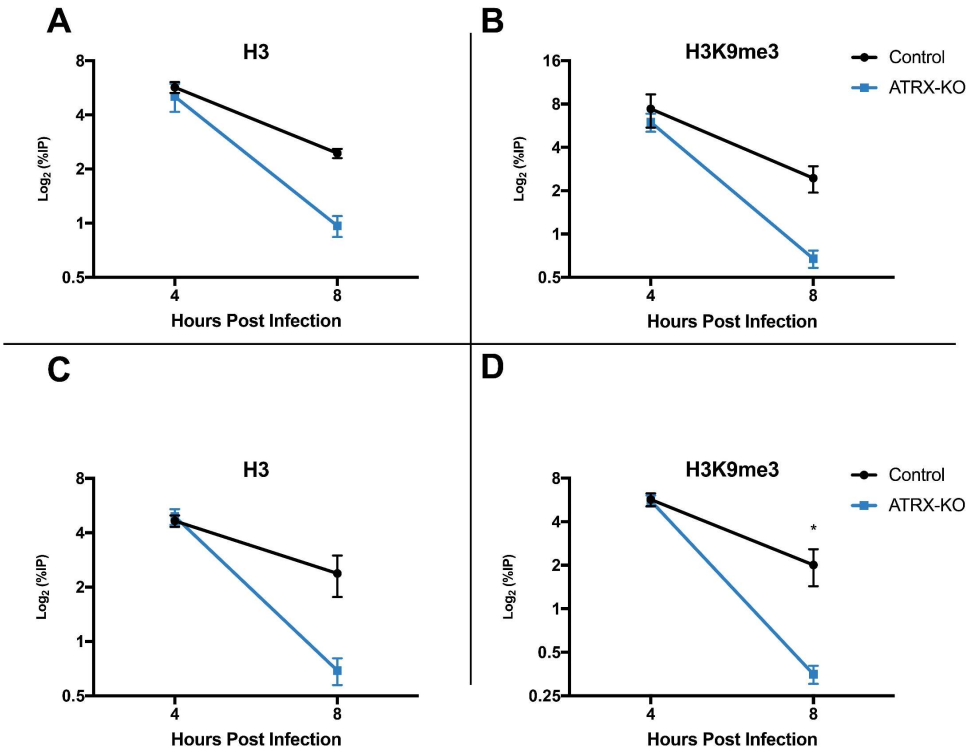

Supplemental Figure 2.9: Untreated controls for flavopiridol and α-amanitin ChIPs.

ATRX-KO and Control cells were infected with HSV 7134 at MOI 3 and fixed at 4 and 8 hpi. ChIP-qPCR was used to detect (A) H3 and (B) H3K9me3 enrichment at the *ICP8* promoter. ATRX-KO and Control cells were infected with HSV 7134 at MOI 3 and fixed at 4 and 8 hpi. ChIP-qPCR was used to detect (C) H3 and (D) H3K9me3 enrichment at the *ICP8* promoter. All data for Supplemental Figure 2.9 are reported as the percent of input immunoprecipitated by each antibody and are the average of 3 independent experiments ± standard error of the mean; two-tailed t-test, $p < 0.05$ (*).

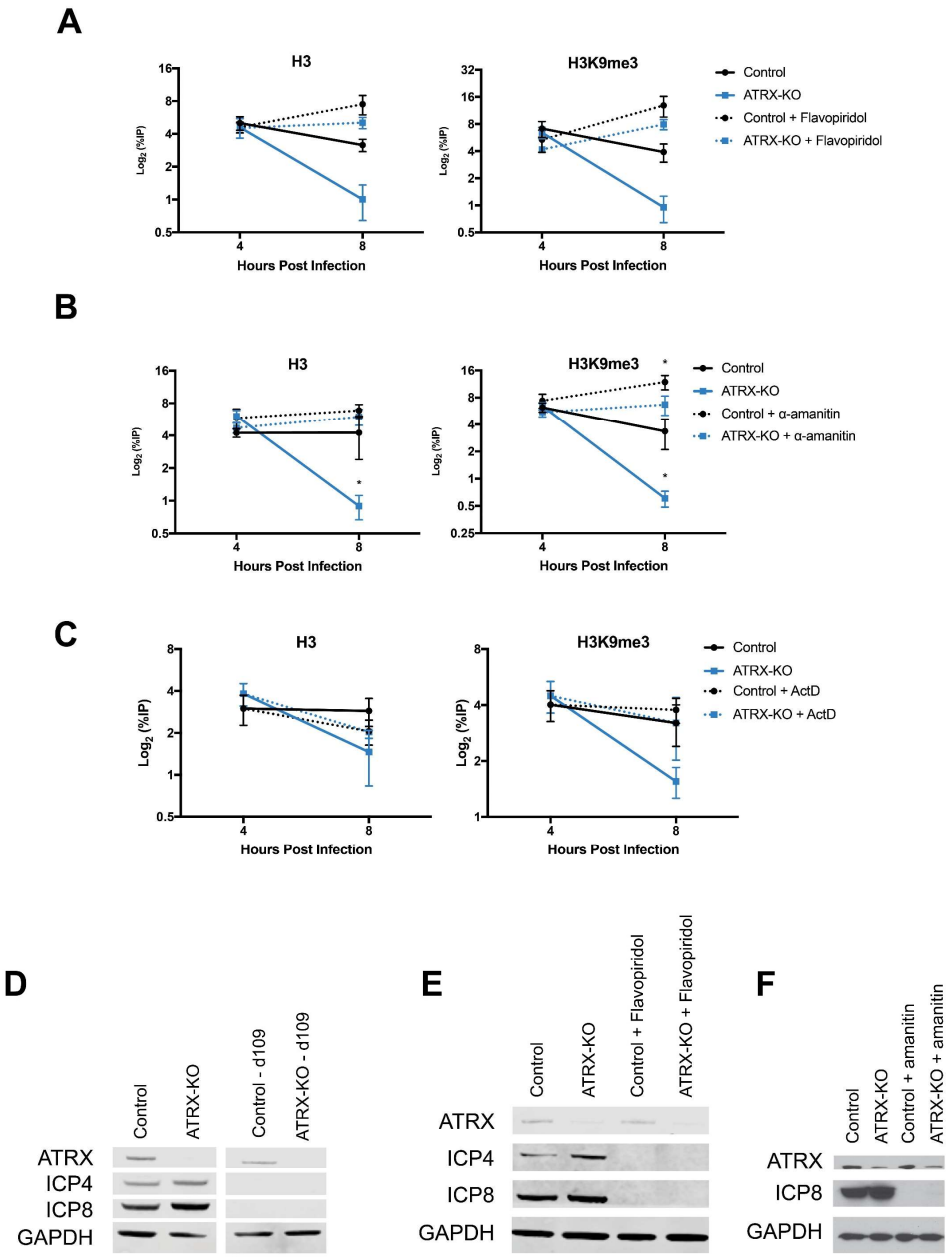

Supplemental Figure 2.10: ATRX promotes heterochromatin maintenance at the ICP27 promoter during chromatin stress.

(A) ATRX-KO and Control cells were treated with flavopiridol (flavopiridol; 1 μM) from 1 h prior to infection until time of harvest. Treated cells were infected with HSV 7134 at MOI 3 and fixed at 4 and 8 hpi. ChIP-qPCR was used to detect H3 and H3K9me3 enrichment at the *ICP27* promoter.

Supplemental Figure 2.10 (Continued) (B) ATRX-KO and Control cells were treated with α-amanitin (2 µg/mL) from 16 h prior to infection until time of harvest. Treated cells were infected with HSV 7134 at MOI 3 and fixed at 4 and 8 hpi. ChIP-qPCR was used to detect H3 and H3K9me3 enrichment at the *ICP27* promoter. (C) ATRX-KO and Control cells were infected with HSV 7134 at an MOI of 3 and treated with ActD (5 µg/mL) at 4 hpi. Samples were fixed and collected a 4 and 8 hpi. Chromatin enrichment is reported as percent input immunoprecipitated by antibodies specific for H3 and H3K9me3 as detected by qPCR using specific primers for the promoter of *ICP27*. (D) Immunoblot showing inhibition of ICP8 production in Control and ATRX-KO cells when treated with cycloheximide (CHX) or infected with HSV *d*109. (E) Immunoblot showing inhibition of ICP8 production in Control and ATRX-KO cells when treated with flavopiridol. (F) Immunoblot showing inhibition of ICP8 production in Control and ATRX-KO cells when treated with α-amanitin. All data for Supplemental Figure 2.10 are reported as the percent of input immunoprecipitated by each antibody and are the average of 3 independent experiments ± standard error of the mean; two-tailed t-test, $p < 0.05$ (*).

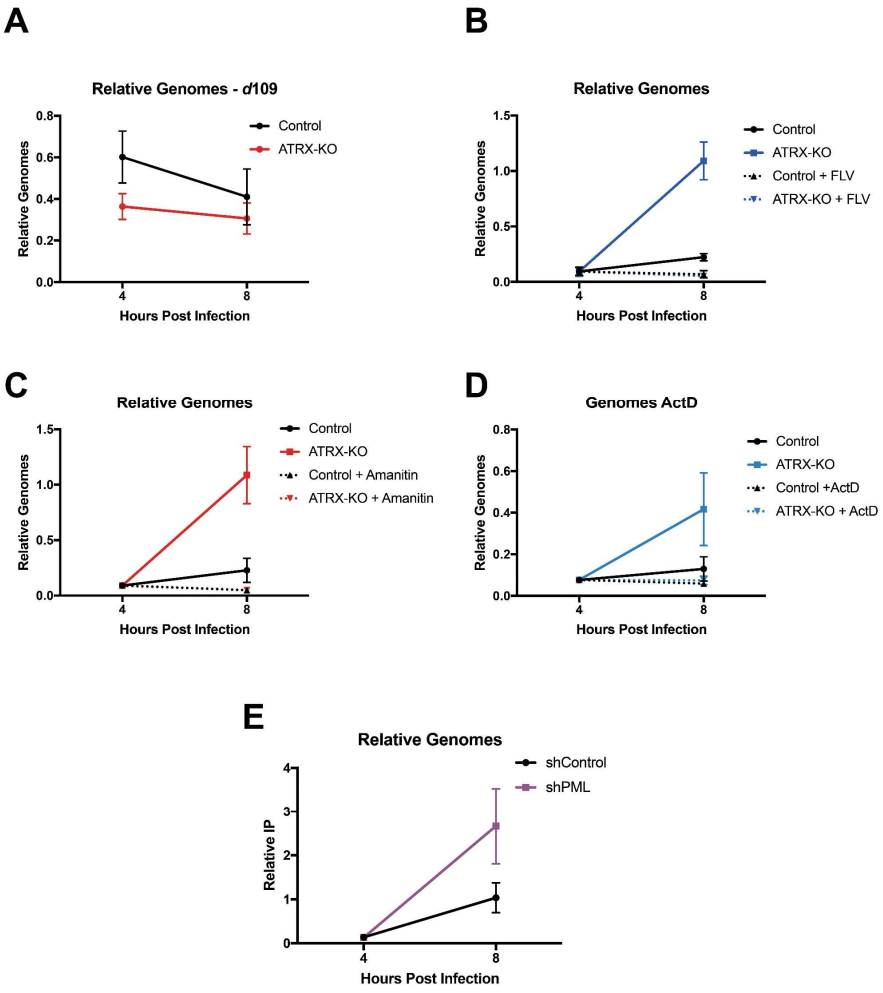

Supplemental Figure 2.11: Relative HSV genomes during drug treatment.

(A) Chromatin input for *ICP8* relative to input *GAPDH* to determine relative viral genome copy numbers in cells infected with HSV *d*109. (B) Chromatin input for *ICP8* relative to input *GAPDH* to determine relative viral genome copy numbers in the absence or presence of flavopiridol. (C) Chromatin input for *ICP8* relative to input *GAPDH* to determine relative viral genome copy numbers in the absence or presence of α-amanitin. (D) Chromatin input for *ICP8* relative to input *GAPDH* to determine relative viral genome copy numbers in the absence or presence of ActD. (E) Chromatin input for *ICP8* relative to input *GAPDH* to determine relative viral genome copy numbers in cells expressing a control short hairpin or short hairpin against PML.

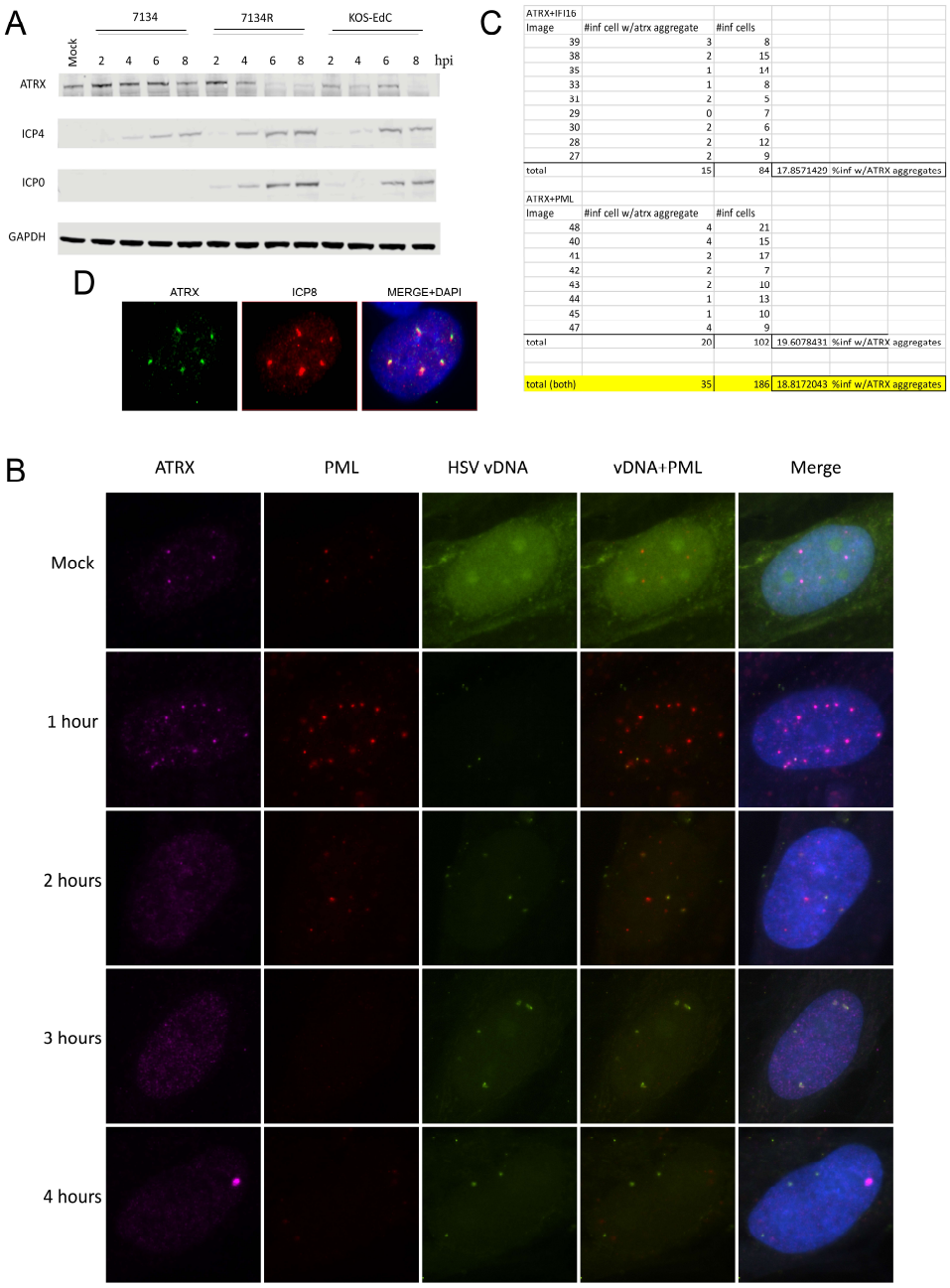

ATRX+IFI16					
Image	#inf cell w/atrx aggregate	#inf cells			
39	3	8			
38	2	15			
35	1	14			
33	1	8			
31	2	5			
29	0	7			
30	2	6			
28	2	12			
27	2	9			
total	15	84	17.8571429	%inf w/ATRX aggregates	
ATRX+PML					
Image	#inf cell w/atrx aggregate	#inf cells			
48	4	21			
40	4	15			
41	2	17			
42	2	7			
43	2	10			
44	1	13			
45	1	10			
47	4	9			
total	20	102	19.6078431	%inf w/ATRX aggregates	
total (both)	35	186	18.8172043	%inf w/ATRX aggregates	

Supplemental Figure 3.1: HSV ICP0 promotes ATRX aggregate formation post PML-NB dispersion.

(A) Human foreskin fibroblasts (HFFs) infected with 7134, 7134R (ICP0-competent), and KOS at MOI 5. Cell lysates were harvested at time points indicated for immunoblot probing of ATRX, ICP0,

Supplemental Figure 3.1 (Continued) ICP4, an GAPDH. (B) HFFs infected with HSV-EdC at MOI 5. Cells were fixed at indicated times post infection then stained with antibodies specific for ATRX and PML. Click chemistry followed by a streptavidin-488 probe was used to detect viral DNA. (C) Quantification of the percentage of cells per field of view that contain ATRX aggregates as observed in infected cells at 4 hpi. (D) HFFs infected with 7134 virus. Cells were fixed at 6 hpi and stained with antibodies specific for ATRX and ICP8 in conjunction with DAPI staining to define the nuclear area.

A

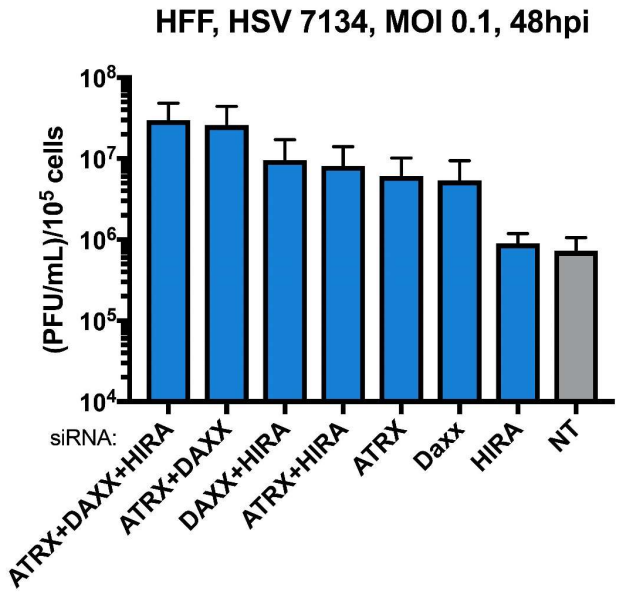

Supplemental Figure 3.2: Depletion of ATRX and DAXX increases HSV 7134 yields in HFFs. (A) HFFs treated with siRNAs against ATRX, DAXX, HIRA, and non-targeting (NT). Cells were infected with 7134 at MOI 0.1 and harvested at 48hpi. Viral yield was determined by infected U2OS cells with serial dilutions of harvested viral lysates. n=3.

A

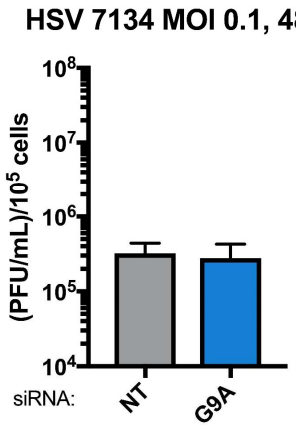

Supplemental Figure 3.3: Depletion of G9A does not enhance HSV yield.

(A) TERT-HFs treated with siRNAs against G9A and non-targeting (NT). Cells were infected with 7134 at MOI 0.1 and harvested at 48hpi. Viral yield was determined by infected U2OS cells with serial dilutions of harvested viral lysates. n=3

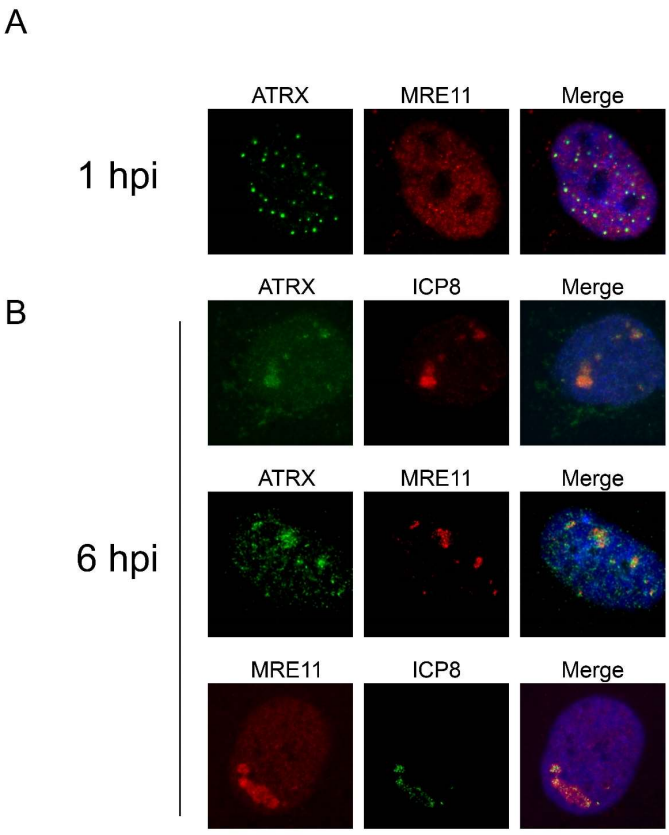

Supplemental Figure 3.4: ATRX and MRE11 localize to replication compartment by 6 hpi. TERT-HF cells were infected with 7134 at an MOI of 5 and fixed at (A) 1 hpi or (B) 6 hpi. Cells were stained using antibodies specific for MRE11, ATRX, or ICP8 with DAPI used to define the nuclear area.

A

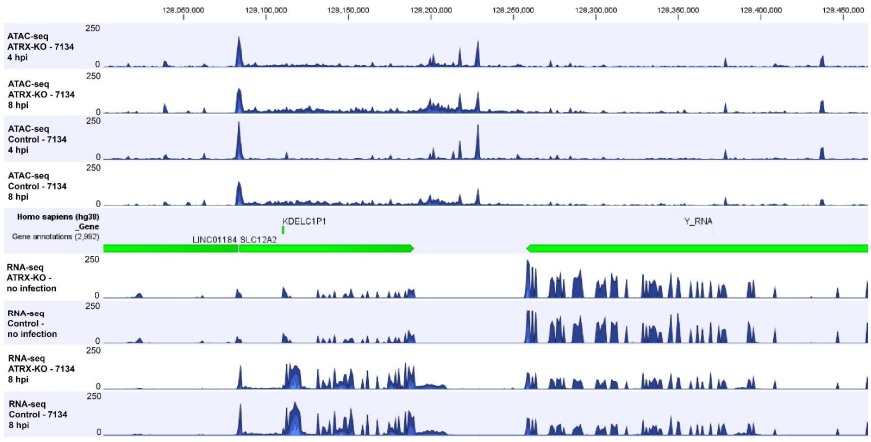

B

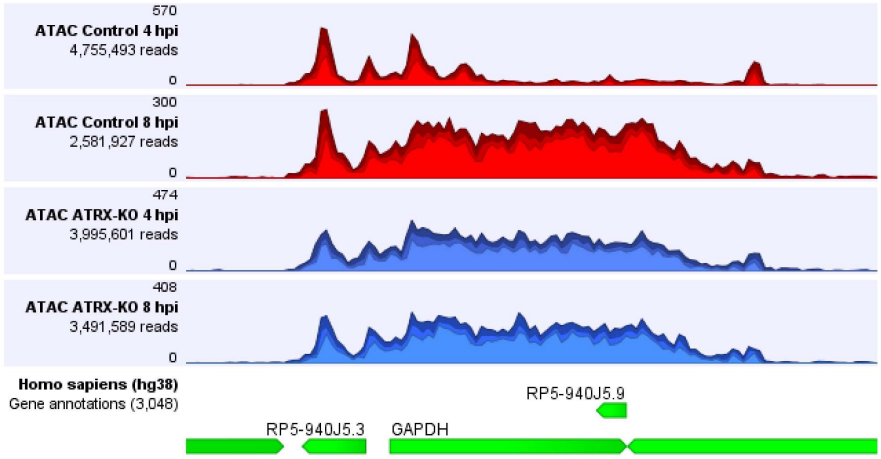

Supplemental Figure 3.5: HSV infection induces DoTT and OCRs.

(A) ATAC-seq and RNA-seq coverage of SLC12A2 and the downstream region in (blue) ATRX-KO and (red) Control cells infected with 7134 at MOI 5, 4 and 8 hpi. Reads are not normalized. (B) ATAC-seq read coverage in in (blue) ATRX-KO and (red) Control cells infected with 7134 at MOI 5, 4 and 8 hpi. Reads are not normalized.

Supplemental Table 3.1: Differential gene expression in uninfected ATRX-KO cells.

Differential gene expression by fold change and difference in RPKM values in uninfected ATRX-KO cells as compare to uninfected Control cells.

Human - ATRX-KO/Control
no infection

Upregulated in ATRX-KO

Gene	Difference - RPKM	Fold Change
AC004980.10	0.505144546	19.5325906
AC079466.1	0.520579022	2.43971145
AK4P3	1.74814476	2.83683323
AL356585.2	0.772109862	6.69958421
AL772307.1	0.502996905	3.39697227
APOBEC3B	0.742016036	2.24799636
BABAM1	1.086596739	4.0379541
CCNG1P1	0.582435451	3.11389125
CNPY4	2.271446337	4.42252878
CSAG4	0.891196864	2.15432984
CTA-29F11.1	1.224312172	2.23576236
CTD-2021A8.3	0.60729835	2.91927305
CTD-2278I10.6	0.853596372	3.37229693
DHFRL1	2.140588259	2.62228322
DHFRP1	2.579376352	2.38229224
DHRS2	2.176915289	2.4649492
EIF3FP1	3.256733252	2.57534687
EPB41L4A-AS1	0.751914792	2.12540292
ERF	1.53134778	2.89719649
FDPSP7	0.666336661	5.71308973
GS1-184P14.2	25.3598604	2.89931088
INHBA	1.140081746	3.64300081
ITGA5	10.90582703	2.00761325
JPX_1	0.901599241	2.12310767
KRTAP1-5	4.48466082	2.6795083
LY6G5B	0.830086333	3.0109527
MAEA	1.633076707	2.25847892
MAMDC2-AS1	0.596416319	2.83671642
MLLT10P1	0.82078279	2.22109726
NDUFC2	2.458386918	2.45033111
PIN4P1	0.725776628	2.24799636
POLR3GP1	0.582930544	2.12310767
PSG2	0.559377259	5.15903811
PSMA2_2	1.434608642	2.28544323
RP11-241F15.9	0.804078305	-
RP11-24C3.2	0.774185092	3.08280143
RP11-302B13.1	0.529463123	2.54772921
RP11-324L17.1	0.542245474	2.01695229
RP11-552F3.10	2.313561205	2.23547824
RP11-603J24.17	2.290603895	2.2400713
RP11-697E2.6	1.014543168	2.03383623
RP11-753H16.5	0.530845853	2.05134774
RP11-7F17.1	0.658831232	2.60838942
RP11-849F2.7	1.737269534	3.96178632
RP11-894P9.2	0.781935197	2.37120115
RPPH1_2	0.54050312	7.64318762
RPS10P3	6.306338248	2.61949623
RPSAP8	1.171497252	2.30303205
SAA1	0.539275779	2.61097071
SAPCD1-AS1	0.661259261	5.45941973
SFRP1	2.634725021	2.0689132
SLC39A3	0.792179106	2.38344111
SNAPC1	1.322225913	2.13733917
SNRPCP9	3.678615828	2.2775155
SNX18P23	0.520760877	14.0125106
SPATA20P1	0.600697217	2.61849946
TAF9P3	0.527439052	5.94470148
TERT	1.614614608	3.74394473
TMEM189-UBE2V1	1.102422822	2.21622336
UFC1	1.745146842	2.86518435
VCY1B	36.35336419	2.80035214
Y_RNA_101	0.549309452	5.09545841
ZNF582	0.533390806	2.22052522

Down regulated in ATRX-KO

Gene	Difference - RPKM	Fold Change
AC018738.2	-1.20005255	-6.476355479
AC104451.2	-0.831978525	-2.060658561
AC129778.2	-0.588579184	-17.1766559
AC144530.1	-0.533679035	-2.355038356
AF196779.12	-0.533734989	-11.23416945
BMS1P14	-0.770639145	-19.37072089
CH507-513H4.3	-0.598583445	-2.067200335
CH507-513H4.4	-0.580882295	-2.259563828
CH507-513H4.5	-3.417880654	-2.66190699
CH507-513H4.6	-0.599984479	-2.234267158
COL3A1	-3.343039545	-2.170719198
CTC-250I14.3	-0.497596969	-2.379570006
CTC-428G20.6	-0.505438136	-2.481201125
CTD-2369P2.4	-0.554766484	-2.558058904
DLEU2_1_2	-0.51963485	-2.355038356
DUX4	-0.894603885	-40.42815844
EDN1	-1.165097577	-2.190874753
HIST1H4C	-1.371191425	-2.296162397
IGHVII-44-2	-1.344332295	-3.434430936
PCDH18	-0.794210756	-2.039118577
RMRP_1	-0.56643998	-2.64941815
RNA5-8S5_4	-0.673179789	-3.238177739
ROCK1P1	-0.646118368	-7.778108332
RP11-1252D15.1	-0.582677774	-8.242634246
RP11-16F15.2	-0.533320516	-2.11953452
RP11-1E6.1	-0.716380504	-2.307937589
RP11-305M3.2	-2.20978231	-2.054395162
RP11-330L19.1	-0.498625778	-2.256911758
RP11-397E7.2	-1.566577022	-2.191494026
RP11-506M12.1	-1.190782574	-2.656925823
RP11-613E4.5	-0.563734813	-2.878380213
RP11-753H16.3	-2.434985693	-2.958512206
RP11-775C24.5	-0.646444726	-2.285772522
RP11-804A23.2	-2.265423212	-2.401946679
RP11-867G23.3	-0.586399056	-4.853426873
RPL21P119	-1.623858907	-2.355038356
RPL7P6	-2.645218417	-2.212053884
RPS26P6	-27.71003082	-2.081550031
RPS26P8	-17.40569841	-5.920610446
SETP8	-1.729395814	-2.004287963
SLC7A5P1	-0.565385157	-2.64941815
SNORD116-4	-0.585722617	-5.88759589
SPTLC1P1	-0.721692336	-3.72881073
TBX2-AS1	-1.596139783	-2.073621844
UBE2L4	-1.007912425	-2.355038356
UBE2V1	-2.369884459	-2.676655159
USHBP1	-0.633608212	-2.273997807
VCX	-0.557943051	-2.099672751

Supplemental Table 3.2: Differential gene expression in ATRX-KO cells infected with HSV 7134 at 8 hpi.

Differential gene expression by fold change and difference in RPKM values in 7134 infected ATRX-KO cells 8 hpi as compare to 7134 infected Control cells 8 hpi.

Human - ATRX-KO/Control
8 hpi

Upregulated in ATRX-KO

Gene	Difference - RPKM	Fold Change
AC005363.11	0.59700152	2.304587422
AC005776.1	0.661847583	4.033027988
AC006129.1	0.536381389	2.729116684
AC008914.1	0.536171654	?
AC009237.14	0.716456446	?
AC016700.6	6.793763093	2.240571104
AC016722.4	0.915147898	2.66865568
AC017079.3	0.711160906	3.072783229
AC018462.3	0.939094316	2.832722039
AC022210.2	8.847257163	2.508394473
AC024590.1	0.499447568	?
AC093824.1	0.565335325	4.609174843
AC122714.1	0.663940324	4.609174843
AC132812.1	0.721973712	?
AC134878.1	0.878546325	?
AC144831.3	1.150731531	2.64600778
ACTL7B	0.604959734	3.021570175
AE000658.30	0.601093202	2.880734277
AL021918.2	1.214230843	2.496636373
AL022393.7	0.596125375	3.62149452
AL022393.9	0.543577217	2.087173514
AL132780.1	0.858335232	6.913762265
AL442127.1	0.660501313	?
APOA1	0.682616074	6.273599092
APOA1-AS	0.761338056	4.03488055
ATP6V0C	0.680309122	2.070596745
BTF3P8	1.084922801	2.442862667
C14orf178	0.500778224	3.089854247
C1orf162	1.217686524	2.321348057
C1QTNF5	1.380747577	2.11506543
CALM2P2	0.526931517	2.127311466
CDH12P3	1.136830948	8.066055976
CTC-350I8.1	0.660965728	2.650275535
CTD-2235C13.3	1.862385503	2.184556827
CTD-2545G14.6	2.725452574	2.503903091
DHFRP1	4.04227016	2.45744271
DLX3	1.165757312	3.331176364
EEF1G	3.181219406	2.029649898
EIF3KP1	0.67588388	3.802569246
FGF18	0.842806137	3.239948762
GAPDHP45	0.745090045	9.218349687
GNRH2	0.553847213	2.145039062
GS1-259H13.7	0.731780675	2.520642492
GUCA2A	0.511389434	2.771733521
HIST1H2AC	1.355654804	2.112705034
HIST1H2AE	0.837613459	3.600917846
HIST1H3H	0.724137847	2.048522153
HIST1H3PS1	0.6112672	2.07412868
HIST2H2AA3	2.609066661	2.131743365
HMGA1P2	1.049950148	5.30055107
HMGB1P3	0.686267256	3.969011671
HSPE1P2	1.757072279	1.999568498
IDI2	0.591297692	2.459952866
JKAMP	0.739364579	2.464771749
KRT8P11	1.496216153	2.131743365
LA16c-335H7.2	3.884447124	2.139974034
LAP3P2	0.63185687	20.35718889
LDHBP1	0.796763511	3.561635106
LINC01018	0.720336825	2.704501121
MAMDC2-AS1	1.099094956	6.377826313
MIR3925	0.741543738	4.609174843
MIR410	0.50638434	?
MIR600HG	0.6351758	3.761510504
NDUFA5P11	0.870513621	2.048522153
OOEP-AS1	0.540509414	2.041373122
PKMP3	0.531605478	2.71612089
POLG2	2.460063815	2.092975981
PPP1R35	0.603560182	3.578175207
PRRG3	1.186076756	2.791507994
PVT1_1	1.083328017	4.321101416
PVT1_1	1.083328017	4.321101416
PYCARD	14.75270489	2.039880131
RANP4	1.602234892	3.456881132
RMRP_1	1.237281524	3.328848498
RN7SL1	2.473433572	2.73136287
RN7SL472P	0.497742969	?
RN7SL832P	1.814341374	2.418193844
RNA5-8S5_1	0.809380212	2.304587422
RNA5-8S5_2	0.840875103	2.016513994
RNA5-8S5_3	0.611493728	6.913762265
RNA5-8S5_4	1.222987455	6.913762265
RNU4-2	0.534246128	5.761468554
RNU6-30P	0.941931008	2.592660849
RNU6-322P	1.262312746	9.218349687
RNU6-415P	0.989359789	4.033027988
RNU6-4P	0.601186405	2.016513994
RNU6-510P	0.50638434	?
RP11-100N3.2	0.900867836	5.185321699
RP11-106M3.1	0.979884149	7.144221007
RP11-1112J20.1	1.439362159	6.913762265
RP11-111F16.2	0.533333684	4.22507694
RP11-116K4.1	0.701117506	2.232569065
RP11-158M2.3	2.014466829	2.547294955
RP11-15I22.8	2.900097106	2.174751511
RP11-166N17.1	1.468485571	2.197288817
RP11-206L10.9	1.469269871	3.356884841
RP11-20I23.2	1.476187387	2.128110006
RP11-20I23.3	1.371770973	4.578582975
RP11-324E6.10	0.649403825	2.240571104
RP11-357K9.2	0.600983612	?
RP11-365H22.2	2.519046903	2.044392068
RP11-390K5.1	2.068714888	2.029038926
RP11-428G5.2	0.504118759	4.148257359
RP11-434O22.1	3.128305976	2.538647082
RP11-434P11.1	0.83752324	2.005844608
RP11-464D20.2	1.957761345	2.043690732
RP11-492M23.2	1.053036499	2.914625269
RP11-603J24.17	3.772698933	3.76291425
RP11-640N20.1	1.287128678	2.441493605
RP11-644F5.15	0.562419385	2.551507503
RP11-681L4.1	0.820434385	2.101241473
RP11-707G14.1	0.566739564	4.033027988
RP11-779O18.2	0.52483197	2.440151388
RP11-977G19.12	0.507099271	3.072783229
RP3-336K20__B.	0.539661505	4.897248271
RP3-522D1.2	2.546684076	5.185321699
RP4-713B5.2	0.756496082	2.440151388
RP5-1182A14.5	0.555050495	2.189358051
RP5-862P8.3	0.611973468	4.897248271
RP5-940J5.3	0.993784602	4.452043883
RP6-201G10.2	0.577243612	2.088532351
RPL12P8	14.44668521	4.756276168
RPL21P119	1.956332916	4.123998544
RPL21P75	0.814718498	3.072783229
RPL29P11	1.537443399	2.406260396
RPL38P4	2.195713905	2.41432968
RPL7P6	1.511601068	2.13731898
RPL9P18	1.094289409	3.312844419
RPS15AP24	3.785641165	2.114797869
RPS6KL1	0.512993413	2.002316416
RPSAP8	1.788463214	2.004991057
SLX1A-SULT1A3	0.944293746	4.078663382
SNORD116-22	0.594451182	?
snoU13_26	0.707954805	?
TACSTD2	0.516312916	7.393884644
TAL2	0.644421691	3.969011671
Telomerase-vert	0.510449208	8.066055976
TERT	22.37917407	5.852550767
TUBB3_1	0.548667332	4.787594515
VTRNA1-1	0.809569923	2.688685325
XXbac-BPGBPG5	0.800993051	10.7547413
Y_RNA_319	2.154932077	2.736697563

Down regulated in ATRX-KO

Gene	Difference - RPKM	Fold Change
AC005702.2	-0.546701447	-2.169585737
AC066694.1	-0.559803111	-5.207005769
AF111168.2	-0.878915393	-?
AKIRIN2P1	-2.942588609	-2.014615327
ALKBH6	-0.544140701	-3.351175508
BOLA2B	-1.284902918	-2.180169082
BTF3L4P1	-0.720871842	-2.682396911
CALM2	-3.476255764	-2.105335549
CCIN	-1.404474856	-2.451842522
COL3A1	-2.043596943	-2.295949094
CTC-518P12.6	-1.253815061	-2.800737952
CTC-756D1.1	-0.734826699	-2.101072503
CTD-2022H16.2	-0.611206359	-2.110948285
CTD-2228K2.7	-0.870901245	-3.537630077
CTD-2269E23.2	-2.57513614	-2.033211777
CTD-2545G14.7	-1.24014496	-2.812222525
CTD-3193O13.12	-0.693563699	-5.39750598
CTD-3203P2.3	-0.761396568	-2.756650113
ELP5	-1.14652462	-2.935598319
ERF	-1.265425297	-2.309907203
FEN1	-5.113545972	-2.420399385
FOXG1	-0.744041104	-2.084688904
FTX_4	-0.93582024	-4.773088622
GNG10	-0.995678569	-3.173019141
GPS2	-1.648643167	-2.767471576
GS1-393G12.14	-0.51975793	-2.975431868
HAUS6P3	-1.680919761	-2.01062599
HMGN1P30	-0.586416917	-2.231573901
HRCT1	-2.452563368	-2.659855761
IGHV3-38	-0.577933966	-2.524608858
IGHVII-44-2	-0.910678878	-4.122212901
KCTD12	-0.54249758	-2.251678171
LAMTOR3P1	-0.540006612	-2.217798754
LSM6P2	-1.039446155	-2.121372721
MIR3143	-0.502237367	-?
MIR4477A	-1.337456548	-6.942674359
MIR762	-0.542796049	-3.47133718
MRPL2P1	-0.71471762	-2.00084018
NHLRC1	-0.593713772	-2.334175
PA2G4	-5.491846035	-2.082737253
PCDH18	-1.200439734	-2.421381856
PFN1P3	-0.621077704	-2.711982172
PLAU	-5.678883918	-5.531685033
POLR3GP1	-1.007986034	-2.603502885
PYCR2	-1.282984947	-6.324894013
RAD17P1	-0.908068487	-2.21091118
RBPJP6	-0.614505387	-2.663353526
RNU6-9	-0.546384953	-2.603502885
RP1-198K11.5	-0.741803655	-2.132392839
RP11-1057B6.1	-0.921910739	-2.192423482
RP11-108L7.15	-0.505100019	-2.082802308
RP11-259N19.1	-0.507746525	-5.640922917
RP11-323N12.5	-0.557550858	-2.603502885
RP11-328J14.2	-1.367613585	-2.737015853
RP11-329A14.1	-0.56470278	-3.781277999
RP11-363I22.3	-0.675824655	-2.975431868
RP11-395A13.2	-1.31116194	-2.192423482
RP11-434E6.4	-0.884251103	-2.024946688
RP11-452L6.1	-0.555594267	-2.675822409
RP11-460N20.3	-0.63997143	-7.810508654
RP11-498C9.4	-0.520635475	-5.640922917
RP11-566K11.5	-1.367749741	-2.861507675
RP11-732A19.8	-1.233054773	-4.512738333
RP11-76N22.1	-0.499951004	-2.121372721
RP11-7F17.1	-0.825961326	-2.748141934
RP11-800A3.7	-0.746317731	-2.243971534
RP11-96J19.1	-0.950255441	-2.169585737
RPL10L	-2.066807525	-2.770394095
RPL7L1P8	-0.943951694	-2.009721525
SRSF2	-4.673616242	-2.326622419
TBX2	-1.077926791	-3.057932479
TCEAL7	-0.510442072	-2.455336054
TERF1P2	-0.634433296	-2.004283967
TIGD2	-1.050810857	-2.409957107
TMPO-AS1	-1.110416049	-2.072175765
UBE2L5P	-2.001960444	-2.08649522
UFC1	-0.537132724	-2.210631954
USP27X	-0.549477156	-2.488883261
Y_RNA_700	-0.789827559	-2.314224786
ZBTB9	-0.699179665	-12.43895823

Supplemental Table 3.3: Changes in accessibility and expression of histone genes during HSV 7134 infection.

Differential gene expression of histone genes by fold change and difference in RPKM values in 7134 infected ATRX-KO cells 8 hpi as compare to uninfected ATRX-KO cells.

Histone Genes

ATAC-seq - ATRX-KO 4 hpi/Control 4 hpi

RNA-seq - ATRX-KO 8 hpi/ATRX-KO no infection

Gene	ATAC-seq Difference	ATAC-seq Fold Change	RNA-seq Difference (RPKM)	RNA-seq Fold Change
H1F0	742.7	2.6578125	-94.41700924	-3.284995051
H1FNT	-3.2	-1.296296296	0	1
H1FOO	-37.1	-1.115720524	0	1
H1FX	351.3	1.76820468	92.5455564	2.75768344
H1FX-AS1	8.2	1.02173913	0.120846135	1.236105782
H2AFB1	-0.9	-	0.062111878	-
H2AFB2	0.3	1.157894737	0.104769174	-
H2AFB3	1.3	1.684210526	0.215920226	-
H2AFJ	268.6	1.720880301	-2.206635107	-1.471165387
H2AFV	115.8	1.242818201	-3.33677627	-1.664414523
H2AFX	1111.2	3.229981939	296.7404933	3.414346396
H2AFY	-554.7	-1.180613441	-0.223069626	-1.108283297
H2AFY2	-11.1	-1.028645161	9.05E-03	4.11991427
H2AFZ	535.5	1.998136067	-66.78574593	-2.01996302
H2AFZP1	0.2	1.222222222	-0.016553245	-
H2AFZP3	0	1	6.620807703	1.280854131
H2AFZP4	0	1	-1.178424557	-1.609256787
H2AFZP5	-2.8	-	0	1
H2AFZP6	0	1	0	1
H2BFM	1.5	1.094936709	0.881617303	3.704798314
H2BFS	0.3	1.157894737	-3.857774123	-1.731914278
H2BFWT	-10.8	-2.113402062	0.022288731	2.640970686
H3F3A	31	1.022750624	-2.237489108	-1.291714099
H3F3AP1	0	1	0	1
H3F3AP3	0.3	1.157894737	0.044790752	-
H3F3AP4	0.2	1.222222222	-2.202936952	-1.20694259
H3F3AP5	0.3	1.157894737	0.042493791	-
H3F3AP6	0.2	1.222222222	-0.647340896	-1.147420169
H3F3B	635.8	1.293604248	2.429910513	1.055249075
H3F3BP1	-0.9	-	-0.527908491	-2.9450451
H3F3BP2	-17.7	-1.260294118	0	1
H3F3C	0.7	1.14893617	3.617253057	1.104906107
HIST1H1A	-11.2	-1.207407407	0	1
HIST1H1B	264.4	3.057587549	0.05925402	1.584582411
HIST1H1C	14.9	3.660714286	-0.50727971	-1.893243279
HIST1H1D	108.4	2.293556086	-0.069096126	-
HIST1H1E	222.8	2.69687738	0.216675263	3.486081305
HIST1H1PS1	21.4	2.768595041	0.419271881	4.753747234
HIST1H1PS2	-0.8	-1.727272727	0	1
HIST1H1T	0	1	0	1
HIST1H2AA	2.2	-	0	1
HIST1H2AB	70.6	1.773274918	0.202658209	7.922912057
HIST1H2AC	704.4	1.983524155	1.944675676	4.090118703
HIST1H2AD	138.2	2.348292683	0.139597835	1.250986114
HIST1H2AE	88.5	1.569131833	1.042564595	9.903640071
HIST1H2AG	443.5	2.055701024	-0.173145133	-1.496983058
HIST1H2AH	78.4	1.51008458	0.163723508	2.376873617
HIST1H2AI	167.2	1.915662651	0.578112368	4.15952883
HIST1H2AJ	63.5	1.592903828	0.451385459	3.169164823
HIST1H2AK	8.2	3.216216216	0.034223604	1.584582411
HIST1H2AL	-0.4	-1.093023256	-0.024321495	-1.262162186
HIST1H2AM	108.8	3.385964912	0.097724758	2.112776548
HIST1H2APS1	1.3	1.684210526	0	1
HIST1H2APS2	-0.9	-	0	1
HIST1H2APS3	-6.9	-2.604651163	-0.085854515	-
HIST1H2APS4	15.2	1.44057971	0.044243736	1.267665929
HIST1H2APS6	-2.6	-3.363636364	0	1
HIST1H2BA	-0.6	-1.272727273	0	1
HIST1H2BB	1333.4	1.297507753	-0.074907819	-1.233295
HIST1H2BC	7.4	1.11028316	-5.71E-03	-1.47252255

Gene	ATAC-seq Difference	ATAC-seq Fold Change	RNA-seq Difference (RPKM)	RNA-seq Fold Change
HIST1H2BD	322.4	1.663101604	0.156690287	1.725150206
HIST1H2BE	39.8	1.59314456	0.529586823	3.961456028
HIST1H2BF	61.1	1.612838516	-0.080370603	-1.419932459
HIST1H2BG	191.5	1.846221829	1.120358157	5.070663716
HIST1H2BH	69.3	1.506208912	8.812251348	9.84361801
HIST1H2BI	109.9	1.710866753	0.083150915	2.376873617
HIST1H2BJ	228.6	1.251734391	9.27E-04	1.008370625
HIST1H2BK	141.9	2.199492815	-13.74117446	-1.839730555
HIST1H2BL	153.8	2.162509448	0.222319998	2.178800816
HIST1H2BM	55.7	1.712276215	-0.072934865	-2.524324372
HIST1H2BN	699.8	1.438086891	0.063070791	2.259978193
HIST1H2BO	95.7	1.796173045	0.463601916	2.535331858
HIST1H2BPS1	-0.9	-	0	1
HIST1H2BPS2	0	1	0	1
HIST1H2BPS3	-0.8	-1.727272727	-0.014015172	-1.262162186
HIST1H3A	116.8	2.306487696	0.282492333	11.09207688
HIST1H3B	66.1	1.63926499	0.242872676	3.169164823
HIST1H3C	1.8	1.382978723	4.74E-03	1.056388274
HIST1H3D	121.8	2.390410959	0.156740381	1.373304757
HIST1H3E	2.3	3.555555556	-0.832432343	-3.085285343
HIST1H3F	83.8	1.908893709	0.165791171	3.961456028
HIST1H3G	152.7	1.348789402	-0.106008812	-1.519269298
HIST1H3H	383.9	2.84833895	1.154355812	5.432853982
HIST1H3I	97.4	2.742397138	0.126171515	1.901498894
HIST1H3J	441.3	1.858393309	1.108299906	4.500214048
HIST1H3PS1	22.3	1.260210035	1.125171627	21.39186255
HIST1H4A	63.9	2.805084746	0.116857925	-
HIST1H4B	209.4	2.346623794	-0.010911356	-1.262162186
HIST1H4C	3.9	1.348214286	6.904571691	7.526766454
HIST1H4D	91.1	1.931492843	-0.089064691	-2.524324372
HIST1H4E	107.3	1.959749553	1.254801441	9.507494468
HIST1H4F	1.1	-	0	1
HIST1H4G	0.2	1.222222222	0	1
HIST1H4H	69.1	1.363684211	-8.94E-03	-1.009729749
HIST1H4I	167.8	1.677158999	-0.5784636	-1.500741624
HIST1H4J	370.5	2.043956044	2.776744427	2.765251659
HIST1H4K	-3.4	-2.545454546	0.058428962	-
HIST1H4L	48.8	1.6981402	-0.11062024	-
HIST1H4PS1	38.4	2.58677686	0.206375505	-
HIST2H2AA3	7.5	2.153846154	4.034292447	5.583766592
HIST2H2AA4	2.1	1.323076923	3.018519471	4.794377552
HIST2H2AB	183.8	3.405759162	0.27831811	-
HIST2H2AC	241.1	3.669988926	3.272906197	3.919756491
HIST2H2BA	192.8	3.091106291	0.061143482	1.284543138
HIST2H2BB	-62.8	-1.104440379	0.287062754	1.624971088
HIST2H2BC	6.5	-	0.132433897	2.112776548
HIST2H2BD	2.4	2.263157895	0.128521293	2.376873617
HIST2H2BE	7105.1	2.020393216	1.297901201	5.060399215
HIST2H2BF	560.5	1.572581469	0.236157412	12.4972726
HIST2H3A	-1	-1.153846154	0.052155802	4.753747234
HIST2H3C	2.4	1.285714286	0.052155802	4.753747234
HIST2H3D	276.8	4.580853816	0.263971189	2.178800816
HIST2H3DP1	0.4	1.142857143	0	1
HIST2H3PS2	0	1	0	1
HIST2H4A	33.9	3.14556962	0.097593624	6.482382592
HIST2H4B	4.5	6	5.43E-04	1.056388274
HIST3H2A	263.9	2.276112186	14.3566222	11.34150189
HIST3H2BA	9.5	1.484693878	0	1
HIST3H2BB	366.2	2.191281718	0.153853581	4.951820035
HIST3H3	2.2	-	0.069909888	1.584582411
HIST4H4	426.9	2.222158603	0.072929723	2.324054203

References

Ace, C.I., McKee, T.A., Ryan, J.M., Cameron, J.M., and Preston, C.M. (1989). Construction and characterization of a herpes simplex virus type 1 mutant unable to transinduce immediate-early gene expression. Journal of virology.

Alandijany, T., Roberts, A.P.E., Conn, K.L., Loney, C., McFarlane, S., Orr, A., and Boutell, C. (2018). Distinct temporal roles for the promyelocytic leukaemia (PML) protein in the sequential regulation of intracellular host immunity to HSV-1 infection. PLoS Pathog *14*, e1006769.

Albright, E.R., and Kalejta, R.F. (2016). Canonical and variant forms of histone H3 are deposited onto the human cytomegalovirus genome during lytic and latent infections. Journal of virology *90*, 10309-10320.

Barrangou, R., Fremaux, C., Deveau, H., Richards, M., Boyaval, P., Moineau, S., Romero, D.A., and Horvath, P. (2007). CRISPR provides acquired resistance against viruses in prokaryotes. Science *315*, 1709-1712.

Bearer, E.L., Breakefield, X.O., Schuback, D., Reese, T.S., and LaVail, J.H. (2000). Retrograde axonal transport of herpes simplex virus: Evidence for a single mechanism and a role for tegument. Proceedings of the National Academy of Sciences *97*, 8146-8150.

Belotserkovskaya, R., Oh, S., Bondarenko, V.A., Orphanides, G., Studitsky, V.M., and Reinberg, D. (2003). FACT facilitates transcription-dependent nucleosome alteration. Science *301*, 1090-1093.

Bender, F.C., Whitbeck, J.C., Lou, H., Cohen, G.H., and Eisenberg, R.J. (2005). Herpes simplex virus glycoprotein B binds to cell surfaces independently of heparan sulfate and blocks virus entry. Journal of virology *79*, 11588-11597.

Benson, L.J., Gu, Y., Yakovleva, T., Tong, K., Barrows, C., Strack, C.L., Cook, R.G., Mizzen, C.A., and Annunziato, A.T. (2006). Modifications of H3 and H4 during Chromatin Replication, Nucleosome Assembly, and Histone Exchange. Journal of Biological Chemistry *281*, 9287-9296.

Bérubé, N.G. (2011). ATRX in chromatin assembly and genome architecture during development and disease. Biochemistry and Cell Biology *89*, 435-444.

Berube, N.G., Smeenk, C.A., and Picketts, D.J. (2000). Cell cycle-dependent phosphorylation of the ATRX protein correlates with changes in nuclear matrix and chromatin association. Hum Mol Genet *9*, 539-547.

Bieniasz, P.D. (2004). Intrinsic immunity: a front-line defense against viral attack. Nature Immunology *5*, 1109.

Boutell, C., Cuchet-Lourenço, D., Vanni, E., Orr, A., Glass, M., McFarlane, S., and Everett, R.D. (2011). A viral ubiquitin ligase has substrate preferential SUMO targeted ubiquitin ligase activity that counteracts intrinsic antiviral defence. PLoS pathogens *7*, e1002245-e1002245.

Boutell, C., Orr, A., and Everett, R.D. (2003). PML residue lysine 160 is required for the degradation of PML induced by herpes simplex virus type 1 regulatory protein ICP0. Journal of virology *77*, 8686-8694.

Boutell, C., Sadis, S., and Everett, R.D. (2002). Herpes Simplex Virus Type 1 Immediate-Early Protein ICP0 and Its Isolated RING Finger Domain Act as Ubiquitin E3 Ligases In Vitro. Journal of virology *76*, 841-850.

Brand, P., Lenser, T., and Hemmerich, P. (2010). Assembly dynamics of PML nuclear bodies in living cells. PMC biophysics *3*, 3-3.

Bresnahan, W.A., Hultman, G.E., and Shenk, T. (2000). Replication of wild-type and mutant human cytomegalovirus in life-extended human diploid fibroblasts. Journal of virology *74*, 10816-10818.

Bringhurst, R.M., and Schaffer, P.A. (2006). Cellular Stress Rather than Stage of the Cell Cycle Enhances the Replication and Plating Efficiencies of Herpes Simplex Virus Type 1 ICP0− Viruses.

Buenrostro, J.D., Wu, B., Chang, H.Y., and Greenleaf, W.J. (2015). ATAC-seq: A Method for Assaying Chromatin Accessibility Genome-Wide. Current protocols in molecular biology *109*, 21.29.21-21.29.29.

Busskamp, V., Lewis, N.E., Guye, P., Ng, A.H., Shipman, S.L., Byrne, S.M., Sanjana, N.E., Murn, J., Li, Y., Li, S.*, et al.* (2014). Rapid neurogenesis through transcriptional activation in human stem cells. Mol Syst Biol *10*, 760.

Cabral, J.M., Oh, H.S., and Knipe, D.M. (2018). ATRX promotes maintenance of herpes simplex virus heterochromatin during chromatin stress. eLife *7*, e40228.

Cai, W., and Schaffer, P.A. (1992). Herpes simplex virus type 1 ICP0 regulates expression of immediate-early, early, and late genes in productively infected cells. Journal of virology *66*, 2904-2915.

Catez, F., Picard, C., Held, K., Gross, S., Rousseau, A., Theil, D., Sawtell, N., Labetoulle, M., and Lomonte, P. (2012). HSV-1 Genome Subnuclear Positioning and Associations with Host-Cell PML-NBs and Centromeres Regulate LAT Locus Transcription during Latency in Neurons. PLoS Pathog *8*, e1002852.

Cereghini, S., and Yaniv, M. (1984). Assembly of transfected DNA into chromatin: structural changes in the origin-promoter-enhancer region upon replication. The EMBO journal *3*, 1243-1253.

Chang, H.R., Munkhjargal, A., Kim, M.J., Park, S.Y., Jung, E., Ryu, J.H., Yang, Y., Lim, J.S., and Kim, Y. (2018). The functional roles of PML nuclear bodies in genome maintenance. Mutat Res *809*, 99-107.

Chelbi-Alix, M.K., and de The, H. (1999). Herpes virus induced proteasome-dependent degradation of the nuclear bodies-associated PML and Sp100 proteins. Oncogene *18*, 935-941.

Chu, H.-P., Cifuentes-Rojas, C., Kesner, B., Aeby, E., Lee, H.-g., Wei, C., Oh, H.J., Boukhali, M., Haas, W., and Lee, J.T. (2017). TERRA RNA Antagonizes ATRX and Protects Telomeres. Cell *170*, 86-101.e116.

Cicconet, M., Hochbaum, D.R., Richmond, D.L., and Sabatini, B.L. (2017). Bots for Software-Assisted Analysis of Image-Based Transcriptomics. In 2017 IEEE International Conference on Computer Vision Workshop (Venice, ITALY), pp. 134-142.

Cliffe, Anna R., Arbuckle, Jesse H., Vogel, Jodi L., Geden, Matthew J., Rothbart, Scott B., Cusack, Corey L., Strahl, Brian D., Kristie, Thomas M., and Deshmukh, M. (2015). Neuronal Stress Pathway Mediating a Histone Methyl/Phospho Switch Is Required for Herpes Simplex Virus Reactivation. Cell Host & Microbe *18*, 649-658.

Cliffe, A.R., Garber, D.A., and Knipe, D.M. (2009). Transcription of the Herpes Simplex Virus Latency-Associated Transcript Promotes the Formation of Facultative Heterochromatin on Lytic Promoters. Journal of virology *83*, 8182-8190.

Cliffe, A.R., and Knipe, D.M. (2008). Herpes simplex virus ICP0 promotes both histone removal and acetylation on viral DNA during lytic infection. Journal of virology *82*, 12030-12038.

Clynes, D., Jelinska, C., Xella, B., Ayyub, H., Scott, C., Mitson, M., Taylor, S., Higgs, D.R., and Gibbons, R.J. (2015). Suppression of the alternative lengthening of telomere pathway by the chromatin remodelling factor ATRX. Nature communications *6*, 7538-7538.

Clynes, D., Jelinska, C., Xella, B., Ayyub, H., Taylor, S., Mitson, M., Bachrati, C.Z., Higgs, D.R., and Gibbons, R.J. (2014). ATRX dysfunction induces replication defects in primary mouse cells. PloS one *9*, e92915-e92915.

Cohen, C., Corpet, A., Roubille, S., Maroui, M.A., Poccardi, N., Rousseau, A., Kleijwegt, C., Binda, O., Texier, P., Sawtell, N.*, et al.* (2018). Promyelocytic leukemia (PML) nuclear bodies (NBs) induce latent/quiescent HSV-1 genomes chromatinization through a PML NB/Histone H3.3/H3.3 Chaperone Axis. PLOS Pathogens *14*, e1007313.

Colgrove, R.C., Liu, X., Griffiths, A., Raja, P., Deluca, N.A., Newman, R.M., Coen, D.M., and Knipe, D.M. (2016). History and genomic sequence analysis of the herpes simplex virus 1 KOS and KOS1.1 sub-strains. Virology *487*, 215-221.

Corces, M.R., Trevino, A.E., Hamilton, E.G., Greenside, P.G., Sinnott-Armstrong, N.A., Vesuna, S., Satpathy, A.T., Rubin, A.J., Montine, K.S., Wu, B.*, et al.* (2017). An improved ATAC-seq protocol reduces background and enables interrogation of frozen tissues. Nature Methods *14*, 959.

Cuchet-Lourenco, D., Anderson, G., Sloan, E., Orr, A., and Everett, R.D. (2013). The viral ubiquitin ligase ICP0 is neither sufficient nor necessary for degradation of the cellular DNA sensor IFI16 during herpes simplex virus 1 infection. Journal of virology *87*, 13422-13432.

Cuchet-Lourenço, D., Vanni, E., Glass, M., Orr, A., and Everett, R.D. (2012). Herpes simplex virus 1 ubiquitin ligase ICP0 interacts with PML isoform I and induces its SUMO-independent degradation. Journal of virology *86*, 11209-11222.

Cutter, A.R., and Hayes, J.J. (2015). A brief review of nucleosome structure. FEBS letters *589*, 2914-2922.

Dai-Ju, J.Q., Li, L., Johnson, L.A., and Sandri-Goldin, R.M. (2006). ICP27 Interacts with the C-Terminal Domain of RNA Polymerase II and Facilitates Its Recruitment to Herpes Simplex Virus 1 Transcription Sites, Where It Undergoes Proteasomal Degradation during Infection. Journal of virology *80*, 3567-3581.

Davison, A.J., Eberle, R., Ehlers, B., Hayward, G.S., McGeoch, D.J., Minson, A.C., Pellett, P.E., Roizman, B., Studdert, M.J., and Thiry, E. (2009). The Order Herpesvirales. Arch Virol *154*, 171-177.

Deaton, A.M., Gómez-Rodríguez, M., Mieczkowski, J., Tolstorukov, M.Y., Kundu, S., Sadreyev, R.I., Jansen, L.E.T., and Kingston, R.E. (2016). Enhancer regions show high histone H3.3 turnover that changes during differentiation. eLife *5*, e15316.

Delbarre, E., Ivanauskiene, K., Spirkoski, J., Shah, A., Vekterud, K., Moskaug, J.O., Boe, S.O., Wong, L.H., Kuntziger, T., and Collas, P. (2017). PML protein organizes heterochromatin domains where it regulates histone H3.3 deposition by ATRX/DAXX. Genome Res *27*, 913-921.

Dembowski, J.A., and DeLuca, N.A. (2018). Temporal Viral Genome-Protein Interactions Define Distinct Stages of Productive Herpesviral Infection. mBio *9*, e01182-01118.

Dembowski, J.A., Dremel, S.E., and DeLuca, N.A. (2017). Replication-Coupled Recruitment of Viral and Cellular Factors to Herpes Simplex Virus Type 1

Replication Forks for the Maintenance and Expression of Viral Genomes. PLOS Pathogens *13*, e1006166.

Deshmane, S.L., and Fraser, N.W. (1989). During latency, herpes simplex virus type 1 DNA is associated with nucleosomes in a chromatin structure. Journal of virology *63*, 943-947.

Dhayalan, A., Tamas, R., Bock, I., Tattermusch, A., Dimitrova, E., Kudithipudi, S., Ragozin, S., and Jeltsch, A. (2011). The ATRX-ADD domain binds to H3 tail peptides and reads the combined methylation state of K4 and K9. Human molecular genetics *20*, 2195-2203.

Diner, B.A., Lum, K.K., Toettcher, J.E., and Cristea, I.M. (2016). Viral DNA Sensors IFI16 and Cyclic GMP-AMP Synthase Possess Distinct Functions in Regulating Viral Gene Expression, Immune Defenses, and Apoptotic Responses during Herpesvirus Infection. MBio *7*, e01553-01516.

Dixon, J.R., Gorkin, D.U., and Ren, B. (2016). Chromatin Domains: The Unit of Chromosome Organization. Molecular cell *62*, 668-680.

Dohner, K., Wolfstein, A., Prank, U., Echeverri, C., Dujardin, D., Vallee, R., and Sodeik, B. (2002). Function of dynein and dynactin in herpes simplex virus capsid transport. Mol Biol Cell *13*, 2795-2809.

Dolan, A., Jamieson, F.E., Cunningham, C., Barnett, B.C., and McGeoch, D.J. (1998). The Genome Sequence of Herpes Simplex Virus Type 2. Journal of virology *72*, 2010-2021.

Drane, P., Ouararhni, K., Depaux, A., Shuaib, M., and Hamiche, A. (2010). The death-associated protein DAXX is a novel histone chaperone involved in the replication-independent deposition of H3.3. Genes Dev *24*, 1253-1265.

Elsasser, S.J., Noh, K.M., Diaz, N., Allis, C.D., and Banaszynski, L.A. (2015). Histone H3.3 is required for endogenous retroviral element silencing in embryonic stem cells. Nature *522*, 240-244.

Eustermann, S., Yang, J.C., Law, M.J., Amos, R., Chapman, L.M., Jelinska, C., Garrick, D., Clynes, D., Gibbons, R.J., Rhodes, D.*, et al.* (2011). Combinatorial readout of histone H3 modifications specifies localization of ATRX to heterochromatin. Nat Struct Mol Biol *18*, 777-782.

Everett, R.D. (2000). ICP0, a regulator of herpes simplex virus during lytic and latent infection. BioEssays *22*, 761-770.

Everett, R.D. (2016). Dynamic Response of IFI16 and Promyelocytic Leukemia Nuclear Body Components to Herpes Simplex Virus 1 Infection. Journal of virology *90*, 167-179.

Everett, R.D., Parada, C., Gripon, P., Sirma, H., and Orr, A. (2008). Replication of ICP0-Null Mutant Herpes Simplex Virus Type 1 Is Restricted by both PML and Sp100. Journal of virology *82*, 2661-2672.

Everett, R.D., Rechter, S., Papior, P., Tavalai, N., Stamminger, T., and Orr, A. (2006). PML Contributes to a Cellular Mechanism of Repression of Herpes Simplex Virus Type 1 Infection That Is Inactivated by ICP0. Journal of virology *80*, 7995-8005.

Ferenczy, M.W., and DeLuca, N.A. (2009). Epigenetic modulation of gene expression from quiescent herpes simplex virus genomes. Journal of virology *83*, 8514-8524.

Fox, H.L., Dembowski, J.A., and DeLuca, N.A. (2017). A Herpesviral Immediate Early Protein Promotes Transcription Elongation of Viral Transcripts. mBio *8*, e00745-00717.

Freeman, E.E., Weiss, H.A., Glynn, J.R., Cross, P.L., Whitworth, J.A., and Hayes, R.J. (2006). Herpes simplex virus 2 infection increases HIV acquisition in men and women: systematic review and meta-analysis of longitudinal studies. AIDS *20*, 73-83.

Full, F., Jungnickl, D., Reuter, N., Bogner, E., Brulois, K., Scholz, B., Stürzl, M., Myoung, J., Jung, J.U., Stamminger, T.*, et al.* (2014). Kaposi's sarcoma associated herpesvirus tegument protein ORF75 is essential for viral lytic replication and plays

a critical role in the antagonization of ND10-instituted intrinsic immunity. PLoS pathogens *10*, e1003863-e1003863.

Garber, D.A., Beverley, S.M., and Coen, D.M. (1993). Demonstration of Circularization of Herpes Simplex Virus DNA Following infection Using Pulsed Field Gel Electrophoresis. Virology *197*, 459-462.

Garrick, D., Samara, V., McDowell, T.L., Smith, A.J.H., Dobbie, L., Higgs, D.R., and Gibbons, R.J. (2004). A conserved truncated isoform of the ATR-X syndrome protein lacking the SWI/SNF-homology domain. Gene *326*, 23-34.

Gibbons, R.J., Pellagatti, A., Garrick, D., Wood, W.G., Malik, N., Ayyub, H., Langford, C., Boultwood, J., Wainscoat, J.S., and Higgs, D.R. (2003). Identification of acquired somatic mutations in the gene encoding chromatin-remodeling factor ATRX in the α-thalassemia myelodysplasia syndrome (ATMDS). Nature Genetics *34*, 446.

Gibeault, R.L., Conn, K.L., Bildersheim, M.D., and Schang, L.M. (2016). An Essential Viral Transcription Activator Modulates Chromatin Dynamics. PLOS Pathogens *12*, e1005842.

Gibson, W., and Roizman, B. (1971). Compartmentalization of spermine and spermidine in the herpes simplex virion. Proceedings of the National Academy of Sciences of the United States of America *68*, 2818-2821.

Goldberg, A.D., Banaszynski, L.A., Noh, K.M., Lewis, P.W., Elsaesser, S.J., Stadler, S., Dewell, S., Law, M., Guo, X., Li, X.*, et al.* (2010). Distinct factors control histone variant H3.3 localization at specific genomic regions. Cell *140*, 678-691.

Gu, H., and Roizman, B. (2003). The degradation of promyelocytic leukemia and Sp100 proteins by herpes simplex virus 1 is mediated by the ubiquitin-conjugating enzyme UbcH5a. Proceedings of the National Academy of Sciences *100*, 8963-8968.

Gu, H., and Roizman, B. (2009). The two functions of herpes simplex virus 1 ICP0, inhibition of silencing by the CoREST/REST/HDAC complex and degradation of PML, are executed in tandem. Journal of virology *83*, 181-187.

Hardwicke, M.A., and Sandri-Goldin, R.M. (1994). The herpes simplex virus regulatory protein ICP27 contributes to the decrease in cellular mRNA levels during infection. Journal of virology *68*, 4797-4810.

Harkness, J.M., Kader, M., and DeLuca, N.A. (2014). Transcription of the herpes simplex virus 1 genome during productive and quiescent infection of neuronal and nonneuronal cells. Journal of virology *88*, 6847-6861.

He, Q., Kim, H., Huang, R., Lu, W., Tang, M., Shi, F., Yang, D., Zhang, X., Huang, J., Liu, D.*, et al.* (2015). The Daxx/Atrx Complex Protects Tandem Repetitive Elements during DNA Hypomethylation by Promoting H3K9 Trimethylation. Cell Stem Cell *17*, 273-286.

Hennig, T., Michalski, M., Rutkowski, A.J., Djakovic, L., Whisnant, A.W., Friedl, M.-S., Jha, B.A., Baptista, M.A.P., L'Hernault, A., Erhard, F.*, et al.* (2018). HSV-1-induced disruption of transcription termination resembles a cellular stress response but selectively increases chromatin accessibility downstream of genes. PLOS Pathogens *14*, e1006954.

Herrera, F.J., and Triezenberg, S.J. (2004). VP16-dependent association of chromatin-modifying coactivators and underrepresentation of histones at immediate-early gene promoters during herpes simplex virus infection. Journal of virology *78*, 9689-9696.

Hoelper, D., Huang, H., Jain, A.Y., Patel, D.J., and Lewis, P.W. (2017). Structural and mechanistic insights into ATRX-dependent and -independent functions of the histone chaperone DAXX. Nat Commun *8*, 1193.

Hollenbach, A.D., McPherson, C.J., Mientjes, E.J., Iyengar, R., and Grosveld, G. (2002). Daxx and histone deacetylase II associate with chromatin through an interaction with core histones and the chromatin-associated protein Dek. Journal of Cell Science *115*, 3319-3330.

Honess, R., and Roizman, B. (1974). Regulation of herpesvirus macromolecular synthesis. I. Cascade regulation of the synthesis of three groups of viral proteins. Journal of virology.

Huang, C., and Zhu, B. (2014). H3.3 turnover: a mechanism to poise chromatin for transcription, or a response to open chromatin? Bioessays *36*, 579-584.

Huh, M.S., Ivanochko, D., Hashem, L.E., Curtin, M., Delorme, M., Goodall, E., Yan, K., and Picketts, D.J. (2016). Stalled replication forks within heterochromatin require ATRX for protection. Cell death & disease *7*, e2220-e2220.

Huh, M.S., Price O'Dea, T., Ouazia, D., McKay, B.C., Parise, G., Parks, R.J., Rudnicki, M.A., and Picketts, D.J. (2012). Compromised genomic integrity impedes muscle growth after Atrx inactivation. The Journal of Clinical Investigation *122*, 4412-4423.

Ivanauskiene, K., Delbarre, E., McGhie, J.D., Küntziger, T., Wong, L.H., and Collas, P. (2014). The PML-associated protein DEK regulates the balance of H3.3 loading on chromatin and is important for telomere integrity. Genome research *24*, 1584-1594.

Iwase, S., Xiang, B., Ghosh, S., Ren, T., Lewis, P.W., Cochrane, J.C., Allis, C.D., Picketts, D.J., Patel, D.J., Li, H.*, et al.* (2011). ATRX ADD domain links an atypical histone methylation recognition mechanism to human mental-retardation syndrome. Nat Struct Mol Biol *18*, 769-776.

Jongeneel, C.V., and Bachenheimer, S.L. (1981). Structure of replicating herpes simplex virus DNA. Journal of virology *39*, 656-660.

Juhasz, S., Elbakry, A., Mathes, A., and Lobrich, M. (2018). ATRX Promotes DNA Repair Synthesis and Sister Chromatid Exchange during Homologous Recombination. Mol Cell *71*, 11-24.e17.

Jurak, I., Kramer, M.F., Mellor, J.C., van Lint, A.L., Roth, F.P., Knipe, D.M., and Coen, D.M. (2010). Numerous Conserved and Divergent MicroRNAs Expressed by Herpes Simplex Viruses 1 and 2. Journal of virology *84*, 4659-4672.

Jurak, I., Silverstein, L.B., Sharma, M., and Coen, D.M. (2012). Herpes Simplex Virus Is Equipped with RNA- and Protein-Based Mechanisms To Repress Expression of ATRX, an Effector of Intrinsic Immunity. Journal of virology *86*, 10093-10102.

Kanherkar, R.R., Bhatia-Dey, N., and Csoka, A.B. (2014). Epigenetics across the human lifespan. Front Cell Dev Biol *2*, 49.

Kent, J.R., Zeng, P.-Y., Atanasiu, D., Gardner, J., Fraser, N.W., and Berger, S.L. (2004). During Lytic Infection Herpes Simplex Virus Type 1 Is Associated with Histones Bearing Modifications That Correlate with Active Transcription. Journal of virology *78*, 10178-10186.

Kim, J.A., Choi, M.S., Min, J.S., Kang, I., Oh, J., Kim, J.C., and Ahn, J.K. (2017). HSV-1 ICP27 represses NF-κB activity by regulating Daxx sumoylation. BMB reports *50*, 275-280.

Kivipõld, P., Võsa, L., Ustav, M., and Kurg, R. (2015). DAXX modulates human papillomavirus early gene expression and genome replication in U2OS cells. Virology journal *12*, 104-104.

Knipe, D.M. (2015). Nuclear sensing of viral DNA, epigenetic regulation of herpes simplex virus infection, and innate immunity. Virology *479-480*, 153-159.

Knipe, D.M., and Cliffe, A. (2008). Chromatin control of herpes simplex virus lytic and latent infection. Nature reviews Microbiology *6*, 211-221.

Knipe, D.M., Lieberman, P.M., Jung, J.U., McBride, A.A., Morris, K.V., Ott, M., Margolis, D., Nieto, A., Nevels, M., Parks, R.J.*, et al.* (2013). Snapshots: chromatin control of viral infection. Virology *435*, 141-156.

Knipe, D.M., Senechek, D., Rice, S.A., and Smith, J.L. (1987). Stages in the nuclear association of the herpes simplex virus transcriptional activator protein ICP4. Journal of virology *61*, 276-284.

Kobayashi, K., Ohgitani, E., Tanaka, Y., Kita, M., and Imanishi, J. (1994). Herpes Simplex Virus-Induced Expression of 70 kDa Heat Shock Protein (HSP70) Requires Early Protein Synthesis But Not Viral DNA Replication. Microbiology and Immunology *38*, 321-325.

Komatsu, T., Quentin-Froignant, C., Carlon-Andres, I., Lagadec, F., Rayne, F., Ragues, J., Kehlenbach, R.H., Zhang, W., Ehrhardt, A., Bystricky, K.*, et al.* (2018).

In Vivo Labelling of Adenovirus DNA Identifies Chromatin Anchoring and Biphasic Genome Replication. Journal of virology *92*, e00795-00718.

Kosakovsky Pond, S.L., Wertheim, J.O., Smith, D.M., Scheffler, K., and Smith, M.D. (2014). Evolutionary Origins of Human Herpes Simplex Viruses 1 and 2. Molecular biology and evolution *31*, 2356-2364.

Koschmann, C., Calinescu, A.-A., Nunez, F.J., Mackay, A., Fazal-Salom, J., Thomas, D., Mendez, F., Kamran, N., Dzaman, M., Mulpuri, L.*, et al.* (2016). ATRX loss promotes tumor growth and impairs nonhomologous end joining DNA repair in glioma. Science Translational Medicine *8*, 328ra328-328ra328.

Kraushaar, D.C., Jin, W., Maunakea, A., Abraham, B., Ha, M., and Zhao, K. (2013). Genome-wide incorporation dynamics reveal distinct categories of turnover for the histone variant H3.3. Genome Biol *14*, R121.

Lacasse, J.J., and Schang, L.M. (2010). During lytic infections, herpes simplex virus type 1 DNA is in complexes with the properties of unstable nucleosomes. Journal of virology *84*, 1920-1933.

LaThangue, N.B., Shriver, K., Dawson, C., and Chan, W.L. (1984). Herpes simplex virus infection causes the accumulation of a heat-shock protein. The EMBO journal *3*, 267-277.

Lechner, M.S., Schultz, D.C., Negorev, D., Maul, G.G., and Rauscher, F.J. (2005). The mammalian heterochromatin protein 1 binds diverse nuclear proteins through a common motif that targets the chromoshadow domain. Biochemical and Biophysical Research Communications *331*, 929-937.

Lee, H., Han, J.-W., Park, J., Kang, K., Cho, E.-J., Han, N., Kim, J.-H., Kwak, S., Youn, H.-D., Lee, H.-T.*, et al.* (2018a). Long non-coding RNA ChRO1 facilitates ATRX/DAXX-dependent H3.3 deposition for transcription-associated heterochromatin reorganization. Nucleic Acids Research *46*, 11759-11775.

Lee, J.S., Raja, P., and Knipe, D.M. (2016). Herpesviral ICP0 Protein Promotes Two Waves of Heterochromatin Removal on an Early Viral Promoter during Lytic Infection. MBio *7*, e02007-02015.

Lee, J.S., Raja, P., Pan, D., Pesola, J.M., Coen, D.M., and Knipe, D.M. (2018b). CCCTC-Binding Factor Acts as a Heterochromatin Barrier on Herpes Simplex Viral Latent Chromatin and Contributes to Poised Latent Infection. mBio *9*, e02372-02317.

Leinbach, S.S., and Summers, W.C. (1980). The Structure of Herpes Simplex Virus Type 1 DNA as Probed by Micrococcal Nuclease Digestion. Journal of General Virology *51*, 45-59.

Leoni, V., Gianni, T., Salvioli, S., and Campadelli-Fiume, G. (2012). Herpes Simplex Virus Glycoproteins gH/gL and gB Bind Toll-Like Receptor 2, and Soluble gH/gL Is Sufficient To Activate NF-κB. Journal of virology *86*, 6555-6562.

Lewis, P.W., Elsaesser, S.J., Noh, K.M., Stadler, S.C., and Allis, C.D. (2010). Daxx is an H3.3-specific histone chaperone and cooperates with ATRX in replication-independent chromatin assembly at telomeres. Proc Natl Acad Sci U S A *107*, 14075-14080.

Li, Y.-H., Tao, P.-Z., Liu, Y.-Z., and Jiang, J.-D. (2004). Geldanamycin, a Ligand of Heat Shock Protein 90, Inhibits the Replication of Herpes Simplex Virus Type 1 In Vitro. Antimicrobial Agents and Chemotherapy *48*, 867-872.

Li, Z., Zhao, D., Xiang, B., and Li, H. (2017). Structural and biochemical characterization of DAXX-ATRX interaction. Protein & cell *8*, 762-766.

Lilley, C.E., Carson, C.T., Muotri, A.R., Gage, F.H., and Weitzman, M.D. (2005). DNA repair proteins affect the lifecycle of herpes simplex virus 1. Proceedings of the National Academy of Sciences of the United States of America *102*, 5844-5849.

Lilley, C.E., Chaurushiya, M.S., Boutell, C., Everett, R.D., and Weitzman, M.D. (2011). The Intrinsic Antiviral Defense to Incoming HSV-1 Genomes Includes Specific DNA Repair Proteins and Is Counteracted by the Viral Protein ICP0. PLOS Pathogens *7*, e1002084.

Lilley, C.E., Chaurushiya, M.S., Boutell, C., Landry, S., Suh, J., Panier, S., Everett, R.D., Stewart, G.S., Durocher, D., and Weitzman, M.D. (2010). A viral E3 ligase targets RNF8 and RNF168 to control histone ubiquitination and DNA damage responses. The EMBO Journal *29*, 943-955.

Liu, X., Main, D., Ma, Y., and He, B. (2018). Herpes Simplex Virus 1 Inhibits TANK-Binding Kinase 1 through Formation of the Us11-Hsp90 Complex. Journal of virology *92*, e00402-00418.

Looker, K.J., Elmes, J.A.R., Gottlieb, S.L., Schiffer, J.T., Vickerman, P., Turner, K.M.E., and Boily, M.-C. (2017). Effect of HSV-2 infection on subsequent HIV acquisition: an updated systematic review and meta-analysis.

Looker, K.J., Magaret, A.S., May, M.T., Turner, K.M.E., Vickerman, P., Gottlieb, S.L., and Newman, L.M. (2019a). Global and Regional Estimates of Prevalent and Incident Herpes Simplex Virus Type 1 Infections in 2012.

Looker, K.J., Magaret, A.S., Turner, K.M.E., Vickerman, P., Gottlieb, S.L., and Newman, L.M. (2019b). Global Estimates of Prevalent and Incident Herpes Simplex Virus Type 2 Infections in 2012.

Lovejoy, C.A., Li, W., Reisenweber, S., Thongthip, S., Bruno, J., de Lange, T., De, S., Petrini, J.H., Sung, P.A., Jasin, M.*, et al.* (2012). Loss of ATRX, genome instability, and an altered DNA damage response are hallmarks of the alternative lengthening of telomeres pathway. PLoS Genet *8*, e1002772.

Lukashchuk, V., and Everett, R.D. (2010). Regulation of ICP0-null mutant herpes simplex virus type 1 infection by ND10 components ATRX and hDaxx. Journal of virology *84*, 4026-4040.

Lund, J., Sato, A., Akira, S., Medzhitov, R., and Iwasaki, A. (2003). Toll-like receptor 9-mediated recognition of Herpes simplex virus-2 by plasmacytoid dendritic cells. The Journal of experimental medicine *198*, 513-520.

Maeshima, K., Imai, R., Tamura, S., and Nozaki, T. (2014). Chromatin as dynamic 10-nm fibers. Chromosoma *123*, 225-237.

Mariamé, B., Kappler-Gratias, S., Kappler, M., Balor, S., Gallardo, F., and Bystricky, K. (2018). Real-Time Visualization and Quantification of Human Cytomegalovirus Replication in Living Cells Using the ANCHOR DNA Labeling Technology. Journal of virology *92*, e00571-00518.

Mason, P.B., and Struhl, K. (2003). The FACT complex travels with elongating RNA polymerase II and is important for the fidelity of transcriptional initiation in vivo. Mol Cell Biol *23*, 8323-8333.

McDowell, T.L., Gibbons, R.J., Sutherland, H., O'Rourke, D.M., Bickmore, W.A., Pombo, A., Turley, H., Gatter, K., Picketts, D.J., Buckle, V.J.*, et al.* (1999). Localization of a putative transcriptional regulator (ATRX) at pericentromeric heterochromatin and the short arms of acrocentric chromosomes. Proc Natl Acad Sci U S A *96*, 13983-13988.

McFarlane, S., Orr, A., Roberts, A.P.E., Conn, K.L., Iliev, V., Loney, C., da Silva Filipe, A., Smollett, K., Gu, Q., Robertson, N.*, et al.* (2019). The histone chaperone HIRA promotes the induction of host innate immune defences in response to HSV-1 infection. PLOS Pathogens *15*, e1007667.

McQuillan, G., Kruszon-Moran, D., Flagg, E., and Paulose-Ram, R. (2018). Prevalence of herpes simplex virus type 1 and type 2 in persons aged 14–49: United States, 2015–2016. NCHS Data Brief, no 304 Hyattsville, MD: National Center for Health Statistics.

Melnick, M., Gonzales, P., Cabral, J., Allen, M.A., Dowell, R.D., and Link, C.D. (2019). Heat shock in C. elegans induces downstream of gene transcription and accumulation of double-stranded RNA. PLOS ONE *14*, e0206715.

Merkl, P.E., and Knipe, D.M. (2019). Role for a Filamentous Nuclear Assembly of IFI16, DNA, and Host Factors in Restriction of Herpesviral Infection. mBio *10*, e02621-02618.

Merkl, P.E., Orzalli, M.H., and Knipe, D.M. (2018). Mechanisms of Host IFI16, PML, and Daxx Protein Restriction of Herpes Simplex Virus 1 Replication. Journal of virology *92*, in press.

Moazed, D. (2011). Mechanisms for the inheritance of chromatin states. Cell *146*, 510-518.

Muggeridge, M.I., and Fraser, N.W. (1986). Chromosomal organization of the herpes simplex virus genome during acute infection of the mouse central nervous system. Journal of virology *59*, 764-767.

Nair, N., Shoaib, M., and Sorensen, C.S. (2017). Chromatin Dynamics in Genome Stability: Roles in Suppressing Endogenous DNA Damage and Facilitating DNA Repair. Int J Mol Sci *18*.

Nan, X., Hou, J., Maclean, A., Nasir, J., Lafuente, M.J., Shu, X., Kriaucionis, S., and Bird, A. (2007). Interaction between chromatin proteins MECP2 and ATRX is disrupted by mutations that cause inherited mental retardation. Proceedings of the National Academy of Sciences *104*, 2709-2714.

Netsawang, J., Panaampon, J., Khunchai, S., Kooptiwut, S., Nagila, A., Puttikhunt, C., Yenchitsomanus, P.-t., and Limjindaporn, T. (2014). Dengue virus disrupts Daxx and NF-κB interaction to induce CD137-mediated apoptosis. Biochemical and Biophysical Research Communications *450*, 1485-1491.

Newhart, A., Rafalska-Metcalf, I.U., Yang, T., Joo, L.M., Powers, S.L., Kossenkov, A.V., Lopez-Jones, M., Singer, R.H., Showe, L.C., Skordalakes, E.*, et al.* (2013). Single cell analysis of RNA-mediated histone H3.3 recruitment to a cytomegalovirus promoter-regulated transcription site. J Biol Chem *288*, 19882-19899.

Newhart, A., Rafalska-Metcalf, I.U., Yang, T., Negorev, D.G., and Janicki, S.M. (2012). Single-cell analysis of Daxx and ATRX-dependent transcriptional repression. Journal of Cell Science *125*, 5489-5501.

Noh, K.-M., Maze, I., Zhao, D., Xiang, B., Wenderski, W., Lewis, P.W., Shen, L., Li, H., and Allis, C.D. (2015a). ATRX tolerates activity-dependent histone H3 methyl/phos switching to maintain repetitive element silencing in neurons. Proceedings of the National Academy of Sciences of the United States of America *112*, 6820-6827.

Noh, K.M., Maze, I., Zhao, D., Xiang, B., Wenderski, W., Lewis, P.W., Shen, L., Li, H., and Allis, C.D. (2015b). ATRX tolerates activity-dependent histone H3 methyl/phos switching to maintain repetitive element silencing in neurons. Proc Natl Acad Sci U S A *112*, 6820-6827.

Oh, J., and Fraser, N.W. (2008). Temporal association of the herpes simplex virus genome with histone proteins during a lytic infection. Journal of virology *82*, 3530-3537.

Oh, J., Ruskoski, N., and Fraser, N.W. (2012). Chromatin assembly on herpes simplex virus 1 DNA early during a lytic infection is Asf1a Dependent. Journal of virology *86*, 12313-12321.

Ohta, A., Yamauchi, Y., Muto, Y., Kimura, H., and Nishiyama, Y. (2011). Herpes simplex virus type 1 UL14 tegument protein regulates intracellular compartmentalization of major tegument protein VP16. Virology Journal *8*, 365.

Orzalli, M.H., Broekema, N.M., Diner, B.A., Hancks, D.C., Elde, N.C., Cristea, I.M., and Knipe, D.M. (2015). cGAS-mediated stabilization of IFI16 promotes innate signaling during herpes simplex virus infection. Proceedings of the National Academy of Sciences of the United States of America *112*, E1773-E1781.

Orzalli, M.H., Conwell, S.E., Berrios, C., Decaprio, J.A., and Knipe, D.M. (2013). Nuclear interferon-inducible protein 16 promotes silencing of herpesviral and transfected DNA. Proc Natl Acad Sci U S A *110*, E4492-4501.

Orzalli, M.H., DeLuca, N.A., and Knipe, D.M. (2012). Nuclear IFI16 induction of IRF-3 signaling during herpesviral infection and degradation of IFI16 by the viral ICP0 protein. Proceedings of the National Academy of Sciences *109*, E3008-E3017.

Orzalli, M.H., and Knipe, D.M. (2014). Cellular sensing of viral DNA and viral evasion mechanisms. Annu Rev Microbiol *68*, 477-492.

Pan, D., Flores, O., Umbach, Jennifer L., Pesola, Jean M., Bentley, P., Rosato, Pamela C., Leib, David A., Cullen, Bryan R., and Coen, Donald M. (2014). A Neuron-Specific Host MicroRNA Targets Herpes Simplex Virus-1 ICP0 Expression and Promotes Latency. Cell Host & Microbe *15*, 446-456.

Park, D.J., Pask, A.J., Huynh, K., Renfree, M.B., Harley, V.R., and Marshall Graves, J.A. (2004). Comparative analysis of ATRX, a chromatin remodeling protein. Gene *339*, 39-48.

Park, J., Lee, J.H., La, M., Jang, M.J., Chae, G.W., Kim, S.B., Tak, H., Jung, Y., Byun, B., Ahn, J.K.*, et al.* (2007). Inhibition of NF-κB Acetylation and its Transcriptional Activity by Daxx. Journal of Molecular Biology *368*, 388-397.

Pellett, P.E., and Roizman, B. (2013). Herpesviridae. In Fields Virology, D.M. Knipe, and P.M. Howley, eds. (Philadelphia, PA: Lippincott Williams & Wilkins).

Peng, H., Nogueira, M.L., Vogel, J.L., and Kristie, T.M. (2010). Transcriptional coactivator HCF-1 couples the histone chaperone Asf1b to HSV-1 DNA replication components. Proceedings of the National Academy of Sciences *107*, 2461-2466.

Phelan, A., Carmo-Fonseca, M., McLaughlan, J., Lamond, A.I., and Clements, J.B. (1993). A herpes simplex virus type 1 immediate-early gene product, IE63, regulates small nuclear ribonucleoprotein distribution. Proceedings of the National Academy of Sciences *90*, 9056-9060.

Pignatti, P.F., and Cassai, E. (1980). Analysis of herpes simplex virus nucleoprotein complexes extracted from infected cells. Journal of virology *36*, 816-828.

Pinninti, S., and Kimberlin, D. (2013). Neonatal herpes simplex virus infections. Pediatric Clinics of North America, *60*, 351-365.

Placek, B.J., Huang, J., Kent, J.R., Dorsey, J., Rice, L., Fraser, N.W., and Berger, S.L. (2009). The histone variant H3.3 regulates gene expression during lytic infection with herpes simplex virus type 1. Journal of virology *83*, 1416-1421.

Poon, A.P.W., Liang, Y., and Roizman, B. (2003). Herpes Simplex Virus 1 Gene Expression Is Accelerated by Inhibitors of Histone Deacetylases in Rabbit Skin Cells Infected with a Mutant Carrying a cDNA Copy of the Infected-Cell Protein No. 0. Journal of virology *77*, 12671-12678.

Preston, C.M., and Nicholl, M.J. (2008). Induction of Cellular Stress Overcomes the Requirement of Herpes Simplex Virus Type 1 for Immediate-Early Protein ICP0 and Reactivates Expression from Quiescent Viral Genomes. Journal of virology *82*, 11775-11783.

Rai, T.S., Glass, M., Cole, J.J., Rather, M.I., Marsden, M., Neilson, M., Brock, C., Humphreys, I.R., Everett, R.D., and Adams, P.D. (2017). Histone chaperone HIRA deposits histone H3.3 onto foreign viral DNA and contributes to anti-viral intrinsic immunity. Nucleic Acids Res *45*, 11673-11683.

Ray-Gallet, D., Woolfe, A., Vassias, I., Pellentz, C., Lacoste, N., Puri, A., Schultz, D.C., Pchelintsev, N.A., Adams, P.D., Jansen, L.E.*, et al.* (2011). Dynamics of histone H3 deposition in vivo reveal a nucleosome gap-filling mechanism for H3.3 to maintain chromatin integrity. Mol Cell *44*, 928-941.

Reverón-Gómez, N., González-Aguilera, C., Stewart-Morgan, K.R., Petryk, N., Flury, V., Graziano, S., Johansen, J.V., Jakobsen, J.S., Alabert, C., and Groth, A. (2018). Accurate Recycling of Parental Histones Reproduces the Histone Modification Landscape during DNA Replication. Molecular Cell *72*, 239-249.e235.

Roizman, B., Knipe, D.M., and Whitley, R.J. (2013). Herpes simplex viruses. In Fields Virology, 6th edition (Philadelphia, PA: Lippincott Williams & Wilkins), pp. 1823-1897.

Rutkowski, A.J., Erhard, F., L'Hernault, A., Bonfert, T., Schilhabel, M., Crump, C., Rosenstiel, P., Efstathiou, S., Zimmer, R., Friedel, C.C.*, et al.* (2015). Widespread disruption of host transcription termination in HSV-1 infection. Nature Communications *6*, 7126.

Sadic, D., Schmidt, K., Groh, S., Kondofersky, I., Ellwart, J., Fuchs, C., Theis, F.J., and Schotta, G. (2015). Atrx promotes heterochromatin formation at retrotransposons. EMBO Rep *16*, 836-850.

Saffert, R.T., and Kalejta, R.F. (2006). Inactivating a cellular intrinsic immune defense mediated by Daxx is the mechanism through which the human cytomegalovirus pp71 protein stimulates viral immediate-early gene expression. Journal of virology *80*, 3863-3871.

Samaniego, L.A., Neiderhiser, L., and DeLuca, N.A. (1998). Persistence and expression of the herpes simplex virus genome in the absence of immediate-early proteins. Journal of virology *72*, 3307-3320.

Sandri-Goldin, R.M. (1998). ICP27 mediates HSV RNA export by shuttling through a leucine-rich nuclear export signal and binding viral intronless RNAs through an RGG motif. Genes & development *12*, 868-879.

Sarma, K., Cifuentes-Rojas, C., Ergun, A., del Rosario, A., Jeon, Y., White, F., Sadreyev, R., and Lee, Jeannie T. (2014). ATRX Directs Binding of PRC2 to Xist RNA and Polycomb Targets. Cell *159*, 869-883.

Schreiner, S., Burck, C., Glass, M., Groitl, P., Wimmer, P., Kinkley, S., Mund, A., Everett, R.D., and Dobner, T. (2013). Control of human adenovirus type 5 gene expression by cellular Daxx/ATRX chromatin-associated complexes. Nucleic Acids Res *41*, 3532-3550.

Schwabish, M.A., and Struhl, K. (2004). Evidence for eviction and rapid deposition of histones upon transcriptional elongation by RNA polymerase II. Mol Cell Biol *24*, 10111-10117.

Schwartzentruber, J., Korshunov, A., Liu, X.-Y., Jones, D.T.W., Pfaff, E., Jacob, K., Sturm, D., Fontebasso, A.M., Quang, D.-A.K., Tönjes, M.*, et al.* (2012). Driver mutations in histone H3.3 and chromatin remodelling genes in paediatric glioblastoma. Nature *482*, 226.

Sekine, E., Schmidt, N., Gaboriau, D., and O'Hare, P. (2017). Spatiotemporal dynamics of HSV genome nuclear entry and compaction state transitions using bioorthogonal chemistry and super-resolution microscopy. PLoS Pathog *13*, e1006721.

Shalginskikh, N., Poleshko, A., Skalka, A.M., and Katz, R.A. (2013). Retroviral DNA methylation and epigenetic repression are mediated by the antiviral host protein Daxx. Journal of virology *87*, 2137-2150.

Shapira, L., Ralph, M., Tomer, E., Cohen, S., and Kobiler, O. (2016). Histone Deacetylase Inhibitors Reduce the Number of Herpes Simplex Virus-1 Genomes Initiating Expression in Individual Cells. Front Microbiol *7*.

Showalter, S.D., Zweig, M., and Hampar, B. (1981). Monoclonal antibodies to herpes simplex virus type 1 proteins, including the immediate-early protein ICP 4. Infection and immunity *34*, 684-692.

Silva, A.C., Xu, X., Kim, H.S., Fillingham, J., Kislinger, T., Mennella, T.A., and Keogh, M.C. (2012). The replication-independent histone H3-H4 chaperones HIR,

ASF1, and RTT106 co-operate to maintain promoter fidelity. J Biol Chem *287*, 1709-1718.

Siwek, W., Gómez-Rodríguez, M., Sobral, D., Corrêa, I.R., and Jansen, L.E.T. (2018). time-ChIP: A Method to Determine Long-Term Locus-Specific Nucleosome Inheritance. In Histone Variants: Methods and Protocols, G.A. Orsi, and G. Almouzni, eds. (New York, NY: Springer New York), pp. 131-158.

Skaliter, R., Makhov, A.M., Griffith, J.D., and Lehman, I.R. (1996). Rolling circle DNA replication by extracts of herpes simplex virus type 1-infected human cells. Journal of virology *70*, 1132-1136.

Smith, C.A., Bates, P., Rivera-Gonzalez, R., Gu, B., and DeLuca, N.A. (1993). ICP4, the major transcriptional regulatory protein of herpes simplex virus type 1, forms a tripartite complex with TATA-binding protein and TFIIB. Journal of virology.

Stern, S., Tanaka, M., and Herr, W. (1989). The Oct-1 homoeodomain directs formation of a multiprotein-DNA complex with the HSV transactivator VP16. Nature *341*, 624.

Strang, B.L., and Stow, N.D. (2005). Circularization of the herpes simplex virus type 1 genome upon lytic infection. Journal of virology *79*, 12487-12494.

Stratmann, S.A., Morrone, S.R., van Oijen, A.M., and Sohn, J. (2015). The innate immune sensor IFI16 recognizes foreign DNA in the nucleus by scanning along the duplex. Elife *4*, e11721.

Tagami, H., Ray-Gallet, D., Almouzni, G., and Nakatani, Y. (2004). Histone H3.1 and H3.3 Complexes Mediate Nucleosome Assembly Pathways Dependent or Independent of DNA Synthesis. Cell *116*, 51-61.

Tang, Q., Li, L., Ishov, A.M., Revol, V., Epstein, A.L., and Maul, G.G. (2003). Determination of Minimum Herpes Simplex Virus Type 1 Components Necessary To Localize Transcriptionally Active DNA to ND10. Journal of virology *77*, 5821-5828.

Tanguy Le Gac, N., and Boehmer, P.E. (2002). Activation of the Herpes Simplex Virus Type-1 Origin-binding Protein (UL9) by Heat Shock Proteins. Journal of Biological Chemistry *277*, 5660-5666.

Taylor, T.J., and Knipe, D.M. (2004). Proteomics of Herpes Simplex Virus Replication Compartments: Association of Cellular DNA Replication, Repair, Recombination, and Chromatin Remodeling Proteins with ICP8. Journal of virology *78*, 5856-5866.

Thompson, M.R., Kaminski, J.J., Kurt-Jones, E.A., and Fitzgerald, K.A. (2011). Pattern recognition receptors and the innate immune response to viral infection. Viruses *3*, 920-940.

Tock, M.R., and Dryden, D.T. (2005). The biology of restriction and anti-restriction. Curr Opin Microbiol *8*, 466-472.

Torigoe, S.E., Urwin, D.L., Ishii, H., Smith, D.E., and Kadonaga, J.T. (2011). Identification of a rapidly formed nonnucleosomal histone-DNA intermediate that is converted into chromatin by ACF. Molecular cell *43*, 638-648.

Tsai, K., Chan, L., Gibeault, R., Conn, K., Dheekollu, J., Domsic, J., Marmorstein, R., Schang, L.M., and Lieberman, P.M. (2014). Viral reprogramming of the Daxx histone H3.3 chaperone during early Epstein-Barr virus infection. Journal of virology *88*, 14350-14363.

Tsai, K., Thikmyanova, N., Wojcechowskyj, J.A., Delecluse, H.J., and Lieberman, P.M. (2011). EBV tegument protein BNRF1 disrupts DAXX-ATRX to activate viral early gene transcription. PLoS Pathog *7*, e1002376.

Udugama, M., Sanij, E., Voon, H.P.J., Son, J., Hii, L., Henson, J.D., Chan, F.L., Chang, F.T.M., Liu, Y., Pearson, R.B.*, et al.* (2018). Ribosomal DNA copy loss and repeat instability in ATRX-mutated cancers. PNAS.

Valle-García, D., Qadeer, Z.A., McHugh, D.S., Ghiraldini, F.G., Chowdhury, A.H., Hasson, D., Dyer, M.A., Recillas-Targa, F., and Bernstein, E. (2016). ATRX binds to atypical chromatin domains at the 3' exons of zinc finger genes to preserve H3K9me3 enrichment. Epigenetics *11*, 398-414.

Vlijm, R., Smitshuijzen, J.S.J., Lusser, A., and Dekker, C. (2012). NAP1-Assisted Nucleosome Assembly on DNA Measured in Real Time by Single-Molecule Magnetic Tweezers. PLOS ONE *7*, e46306.

Voon, Hsiao P.J., Hughes, Jim R., Rode, C., De La Rosa-Velázquez, Inti A., Jenuwein, T., Feil, R., Higgs, Douglas R., and Gibbons, Richard J. (2015). ATRX Plays a Key Role in Maintaining Silencing at Interstitial Heterochromatic Loci and Imprinted Genes. Cell Reports *11*, 405-418.

Wadsworth, S., Jacob, R.J., and Roizman, B. (1975). Anatomy of herpes simplex virus DNA. II. Size, composition, and arrangement of inverted terminal repetitions. Journal of virology.

Wagenknecht, N., Reuter, N., Scherer, M., Reichel, A., Muller, R., and Stamminger, T. (2015). Contribution of the Major ND10 Proteins PML, hDaxx and Sp100 to the Regulation of Human Cytomegalovirus Latency and Lytic Replication in the Monocytic Cell Line THP-1. Viruses *7*, 2884-2907.

Wang, G.Z., Wang, Y., and Goff, S.P. (2016). Histones Are Rapidly Loaded onto Unintegrated Retroviral DNAs Soon after Nuclear Entry. Cell Host Microbe *20*, 798-809.

Wang, Q.-Y., Zhou, C., Johnson, K.E., Colgrove, R.C., Coen, D.M., and Knipe, D.M. (2005). Herpesviral latency-associated transcript gene promotes assembly of heterochromatin on viral lytic-gene promoters in latent infection. Proceedings of the National Academy of Sciences of the United States of America *102*, 16055-16059.

Weber, F., Wagner, V., Rasmussen, S.B., Hartmann, R., and Paludan, S.R. (2006). Double-stranded RNA is produced by positive-strand RNA viruses and DNA viruses but not in detectable amounts by negative-strand RNA viruses. Journal of virology *80*, 5059-5064.

Weidtkamp-Peters, S., Lenser, T., Negorev, D., Gerstner, N., Hofmann, T.G., Schwanitz, G., Hoischen, C., Maul, G., Dittrich, P., and Hemmerich, P. (2008). Dynamics of component exchange at PML nuclear bodies. Journal of Cell Science *121*, 2731-2743.

Whitehead, K.A., Dahlman, J.E., Langer, R.S., and Anderson, D.G. (2011). Silencing or stimulation? siRNA delivery and the immune system. Annu Rev Chem Biomol Eng *2*, 77-96.

Wilkinson, D.E., and Weller, S.K. (2006). Herpes simplex virus type I disrupts the ATR-dependent DNA-damage response during lytic infection. Journal of Cell Science *119*, 2695-2703.

Wilson, A.C., LaMarco, K., Peterson, M.G., and Herr, W. (1993). The VP16 accessory protein HCF is a family of polypeptides processed from a large precursor protein. Cell *74*, 115-125.

Woodhall, D.L., Groves, I.J., Reeves, M.B., Wilkinson, G., and Sinclair, J.H. (2006). Human Daxx-mediated repression of human cytomegalovirus gene expression correlates with a repressive chromatin structure around the major immediate early promoter. J Biol Chem *281*, 37652-37660.

Wyler, E., Menegatti, J., Franke, V., Kocks, C., Boltengagen, A., Hennig, T., Theil, K., Rutkowski, A., Ferrai, C., Baer, L.*, et al.* (2017). Widespread activation of antisense transcription of the host genome during herpes simplex virus 1 infection. Genome Biology *18*, 209.

Xin, H., Takahata, S., Blanksma, M., McCullough, L., Stillman, D.J., and Formosa, T. (2009). yFACT induces global accessibility of nucleosomal DNA without H2A-H2B displacement. Mol Cell *35*, 365-376.

Xu, P., Mallon, S., and Roizman, B. (2016). PML plays both inimical and beneficial roles in HSV-1 replication. Proc Natl Acad Sci U S A *113*, E3022-3028.

Yao, S., Sukonnik, T., Kean, T., Bharadwaj, R.R., Pasceri, P., and Ellis, J. (2004). Retrovirus silencing, variegation, extinction, and memory are controlled by a dynamic interplay of multiple epigenetic modifications. Mol Ther *10*, 27-36.

Yao, Z., Zhang, Q., Li, X., Zhao, D., Liu, Y., Zhao, K., Liu, Y., Wang, C., Jiang, M., Li, N.*, et al.* (2014). Death domain-associated protein 6 (Daxx) selectively represses IL-6 transcription through histone deacetylase 1 (HDAC1)-mediated histone deacetylation in macrophages. The Journal of biological chemistry *289*, 9372-9379.

Zhang, S.-Y., Jouanguy, E., Ugolini, S., Smahi, A., Elain, G., Romero, P., Segal, D., Sancho-Shimizu, V., Lorenzo, L., Puel, A.*, et al.* (2007). TLR3 Deficiency in Patients with Herpes Simplex Encephalitis. Science *317*, 1522-1527.

Zhou, C., and Knipe, D.M. (2002). Association of herpes simplex virus type 1 ICP8 and ICP27 proteins with cellular RNA polymerase II holoenzyme. Journal of virology *76*, 5893-5904.

Zwaagstra, J.C., Ghiasi, H., Slanina, S.M., Nesburn, A.B., Wheatley, S.C., Lillycrop, K., Wood, J., Latchman, D.S., Patel, K., and Wechsler, S.L. (1990). Activity of herpes simplex virus type 1 latency-associated transcript (LAT) promoter in neuron-derived cells: evidence for neuron specificity and for a large LAT transcript. Journal of virology *64*, 5019-5028.